Department of Precision and Microsystems Engineering

A Compliant Dynamic Arteriovenous Fistula: The Design and Validation of a Robust Implantable Valve

D.W.Ulijn

Report no : 2024.076
Coach : Dr.ir. T.Horeman, Ir. N.A.White
Professor : Prof.dr.ir. J.L.Herder
Specialisation : MSD
Type of report : Master Thesis
Date : 22 August 2024

Preface

Handing in this report I realise this will be one of the last steps towards my graduation from the Master of Precision and Microsystems Engineering - Mechanical Engineering at the TUDelft. I would like to thank my daily supervisor Ir. Nick White for his uninterrupted support throughout this project and the weekly meetings, keeping me in check and focused on the priorities. I would also like to express my gratitude toward Dr. ir. ing. Tim Horeman for the opportunity to work on this medical subject and Prof.dr.ir. Just Herder for his supervision.
I'm also very grateful for all the help I've received during my thesis. Thank you Koen for your help with the linearstage, optimization and the interesting discussions we shared. Thanks to Jan for your invaluable advice and for allowing me to use the Phantomlab. I'd also like to thank Jelle and Rinus for the fun and not-so-fun times shared studying and the many cups of coffee we shared. And thank you Berend allowing me to study in your awesome workshop. I'm grateful for all the people I've met during my time as a student here in Delft, the people of the workshops of IWS and the Dreamhall and at Delft Hyperloop.
Lastly, I'd like to express my deepest thanks to my family for all of their support. Especially to my parents for the countless visits to the railway and technical museum at a young age, inspiring me to become a Mechanical Engineer.

Dirk Ulijn
Delft, August 2024

Abstract

Each year in the Netherlands almost two thousand people are diagnosed with End Stage Kidney Disease, amounting to a total of 7 million people worldwide. With an insufficient amount of donors available, most of these patients are treated using haemodialysis where the blood is filtered with a dialysis machine. Prior to this treatment an arteriovenous fistula (AVF) or arteriovenous graft(AVG) is created to increase their blood flow sufficiently to speed up the filtration process. Another result of increasing the blood flow is the size increase of the vein, leading to easier access. Unfortunately, the continuous high flow rate is linked to various negative effects. To counter these negative effects a Dynamic Arteriovenous System (DAS) or dynamic AVF (dAVF) was developed that can regulate the flow on demand. This allows for the flow to be increased temporarily during dialysis and to return to nominal values outside of dialysis with the ultimate goal of increasing life expectancy. Earlier iterations of the dAVF encountered reliability issues due to the formation of fibrous tissue on critical locations of the implant hindering actuation on the anastomosis. For this project, a compliant implantable dAVF-Valve is developed that minimizes the influence of ingrowth and provides a more robust solution.

Following an in-depth systems engineering approach, a detailed problem analysis was performed. Following this, the requirements were set to measure the performance of the design and ensure a suitable solution to the problem definition. At the same time, criteria were generated to score generated concepts.

For concept generation, a morphological approach was used to combine solutions for several subfunctionalities to create three concepts.

A broad range of sub-solutions were found, sorted methodologically and discussed in further detail. The selection of these sub-solutions was guided by a focus-based design resulting in a; robust concept, a compact concept and a concept focused on reduced graft traction. These concepts were developed through various iterations until a comparable level of development was reached. Further investigation on the performance of these concepts to the criteria was noted in a Harris Profile with which a concept design was selected.

This concept was further investigated and optimized in two iterations applying various analytical tools and testing of prototypes. For the final optimization iteration, three different design goals were set due to the unknown influence of the silicone protection, resulting in three different concepts.

These designs were prototyped and tested finding that each performed best in their optimized area. All concepts performed within the set requirements bar the volume requirement. The concept focussed on the largest remaining energy budget within the volume constraints is therefore favourable utilizing 32% of the available work from the actuator. For the other concepts that deliberately exceeded the volume requirement by 10 mm in width, this was 30% for the optimization on minimal stiffness and 29% for the goal of reducing this percentage. Other validations performed included a fatigue test, a simulation of fibrous tissue formation and a traction test. From validation, it can be concluded that the application of a stiff compliant mechanism within a soft protective shell can provide a valuable solution for a dAVF-Valve capable of resisting the ingrowth of fibrous tissue.

Contents

Nomenclature

All abbreviations used in the report are summarized below.

Abbreviations

Abbreviation	Definition
AVF	Arteriovenous Fistula
AVG	Arteriovenous Graft
CAD	Computer Aided Design
CAM	Computer Aided Machining
CKD	Chronic Kidney Disease
CNC	Computer Numerical Control
Co-Cr-Mo	Cobalt Chromium Molybdenum alloy
DAS	Dynamic Arteriovenous System
dAVF	Dynamic Arteriovenous Fistula
DL	Double Layer
DoF	Degree of Freedom
EoM	Equations of Motion
ESKD	End Stage Kidney Disease
FACT	Freedom and Constraint Topology
FBD	Free Body Diagram
FBR	Foreign Body Response
FDA	Food and Drug Administration
FDM	Fused Deposition Manufacturing
FEA	Finite Element Analysis
FFF	Fused Filament Fabrication
GFR	Glomerular Filtration Rate
HD	Hemodialysis
ISO	International Organization for Standardization
LUMC	Leids Universitair Medisch Centrum
MDR	Medical Device Regulation
MIM	Metal Injetion Moulding
MoSCoW	Must, Should, Could, Won't
PD	Peritoneal Dialysis
PEEK	PolyEther Ether Ketone
PLA	PolyLactide Acid
PRBM	Pseudo Rigid Body Model
RRT	Renal Replacement Therapies
SS 316L	Stainless Steel 316L alloy
SE	System Engineering
Ti-6Al-4V	Titanium alloy
TL	Triple Layer
TUDelft	Technische Universiteit Delft
VA	Vascular Access
VALID	Verifiable, Achievable, Logical, Integral and Definitive
W-EDM	Wire Electro Discharge Machining

1 Introduction

In this graduation thesis the design and validation of a compliant valve design for the Dynamic Arteriovenous System will be discussed. In this introductory chapter some medical background will be provided together with a short summation of earlier designs that form the state of the art.

1.1. Medical Background

In 2019 it is estimated that 13.4% of the population worldwide suffered from Chronic Kidney Disease (CKD) which is defined as an ”abnormality in the kidney structure or function” [1]. CKD is mostly caused by high blood pressure or diabetes and results in the renal system filtering less than 60 ml/min in a Glomerular Filtration Rate (GFR) Test. If the kidneys can not filter more than 15 ml/min, End Stage Kidney Disease (ESKD) is diagnosed, this accounts for an estimated 7 million people worldwide. In the Netherlands this number was 18071 with 1844 new cases in 2020 [2]. When ESKD is diagnosed there are three Renal Replacement Therapies (RRT) that can be considered;

- **Renal Transplant:** transplanting a donor kidney, either from a living donor or postmortem, is the most durable and least invasive option. However, due to the availability of donor organs not all RRT patients receive a donor organ, 6261 patients are dependent on dialysis. [2].
- **Peritoneal dialysis (PD):** a way of RRT is to insert dialysis fluid in the peritoneal space and use the vascularized tissue as a filtering membrane [3]. After a few hours the fluid is drained and the process is repeated. This therapy can be done at home, is cheaper and less intrusive for the patient. Compared to Hemodialysis however it is less effective in filtering the blood and thus only used on 16% of prevalent RRT patients.
- **Hemodialysis (HD):** when PD is not an option or effective enough, Hemodialysis is most frequently used with 84% of all prevalent RRT patients. With HD the blood is filtered extracorporeal using a dialysis machine. Although in some occurrences HD is done at home (4%), the majority of cases are performed in a medical environment. HD on average is done in 3 sessions of 4 hours per week [3] and thus has a significant impact on the quality of life. Next to that HD is also the most expensive therapy that is covered by insurance at €80.000 to €120.000 per year.

From literature, it shows that HD is the predominant renal replacement therapy due to its effectiveness. However, next to the negative impact on quality of life and the vast expenses associated with HD, the mortality rate is also high. The risk of heart failure in 12 months is 33% and within 3 years this has increased to 57% [4]. According to Malik, Lomonte, Rotmans, *et al.* the mortality is caused by multiple factors however mainly due to the increased blood flow and Vascular Access (VA) failure.
The blood flow of dialysis patients is increased to speed up the dialysis process. This is done by either an Arteriovenous Fistula (AVF) which creates a direct connection of the high-pressure arteries with the low-pressure veins, as illustrated in figure 1.1b. Thus bypassing the narrow flow restrictive blood vessels in the hand and increasing the flow. Alternative to an AVF, an Arteriovenous Graft (AVG), often a PTFE tube, can be placed between the artery and vein. Both these operations increase the blood flow in the brachial artery to an average of 1000 ml/min with outliers up to 2000 ml/min [5], which is orders of magnitude more than the usual flow rate. This increase in blood flow results in significant

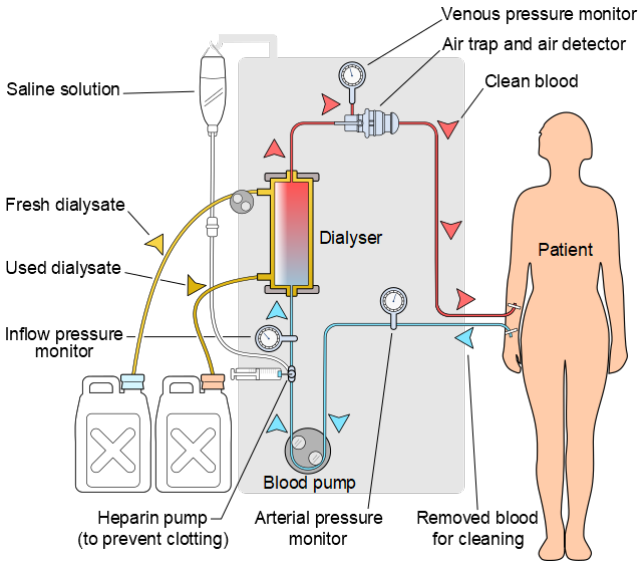

(a) Overview of Hemodialysis. CC3

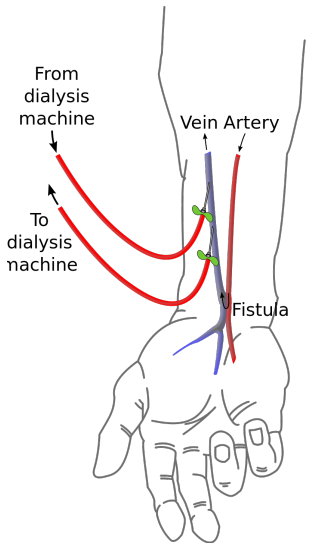

(b) Arterovenious Fistula CC by SA 3.0 - Kbik at English Wikipedia

Figure 1.1: Schematic overviews of Dialysis and AVF placement

growth in the artery and vein diameter, up to 6 mm where prior to the operation this is 2 mm. [5]. This increase in diameter is beneficial for creating the VA in the vein. However, it also introduces increased stresses in the veins. Both the AVF and AVG are linked to a vast amount of complications such as the aforementioned hypertension resulting in problems with vascular wall rigidity [4]. In their research Roy-Chaudhury, Sukhatme, and Cheung state venous stenosis, a blockage in the veins, is identified as one of the risk factors for morbidity. Other identified complications are local swelling of the lymphs, infections, aneurysms (where the diameter of the veins increases due to weakening of the vessels wall), steal syndrome (causing change in flow direction) and thrombosis which can lead to stenosis [7]. These complications are present with either AVF or AVG operations and few effective treatments are known [6].

Due to the complications mentioned above, the Leids Universitair Medisch Centrum (LUMC) and the TUDelft started the research and development on the Dynamic Arteriovenous System (DAS). The approach is to implant a device fitted to a PTFE-coated tube that is capable of opening and closing the blood flow as required. Only opening the anastomosis, the connection between artery and vein, when the patient is to be dialysed. When not connected to the dialyser the anastomosis will be closed and the blood flow will be directed as is nominal. This is expected to reduce the negative effects currently present in HD and thus reducing cost and increasing patient welfare.

1.2. State of the Art

The first dAVF prototype was constructed at the LUMC and is show in figure 1.2. This very first prototype device consisted of a metal valve that uses pin-hinges for joints to close the graft. On the other end an actuator is connected through a cable, this actuator relies on a servomotor for actuation. This device was tested ex-vivo and in-vivo in a goat study and mainly proved the concept of a dAVF. During testing with a modified version the tension on the graft caused the sutures to fail which lead to internal bleeding [8].

The next redesign had the objective of reducing the size of the device as well as the mitigation risks by increasing durability of the parts and improving the overall in-vivo safety. The design that followed the first prototype was developed at the TUDelft and again consisted of two subsystems, an actuator [9] and a valve [8].

The actuator was designed by Kroft and is shown in figure 1.3a. The implantable part of the design consists of a wheel of magnets that can rotate around a central axis once activate by an external ring of magnets. Connected to the internal set of magnets is a magnetic backplate in which a spiral is machined. A follower pin follows the spiral and is connected to a bowdencable which is to be connected

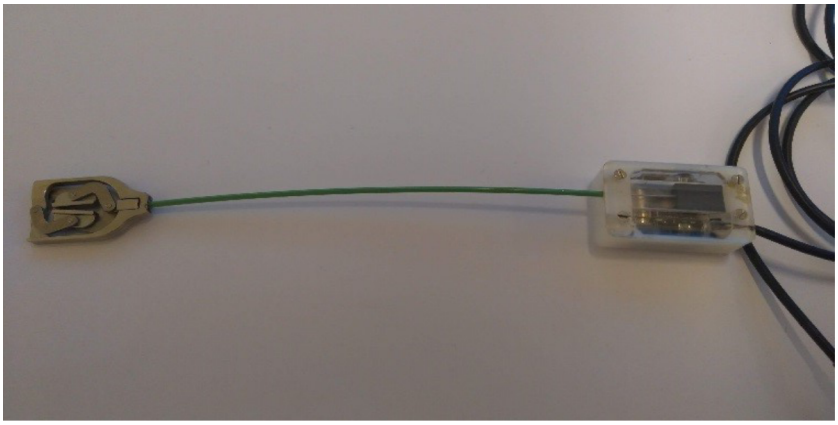

Figure 1.2: dAVF protype constructed at the LUMC

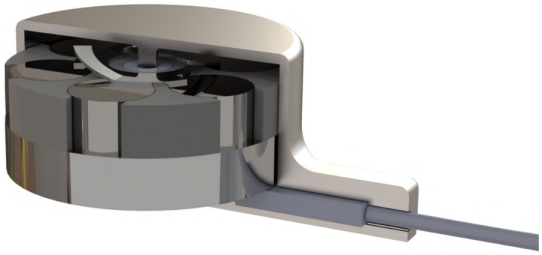

(a) A render of the dAVF actuator developed by Kroft [9]

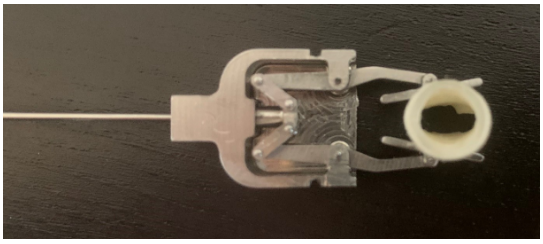

(b) A prototype of a dAVF Valve developed by N. White [8]

Figure 1.3: State of the Art for a dAVF system consisting of both an actuator and a valve.

to the valve. The result is that once the wheel is rotated, this motion is translated to an axial movement. Within the discussion it is mentioned that aspects such as the optimal transmission system to the valve, pushing and pulling tests, bending angels and fixation methods are open for further development [9]. After these two research some smaller projects were undertaken of which the first one was a redesign of the valve in a compliant manner. The results of which can be seen in figure 1.4a which achieved a reduction in size and the number of parts [10]. Although more simple in design this method does lose the favourable transmission ratio present in the dAVF design shown in figure 1.3b. In another project a monitoring system was conceptualized of which the results can be seen in figure 1.4b. The proposal is to attach two magnets to the dAVF-Valve that can be can be used to monitor its position by using three sensors outside of the body [11].
Finally a new, more optimized, version of the actuator was developed. Based on the magnetic working

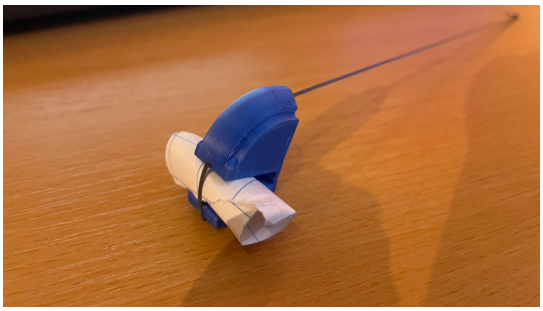

(a) A 3D printed model of a compliant dAVF developed by Hart [10]

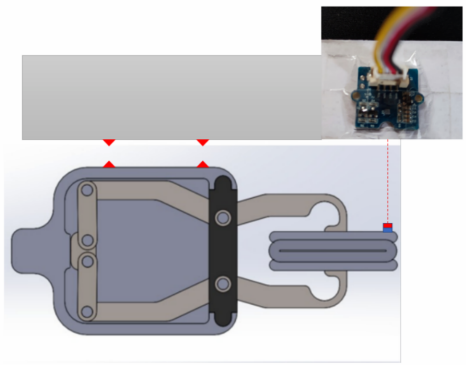

(b) The concept for a monitoring system for a dAVF developed by Wu [11]

Figure 1.4: State of the Art of additional dAVF research done at the TUDelft.

principle but with, most notably, an optimized magnetic array and a reduced overall volume as can be seen in figure 1.5a

(a) An exploded view of the updated DAS-Actuator with the magnet-array and spiral groove visible.
Source:White, Kroft, Bogt, *et al.*[12].

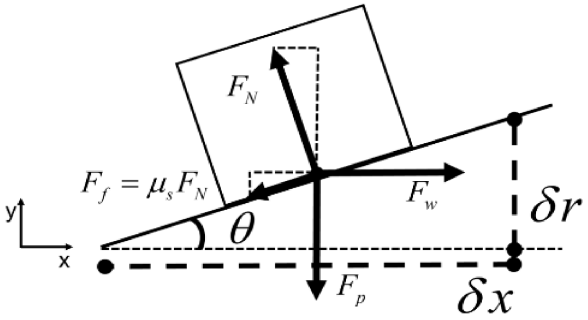

(b) An FBD of the forces acting upon the follower pin during actuation.
Source:White, Kroft, Bogt, *et al.*[12].

Figure 1.5: Version 2 of the dAVF-Actuator.

In figure 1.5b a Free Body Diagram (FBD) is given for the follower pin in the spiral groove where θ is the angle of its pitch. In the following equations the forces from this FBD are decomposed over X and Y and substituted for the normal force , F_N, to find the relation between the force induced by the input torque, F_w, and the outputted force exerted on the bowden cable, F_p.

$$\Sigma F_x \rightarrow^{+} = F_w - cos(\theta)\mu F_N - sin(\theta)F_N = 0 \tag{1.1a}$$

$$\Sigma F_y \uparrow^{+} = cos(\theta)F_N - sin(\theta)\mu F_N - F_P = 0 \tag{1.1b}$$

$$F_p = F_w \frac{cos(\theta) - \mu sin(\theta)}{sin(\theta) + \mu cos(\theta)} \tag{1.1c}$$

However, as F_w is defined by input torque over the radius on the spiral (which is a variable), it will increase over rotation of the spiral due to the radial decrease. Due to the spiral drive, the dAVF-Actuator inherently has a form of stability due to the mechanism being non-backdrivable when no torque is inputted in to the system. With no input torque from the magnet array, F_w becomes zero and the friction force will flip direction in figure 1.5b. Taking the X-components of the forces this gives;

$$\Sigma F_x \rightarrow^{+} = F_N(cos(\theta)\mu - sin(\theta)) = 0 \tag{1.2}$$

To satisfy this stability, $\theta < tan^{-1}(\mu)$ has to be satisfied. For $\mu = 0.25$ this results in a angle of $\theta = 14°$ [12].
Changing the dimensions of the spiral can alter the actuators force-displacement curve. However, as discussed in further detail in section 3.1.1 on design boundaries, the current configuration of the actuator will be used.

2

System Engineering

For any complex project it can be worthwhile to follow the approach of System Engineering (SE). SE is a robust approach to the design, creation, and operation of systems [13]. For this project the dAVF is considered as the system consisting of two subsystems; the actuator and the valve as identified in section 1.2. This project has a focus on the design of the valve subsystem, however the entire system is to be considered for the system engineering aspect due to the influence of the actuator on the overall desired function of the dAVF.

The goal of this chapter is set design requirements and criteria to which the design can be verified and validated to in chapter 5. In order to set these a deeper understanding of the problem is required. As a guideline to develop this understanding the following list of questions will be answered [14];

1. **Who** is involved by the problem? *This will be answered by a stakeholder identification in section 2.1 where all stakeholders involved in this project are to be identified.*
2. **What** is the problem? *The overall problem has been discussed in chapter 1 where a medical need for a dAVF solution is discussed. This will be included in to problem statement.*
3. **Where** is the problem located? *Within section 2.3 an analysis will be provided on the implant location that will provide insight in (among others) implant shape and size.*
4. **When** does the problem occur. *This question will be answered in section 2.2 with a discussion of the effects the body has on the implant and vice versa.*
5. **Why** does the problem need solving? *For this a problem definition based on knowledge from the state of the art is given in section 2.5.*

2.1. Stakeholders

In order to answer the 'Who'-question, a stakeholder analysis is performed to gain a deeper understanding of all of the parties involved. According to the System Engineering Handbook; a stakeholder can be defined as a group or individual that is affected by or has a stake in the product or project [13]. By identifying all parties involved the expectations and limitations can be exposed that will aid in the formulation of requirements the dAVF should fulfil. Below an overview will be given on the stakeholders involved in this project. Prior to that it is of importance to identify the types of stake holders and to investigate the life cycle of the dAVF-valve.

Within the listed stakeholders a differentiation is made between stakeholders based on their involvement with the systems within its lifecycle. With primary parties being most involved in the designing of the system or directly influenced by it. Secondary parties are not actively involved with the development but can still influence the design (e.g. patent offices or regulatory entities). Tertiary parties are even more distanced from the project and are often more involved with the societal impact. Even though the secondary and tertiary parties might not be involved within the time frame of this thesis project, including them in the formulation of requirements will generate a feasible design for application in a

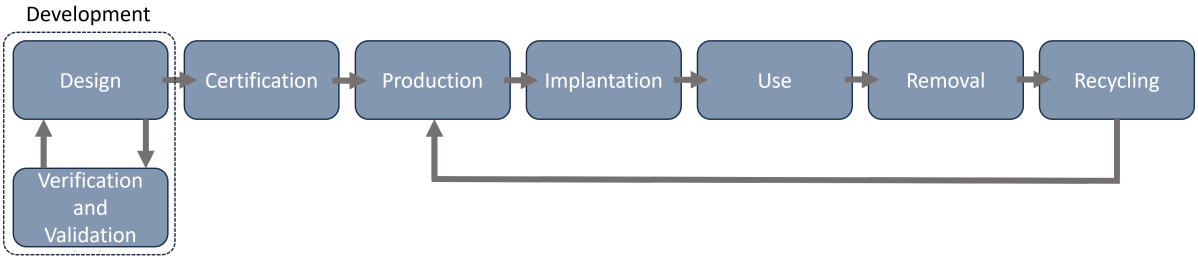

Figure 2.1: The life cycle for the dAVF. It should be noted that this diagram is not to be confused with a planning for this thesis project. It is to be used a tool to identify stakeholders and requirements for all relevant phases of the device.

medical environment.

A list of all identified stakeholder is given below. For each stakeholder a short description is given of their goals together with a list of targets (what the stakeholder expects this study to result in) and their main phases of involvement from figure 2.1. These statements are gathered by speaking with the relevant stakeholders or research on previous literature.

1. **TUDelft Biomedical group** *(primary stakeholder)* A research group within the TUDelft with the goal to develop, design and refine medical devices. By cooperating with healthcare professionals to identify medical problems and provide a solution.
   Targets: Generation of knowledge, patentability, development cost
   Main phases of involvement: development, certification, production and recycling
2. **LUMC Nephrology group** *(primary stakeholder)*A group within the LUMC focussed on the diagnostics and treatment of renal diseases with a special focus on dialysis.
   Targets: Increase quality and duration of life for patients, generation of knowledge and patents
   Main phases of involvement: development, certification, implantation, use and removal
3. **Surgeons** *(primary stakeholder)* The vascular surgeon at the hospital will be responsible for the placement of the dAVF implant as well as any maintenance required on the Vascular Access or the removal of the implant.
   Targets: Low risk, ease of implantation and maintainability
   Main phases of involvement: implantation, use and removal
4. **Dialysis staff** *(primary stakeholder)* The doctors and nurses staff the dialysis department of the hospital, their focus is on treating the patients. They will interact with the dAVF in order to regulate the blood flow rate prior to starting the dialysis process.
   Targets: Reliability, ease of use and feedback
   Main phases of involvement: Use
5. **ESKD-Patient** *(primary stakeholder)* The patient will receive the dAVF-implant in order to prolong their life expectancy as well as increase their quality of life. The mean age of haemodialysis patients in the Netherlands is 67 year, 60% is male and 51% is of a lower socioeconomic status. Current survival rates are 83% for one year and only 53% survive three years [2], the dAVF should increase this.
   Targets: life expectancy, quality of life, risk of side effects and cost of treatment
   Main phases of involvement: Implantation and use
6. **Production Partner** *(secondary stakeholder)* the first batches of implant production will likely be done by design and prototyping LUMC. A production partner with experience in the manufacturing of invivo devices is critical for the safety and success of the device.
   Targets: Manufacturability, supply chains and medical safety
   Main phases of involvement: Production
7. **Health insurances** *(secondary stakeholder)* Currently haemodialysis is the most expensive treatment covered by health insurance, about 80.000 to 120.000 euros per year per patient [15]. The costs of the implant and the procedure will likely be paid by the insurances, with the benefit of a reduction in risk of VA failure.
   Targets: Cost of treatment, implant cost, outcomes
   Main phases of involvement: development

8. **Medical Device Regulation (MDR)** *(secondary stakeholder)* The MDR is the European equivalent of the American FDA, a regulatory body that manage the regulation of medical devices. The MDR has a strong focus on clinical evidence required to demonstrate the safety and performance of a medical device.
   Targets: Medical properties, robustness, safety and contamination risk or other adverse effects
   Main phases of involvement: Certification
9. **Notified Body** *(secondary stakeholder)* Where the MDR is the legislator, a Notified Body is appointed per country to verify the device to legislations. In the Netherlands these are KIWA, DEKRA or BSI which can determine if a medical device and documentation adheres to the law, can do audits (announced or unannounced)
   Targets: Medical properties, robustness, safety and contamination risk or other adverse effects
   Main phases of involvement: Certification
10. **Ministry of Health, Welfare and Sport** *tertiary stakeholder* The government aids a fit and healthy nation. It is the ministry that shapes legislation and controls the budget of the health-sector in the country. **Targets:** Quality, affordable and accessible care for all in the Netherlands.
    Main phases of involvement: Legislation, investment and deployment.
11. **Kidney Foundation** *tertiary stakeholder* This foundation (in Dutch de Nierstichting) is a charity that focusses on prevention, improvement and eventually a cure of kidney disease.
    Targets: stimulating research in prevention, detection, transplantation, dialysis treatment and overall quality of life for ESKD-patients.
    Main Phases of involvement: investment and deployment

2.2. Functional Description

In chapter 1 the introduction and function of a dAVF-valve is given, this section will further elaborate on the expected functioning of the valve and the biological systems that have to be taken into account for the design of such an implant. Based on these functions the requirements in section 2.7 can be formulated.

Flow control

As discussed earlier within chapter 1, ESKD patients that require dialysis often undergo either a AVF or AVG operation where a connection (anastomosis) is created between the artery and vein. This results in an increased bloodflow as the flowresistance in the capillaries is bypassed. Not only does this lead to a reduced dialysis time, the increase in flow will over time cause a larger vein diameter (around 6mm) that will ease access to the dialysis machine. Once this increase in diameter and flow is stable the access can be used and is referred to as matured [16]. Within the concept of the Dynamic Arteriovenous System, a valve is placed over the anastomosis, as illustrated in section 2.2, that is capable of opening and closing the anastomosis on demand. During dialysis sessions the valve is actuated by a healthcare professional, either a doctor or a nurse, and set to the open position. For a successful dialysis session a blood flow rate of at least 250 ml/min is advised by Chang, Kim, Kim, *et al.* as their study showed increased mortality rates for lower flow rates [17]. A general consensus indicates a flow of 600 - 1000 ml/min is considered as acceptable for dialysis [16], [18]. After either a AVF or AVG operation, patients are reported to have an average blood flow through the dialysis machine of 964 $\pm$ 520 ml/min [19]. This increase in flow leads to a faster filtration rate and thus a shorter treatment time. After completion of the dialysis session, the valve is actuated to its closed state where there will be no flow through the valve and the arterial flow should return to its nominal value. In order to redirect the flow its original path the valve will have to withstand the pressure difference between the artery and vein. The maximal arteriovenous pressure is found the be at 180 mmHG in the systolic (beating phase of the heart) phase [20]. On the other side the pressure within the veins is reported to be around 10mmHG [21]. This results in a maximal pressure difference of 170mmHG. In the current state of medical research it is assumed that a complete closure of the graft is required (i.e. a flow through the anastomosis of 0 ml/min). Due to the novelty of a dAVF, the medical effects caused by partial closure are unknown. Further research would have to be performed to determine the feasibility of partially closing the anastomosis to find weither an acceptable flowrate can be created. Research into this falls outside of the reasonable scope of the design of a compliant dAVF. Hence the safe assumption is that a full closure of the dAVF-valve a must.

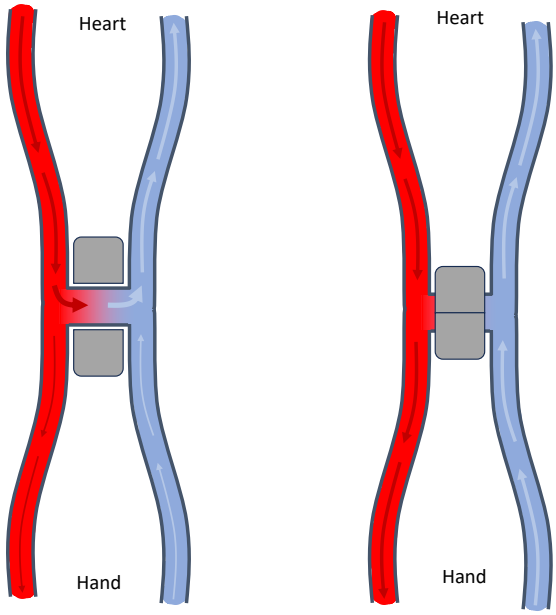

Figure 2.2: Illustration of the redirection of the bloodflow with the dAVF-Valve in open (left) and closed (right) state.

Thrombus formation
After closure of the valve the blood should flow past the graft entrance and through the vascular system in the arm and hand. There is however an increased risk of thrombus formation around the graft inlet and outlet due to the altered geometry. These volumes on both the venous as the arteriovenous side are to be minimized as these can result in zones with stagnant flow can occur. For the same reason it is of great importance that the graft is completely closed. If the graft is not completely closed and compressed to force all blood out, this can also lead to stenosis follow by thrombus formation. An example of this thrombus formation around a AVG is given in figure 2.3. Quencer and Oklu report on an increase of risk for thrombosis formation, for AVG-patients this resulted in an average thrombosis formation 0.5 to 2 times per year, for AVF-patients this number was estimated at 0.1 to 0.5 times per year. Thrombosis is reported to cause 65% to 85% of vascular access losses [22]. The dAVF utilizes a similar type of tube as a graft and can face the same issues. However, it should be noted that for AVGs usually a considerably longer graft is used as compared to the graft length used for the dAVF. Quencer and Oklu reason that the increased occurrences of thrombus formation in AVGs is the lack of endothelium, a single cell film on the inside of the vascular system that acts as an interface between the bloodstream and the blood vessel and prevents clotting. An increased risk for thrombosis for AVG is reported at a flow measured at the VA of less than 500 ml/min [22]. A more specific number could not be found, likely due to patient variety. As discussed earlier, in section 2.2, the question remains whether a complete closure is required or if a partial opening could aid the flush of any thrombus formation. Additional medical research on this topic is required. For the purpose of this further research it would be desirable for dAVF-valve to allow for multiple stages of opening. Zilberman-Rudenko, Sylman, Lakshmanan, *et al.* state that thrombus formation has been associated with junctions and bifurcations in the vascular system. For the dAVF this would be near the anastomosis at the closed state (but could occur during the open state as well) in section 2.2. The flow at these points is hard to predict but can often result in flow separation and locally stagnant flow. It is at these stagnation points that thrombus formation is likely to occur [23]. It is vital for patient wellness that the risk of thrombosis is mitigated by the design as these can lead to missed dialysis sessions, admission to a hospital or the patient needing a temporary catheter for dialysis access [22].

2.3. Implant Location

For the 'where'-question most information can be attained from dialysis procedures with both an AVF or AVG. Additional research on the ideal location for a dynamic arteriovenous system has been performed

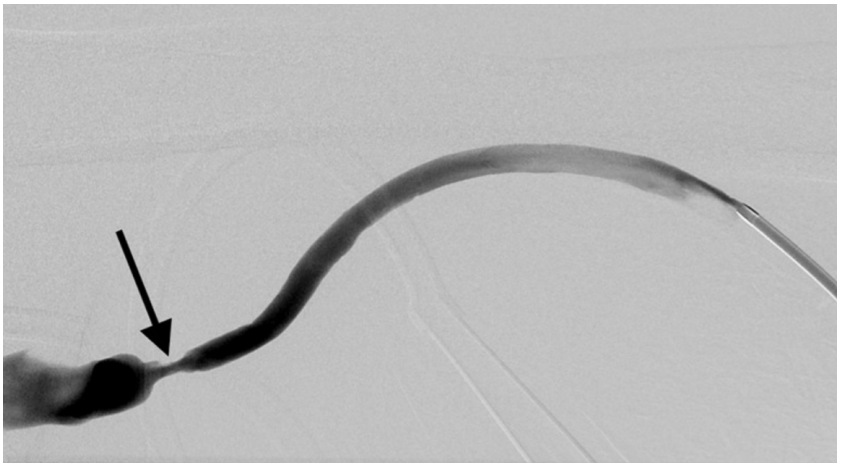

Figure 2.3: Thrombosis formation in a AVG leading to stenosis, narrowing of the graft, indicated by the arrow. Source: Quencer and Oklu [22]

in earlier research [8] which will be discussed in this section. The dAVF is to be implanted around the anastomosis which is near the Vascular Access (VA). An example of a VA is given in figure 1.1b. For a connection to the dialysis machine the VA is often located in the lower (distal) arm with some exceptions where the upper (proximal) arm is used. The location of the VA is dependent on the available flow. With a large blood flow rate comes an increase on the stress and thus wear on the vascular system, to mitigate this the VA is place as distal as can be. For cases where a distal VA results in too little flow, a more proximal location can be considered. In the case of the dAVF, the flow can be regulated so this isn't issue is not relevant. What does matter is the available space for the implant, in this case a proximal location is preferable as due to a large volume to work with and less movement in the arm. Often the non-dominant arm of the patient is used for VA due to the fragility and the loss of strength. The majority of dAVF-implants will thus be located in the upper left arm; ideally the design can be used in either location. In a previous study a dimensional analysis on a dAVF has been performed which resulted in a rectangular maximum set of dimensions [8].

2.4. Foreign Body Response

For a better understanding of when and how previous iterations of the dAVF have been influenced by tissue formation in critical components, the concept of Foreign Body Response is discussed in this section.

Foreign Body Response (FBR) is when the body responds to a foreign material by encapsulating the object with a fibrous tissue. The choice of material is the main impactor on this response, a more in-depth study into biocompatible materials was done as a literature study prior to this thesis [24]. All materials will have some tissue formation due to FBR and this has to be taken into account whilst designing the dAVF-valve. Previous iterations had the formed tissue decrease efficiency up to a point where the implant was no longer functioning as expected. Whilst tissue formation can cause harm to the intricate workings of the implant, the encapsulation can also be used to fixate the outer surface of the implant within the body. Whilst there are methods to simulate FBR [25], the common verification methods still rely on in-vivo testing [8].

2.5. Problem Definition

Condensing all of the topics discussed above, a problem definition can be written. Within section 2.1 a multitude of stakeholders involved with this project where identified. For each a problem statement or project objective could be formulated. The perspective of the research group of which this project is a part of was taken with the challenges faced at the time of writing for which a new iteration dAVF-valve will be developed. The problem definition for this graduation project is formulated below;

The TUDelft and LUMC research group have found that fibrous tissue forms on critical parts of a valve for the dynamic arteriovenous system placed between the proximal artery and vein after long term implantation of the device. The fibrous tissue formed around the pin-hinges and other moving components highly influenced both performance and reliability of the valve. Prevention of tissue formation that forms an obstruction in the valve-mechanism is needed to guarantee long term functioning of the valve and a prolongation in life expectancy of those suffering from ESKD.

2.6. Project Objective

Building upon the problem definition, the project objective presents a statement on why further development on the dAVF is needed and what is to be done to achieve this.

To reduce the adverse effects of fibrous tissue formation on performance and durability of the dAVF valve, a compliant valve is to be designed and tested that performs similarly to previous designs in reducing the negative effects of an AVF treatment but is more resistant against tissue formation.

2.7. Requirements

By formulating the requirements the needs and expectations of the stakeholders are translated to problem definitions. These are in turn to be written as technical requirements that are measurable and verifiable.
The requirements that are to be satisfied during the design of the compliant dAVF valve will be listed below. Each requirement will have a prioritization and relevant Stakeholder attached to it. Since all requirements are to be validated during the project the validation method is also listed. An important note to make is that these requirements cover the important factors to be considered in the design, additional requirements further in the life cycle of the project are omitted. One example topic would be that of shipping requirements.
The two important factors considered here are the completeness of the requirements which is achieved with the VALID-guidelines as elaborated below. Another important aspect to recognize is that not all requirements are equal in prioritization. To make a clear indication of the importance for each requirement the MoSCoW model of prioritization is followed [26].

- **Must** indicates that the requirement is the be satisfied in order for the project to be considered a success. If one of the must requirements is failed during verification, this has to be fixed before the development can be concluded.
- **Should** labelled requirements indicate a high priority that should be completable within the set planning. In case it is not met, other solutions or workarounds are available.
- **Could** requirements are considered to be desirable and could be included if time, money or other resources allow.
- **Won't** requirements are aspects of the project that are to be excluded in this version. In later versions these might increase in priority in order to be added to the system.

The requirements set for the development of the compliant dAVF follow the VALID-guidelines;

- **Verifiable:** the objective should be verifiable through measurements to assure if the requirement is met. For this project all technical requirements are given a quantitative value, for the medical requirements this was not always achievable, more on this in the section below. Also where applicable a proposed verification method is given.
- **Achievable:** in other words, the requirement has to be realistic. Although some requirements can be challenging there is no use for designing for the unachievable.
- **Logical:** the requirement should make sense thus wherever possible a citation is given for any claims. Also the reasoning for each requirement is given.
- **Integral:** the requirement is to be complete so there should be no situations or states that are not encompassed by the requirement.
- **Definitive:** lastly the requirements should be clear and unambiguous so no other interpretations are possible.

The requirements set during this phase are subject to change as the technical design of an implant is an iterative process. Throughout the development cycle it might be changed for reasons such as; new insights from the medical experts, adaptation of requirements that are later found the be unachievable of irrelevant or perhaps a more suitable verification method is found during testing. All changes or other notes on these requirements will be discussed in chapter 6.

Specific values are given to a requirement as often as possible as this is crucial for verification of the prototypes at the final stages of this project. There are however some requirements, mainly in the medical domain that are hard to quantify such as the implantability of the device by a surgeon. The is a connection for that can be made between this requirement and the dimensional requirement, however other design aspects might influence the difficulty of implant placement as well.

Another important note to make is that of safety factors, which is an often discussed aspect within the realm of engineering. In this overview the numbers given are without a multiplication of a safety factor. The reasoning for this is that these safety factors can be applied during different stages of the development. For example; there will be an uncertainty of the blood pressure which the dAVF-valve will have to be able to resist, some patients will have a higher bloodpressure than others. For this one might apply a safety factor stating that the device will have to withstand double that pressure. In this case the safety factor would be applied at the input of the design. Another option would be to apply this safety factor at the output of the design. If it is assumed that there will be some flexure that will apply a force to resist that pressure, it can be opted to apply the safety factor over the dimensions of said flexure. One reason for this might be to account for manufacturing inaccuracies. As the height dimension of a flexure will impact the stiffness by a power 3rd. So a safety factor of 2 will have a 8 times larger stiffness per flexure. For two opposing flexures this can result in an eight times difference than if the safety factor of two was applied on the input. In the end both inaccuracies, in bloodpressure as well as manufacturing tolerances, will have to be accounted for. However, as stated, above where the safety factor applies will impact a design. Safety factors will be discussed during dimensioning in later in the design process.

Technical Requirements

1.1 Size: regardless of the shape of the implant, the device **must** be bound by a boxshaped volume with the size of 30mm by 15mm by 10mm. These measurements are extracted from an earlier cadaver study [8]. The orientation of this box is fixed with the greatest dimension running in parallel in respect to the arm. It is assumed that exceeding this requirement will decrease patient comfort as it can limit mobility of the arm and can feel uncomfortable.
Stakeholders: Biomedical group, Nephrology group, Surgeon, Patient, MDR
Verification method: During the design of the implant a boundary box will be made to ensure the device remains within the defined volume. Once the prototype is produced it is to be measured using callipers to validate the size.
Reasoning: there a multitude of variables that makes it difficult to put an exact number to the volume claim; each person will have a slightly different anatomy, the human body is not rigid but flexible and will adapt around the implant and finally; not much research was found on implants in the proximal arm. In a conversation with a vascular surgeon it was confirmed that the most viable method to evaluate the volume requirement is by experimentation. An example of such is the cadaver study done in an earlier study on the dAVF-valve [8]. It is however not a given that the design of the valve will be bounded by a box, it might assume other forms such as a disk or a cylinder. To gain a better insight in these volumes claim a dimensional state of the art overview is given in table 2.1.

1.2 Mass: compared to other implants it is estimated that the mass **must** be less than 50 grams. Based on earlier design iterations of a dAVF-valve the mass **should** be less than 20 grams to be competitive with other designs.
Stakeholders: Biomedical group, Nephrology group, Surgeon, Patient, MDR
Verification method: During the design a weight sensor feature is to be used in the CAD environment. After production the prototype is to be weighed on a scale to validate the mass.
Reasoning: It is estimated that the volume requirement will be leading the mass requirement, however both are to be met in the final results. The values for the mass are taken

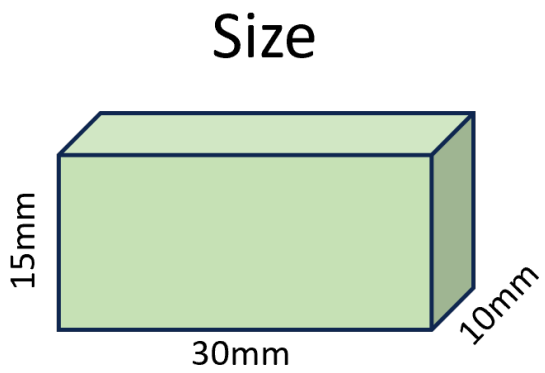

Figure 2.4: Visualization of the Volume requirement .

from other devices that could be worn on the arm. The 20 grams requirement originates from a desire to produce a design with a lower weight compared to the previous prototype. Like the volumetric dimensions it non-trivial to find suitable values. The human upper arm has a mass of 2633 grams for an average male adult [30], for a valve mass of 50 grams the implantation of such a valve would increase the total mass with 1.9%, for the desired 20 grams this is only 0.8%.

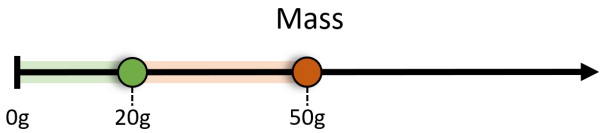

Figure 2.5: Visualization of the mass requirement with the 'must' in red and the 'should' in green.

1.3 Bloodflow in open state: for the haemodialysis to be successful a bloodflow through the anastomosis **must** be at least 600ml/min, for an AVF this results in a vein diameter of 6mm [16]. If this requirement is not met, the treatment time will increase which results in an increase in treatment cost. A lower flow can also lead to a decreased vein diameter after maturation which can complicate vascular access to the dialysis-machine.
Stakeholders: Biomedical group, Nephrology group
Verification method: this can be simulated using CFD software, validated in a mock-flow test setup utilizing a flowmeter and during in-vivo animal studies using an echo.
Reasoning: for a functional dAVF, it is of vital importance that when the anastomosis is opened, a suitable blood flow can be achieved for dialysis.

1.4 Pressure resistance in a closed state: in the closed state the valve **must** block all flow such that the flow is equal to 0 ml/min at the pressure difference of 170mmHG as found in section 2.2. This will allow the flow to return to its normal path trough the arms vascular system.
Stakeholders: Biomedical group, Nephrology group
Verification method: this can be validated in a mock-flow test setup utilizing a manometer and during in-vivo animal studies using an echo.

Table 2.1: Overview of dimensions of comparable implantable devices.

Implant type	Shape	Dimensions	Source
dAVF-Valve LUMC	Box	30mm x 15mm x 10mm	NA
dAVF-Valve Nick White	Box	30mm x 15mm x 10mm	[8]
dAVF-actuator	Cylinder	35mm x 25mm	[9]
Contraceptive Implant	Rod	2mm x 40mm	[27], [28]
PowerPort Vascular Implant	Disk	22mm x 38mm	[29]

Reasoning: upon closure of the graft, a pressure difference between the artery and the venous side will build up. For a flow of 0ml/min this pressure difference is to be held for a continued time. A correct closure is also important for mitigating thrombus formation, any blood left in the graft will increase the risk of stenosis.

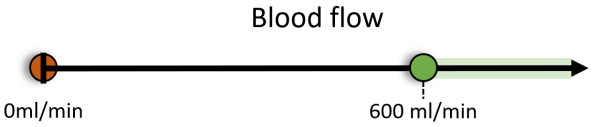

Figure 2.6: Visualization of the blood flow requirements with the closed state in red and the open state in green.

1.5 Compatibility with dAVF-actuator: the dAVF-valve **must** be compatible with the magnetic actuator designed by Kroft of which the output is given in figure 2.7 [9]. Finding the area under this graph gives the work that can be provide by the actuator which is 0.12 Joule.
Stakeholders: Biomedical group, Nephrology group, Dialysis staff
Verification method: By attaching a load cell to the valve mounted to a pressurized graft the force required to actuate the valve can be found.
Reasoning: the forces shown in figure 2.7 are found by an optimization script [9]. Ideally the valve will be designed to utilized this curve. However, a larger force output can be realized at the cost of a decrease in displacement or vice versa (all will have to be within limits of the design of the actuator). Some adjustments might be feasible however, this will result in a less than ideal design for the actuator and as such, a lower Work output.

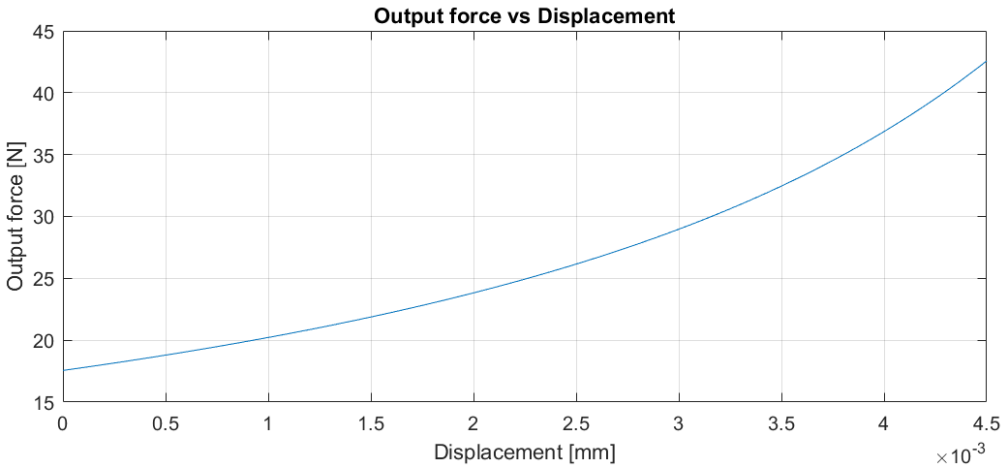

Figure 2.7: Graph of the force output of the magnetic dAVF-actuator over the displacement of its end effector. This graph results from an optimization code written by N. White on the work of Kroft [9].

1.6 Traction on the anastomosis: closing and opening the dAVF-valve system **must** not lead to rupture in the sutures. In previous work on the state of the art, this was coupled to a maximum traction force of 0.76N [8]. This number is based on a paper written by Rodrigues, Horeman, Dankelman, *et al.* where it was found that the first signs of tissue damage by tension on the sutures show at 4.55N for a vena cava and 8.94N for an aorta at 95% CI in a porcine model [31]. To find an equivalent tearout value for the dAVF, this number was scaled linearly to the wall thickness of the veins [8]. Based on performance of the earlier state of the art concept, the compliant dAVF **could** exert no more than 0.19N of tractive force on the anastomosis. Both of these tractive force are measured parallel to the vein and artery.
Stakeholders: Biomedical group, Nephrology group, Surgeon
Verification method: ideally this requirement is to be validated in an animal study. Alternatively a load cell can be placed between the dAVF-valve and the fixed world to validate the force.
Reasoning: due to the limited availability of knowledge on tissue rupture or other ways of harming the body, there is a great uncertainty in appointing a value to the force at which

harm occurs. The data that is available is not tested on human tissue and in the paper by Rodrigues, Horeman, Dankelman, *et al.* the uncertainty of the measurements (specifically determination of first signs of damage) is great [31]. The values found do at least point to a range in where damage to the human tissue can occur but due to the different subject species, different part in the vascular thickness and the uncertainty in the measurements. Considering all of this it would be best practice to apply a considerable safety factor and validate this requirement in animal studies that will follow later on in the development progress.

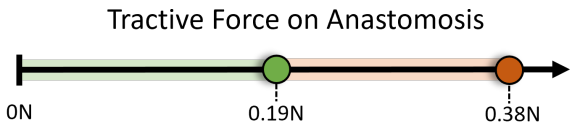

Figure 2.8: Visualization of the resultant force requirement with the 'must' in red and the 'should' in green.

1.7 Life cycle time: the dAVF-valve **must** last 836 cycles, equalling 4 years of use. The valve **should** last 2080 cycles, equalling 10 years of use. A cycle is defined as opening and closing the valve.
Stakeholders: Biomedical group, Nephrology group
Verification method: A mockflow test setup can be created where the valve is actuated with a linear stage and the pressure or flow is monitored. It is estimated that to verify 2080 cycles, assuming a cycle time of 10 seconds, will take slightly less than 6 hours of continuous testing.
Reasoning: In order to be a significant improvement the dAVF-Valve must last for at least a similar duration as the state of the art concept. Thus, like the earlier iteration, the compliant dAVF must last 836 cycles. This is equal to four years of use, which is double the average primary patency (the time between start of haemodialysis and the first required intervention on the AVF) [22].) of an AVF treatment [8]. At best an AVF treatment lasts for 10 years [22]. For the dAVF to equal this, the expected life cycle time should be equal to 2080 cycles.

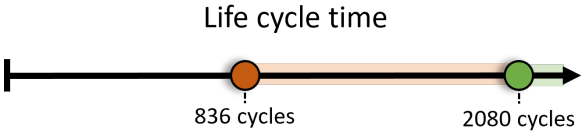

Figure 2.9: Visualization of the life cycle requirements with the 'must' value in red and the 'should' value in green.

1.8 Fail safety: when the device does malfunction it **should** return to a failsafe state where the valve is in the fully open position.
Stakeholders: Biomedical group, Nephrology group
Verification method: a study on failure modes can be done on a mockflow test setup where for every failure mode the reaction of the valve is tested.
Reasoning: Although the device is designed to last for a long time, it should be assumed that malfunctions can always occur. It is vital for the patient that when this happens, the valve returns to a safe state. This state is considered to be the open position as this will lead to a state where the patients blood can still be dialysed. In the case of a failure leading to the closed position this is no longer the case.

1.9 Multiple stages: the valve **should** have three distinct stages of opening or more with minimal force required from the actuator. The valve **could** be stable at all these positions meaning no force is to be applied. A continuous range of opening is considered as infinite stages.
Stakeholders: Biomedical group, Nephrology group, Dialysis staff
Verification method: A setup similar to the input force test can be utilized where a loadcell is attached to the input of the valve and a pressurized PTFE-tube is compressed.
Reasoning: Dialysis patients are reported to have varying flowrate through the anastomosis after their AVF or AVG surgery [19]. It can be desirable to have finer control over the surface

area in the anastomosis and thus the bloodflow rate in the open state of the valve. Ideally this would be a contineous process with infinite steps, another option would be to have multiple stable positions. The minimal amount of these stages would be three.

1.10 Control of opening: the opening and closing of the valve **could** be controlled so the valve opens gradually in a time span of 10 seconds.
Stakeholders: Biomedical group, Nephrology group, Dialysis staff
Verification method: A similar setup as described in the multiple stages test setup where the time of opening and closing is measured.
Reasoning: By having a controlled redirection of flow rather than a sudden change, the stress on the vascular system should be less. If requirement 1.8 is realized by a continuous range of opening this requirement is also satisfied.

Medical Requirements

2.1 Resistance to Fibrous Tissue Encapsulation: the required input force for opening and closing the dAVF-valve after encapsulation by fibrous tissue **must** not exceed the maximum force of 42.5 N that the actuator can provide to the input of the valve at the end of its displacement (as seen in figure 2.7). Ideally the input force after encapsulation **should** not exceed 20% of the original required opening force prior to implantation and encapsulation by fibrous tissue.
Stakeholders: Biomedical group, Neprhology group, surgeons, dialysis staff
Verification method: this can be verified by animal studies after invivo testing for several months. Alternatively the mechanism can be encapsulated by a synthetic material with similar material properties as fibrous tissue.
Reasoning: As discussed in section 2.4 the formation of fibrous tissue around the valve mechanism proved to hinder the functionality of the valve after maturation. The input force was chosen as a metric as this a measurable quantity and directly impact the use of the device.

2.2 Biocompatible material: the materials to be used for the construction of the valve **must** be used in other implantable devices prior to this study.
Stakeholders: Biomedical group, Nephrology group, MDR, Production Partner
Verification method: for within the time frame of this project the biocompatibility of the materials is best assessed by available datasheets or other studies on the biocompatibility of materials.
Reasoning: this study does not aim to prove the effects of materials on the body. To ensure safe implantation, all materials to be used for the dAVF-valve have to be used in other implants before. Prior to this project a literature review was performed listing all biocompatible materials and production processes that can be applied for the creation of a compliant dAVF [24].

2.3 Resistance of Tissue ingrowth: the ingrowth of tissue in the valve mechanism **must** not affect the dAVF valve to ensure that the valve functions as intended for a duration of 4 years. This **could** be extend to a total of 10 years.
Stakeholders: Biomedical group, Nephrology group
Verification method: in early development testing the device can be tested for water tightness. A full verification can be done with the final device in either a simulated environment or with an animal study.
Reasoning: the ingrowth of tissue has shown to limit the function of earlier prototypes of valves by blocking the mechanism or the bowden cable used as an interface between valve and actuator. As with biocompatibility it is impossible to test the device over the selected time span as the process of tissue ingrowth can not be sped up. However, through the means of shorter invivo test or even tests on water tightness a few conclusions can be made on whether this requirement is satisfied.

2.4 Tissue Anchoring: the dAVF-valve **could** utilize tissue ingrowth in order to fixate itself to the other tissue in the arm.
Stakeholders: Biomedical group, Nephrology group, Surgeons
Verification method: if tissue ingrowth is incorporated in to the design in-vivo testing is likely the only method of validation.

Reasoning: where tissue formation can be troublesome for the functioning of the inner mechanisms of the valve, the outer casing can be designed in such a way that it will bond with the tissue in the arm as to fixate the valve.

2.5 Removable: in case of malfunctioning the valve **could** be designed as to be easily removable by surgery.
Stakeholders: Biomedical group, Nephrology group, Surgeons
Verification method: consolidate with a medical expert or assess the explantation on a in-vivo study.
Reasoning: although the valve is to be designed with a reasonable life time, malfunctions can always occur resulting in the need of removal of the dAVF-valve via surgery in order to either fix the valve or, more likely, implant a new one.

2.8. Criteria

In this section the criteria that are to be used for the development of a compliant dAVF are listed. The goal of a criterium is to aid the concept-design selection following their generation. So whereas the requirements set in section 2.7 will be used to validate the design at the end of this thesis project, the criteria are to be used in an earlier stage where no design is finalized. The selection of concepts will happen when multiple technical details are yet to be worked out. This requires a pragmatic approach based on fundamental working principles or estimated performance specifications. The criteria have to be formulated accordingly. Another approach to be used is to rank concepts comparatively (ideally referencing to a state of the art concept). A more in-depth discussion on concept selection will be given in section 3.3 but a basic definition of the need for criteria is required to make a distinction between criteria and requirements.
A note of importance is that, although requirements are validated at the end of the development cycle, all concepts are to be developed with the requirements in mind. If there is a strong indication that a concept is by no means able to achieve the requirements, there is no sense in further efforts on the development of that concept.
To summarize; Requirements are set absolute targets to be met at the end of the development in order for the compliant dAVF-valve to be considered a success. Criteria are used to compare conceptual designs relatively to one another at the end of the conceptual design.
The criteria to be used for selection of a compliant dAVF-valve are listed below ranked in order of importance. This order will replace the weighing factors used to multiply scores with in a conventional decision matrix.

1. Resistance to Fibrous Tissue formation: as indicated in the functional description in section 2.2, in previous prototypes the formation of fibrous tissue around critical parts of the valve mechanism affects the valves function over a prolonged period of time. It is therefore crucial that the effects of this are mitigated.
   Stakeholders: Biomedical group, Nephrology group
   Evaluation method: material, open volumes and surface area.
   Reasoning: as learned in section 2.4, the foreign body response is mainly impacted by material choice. In-depth research on this was done in a prior literature study [24]. Additional factors of impact are the open volumes in which fibrous tissue can form and the surface area to which it can attach. In case of similar materials being used, these factors are to be taken into consideration.
2. Traction on Anastomosis: the graft is secured to the artery and the vein by sutures. As discussed in requirement 1f, this tractive force on the graft is to be limited to no more than 0.76N [8] by the tearout strength of the suture in the vein.. The base line is set by the hinged dAVF-Valve at 0.19N [8].
   Stakeholders: Biomedical group, Nephrology group
   Evaluation method: concepts will be scored on both approach direction towards the graft and the contraction of the graft caused by the end-effector shape. Each can be scored as better than the state of the art (+), worse (-) or similar (0).
   Reasoning: no force measurements can be done for the conceptual selection as no physical prototype is available. However, reasonable assumptions can be made of the effect of the design choices on the tractive forces on the graft. As the graft contracts and deforms, this will inevitably result in a load on the sutures. To keep this load to a minimum the motion of the mechanism

and the shape of the end effectors will be assessed. Motions that result in a parallel approach to the graft and end effectors that keep deformation of the graft to a minimum will score better than those that don't.

3. Energy storage: as the compliant mechanism opens the graft, potential energy is stored in deformation of the flexures. This energy storage is to kept at a minimum to ease opening of the anastomosis and to ensure the valve is compatible with the actuator.
   Stakeholders: Biomedical group, Nephrology group, Dialysis staff
   Evaluation method: for each concept, for all of the flexures their stiffness and required displacement is to be determined. With these the energy required to actuate the valve can be found and thus the valve concepts can be compared to one another.
   Reasoning: the valve that is to be designed has to be compatible with the already developed actuator (described in section 1.2). The energy that this actuator can introduce in the valve subsystem is limited to 0.12J. For the pinhole-concept the energy provided is mainly stored in deformation of the pressurized graft. With the addition of flexures, more energy will be stored in the system as the flexures act as springs and thus store energy upon displacement. This total energy budget is not to exceed what the actuator is capable of delivering.
4. Design Complexity: Occams Razor is originally formulated as; "plurality should not be posited without necessity". In the engineering perception this could be interpreted as the design with the least parts will be the least complex and is therefore favourable over other options. For the purpose of this criterium it is better to interpret it more freely as; the simplest design is the best design. Here the complexity is determined for the timespan of this project.
   Stakeholders: Biomedical group, Nephrology group
   Evaluation method: a workload estimation for both the design phase as well as a production as verification and validation is made.
   Reasoning: in many engineering efforts the number of parts will give a good indication of their complexity. However, specifically for compliant mechanisms this isn't applicable as compared to their pinhole-counterparts they will inherently consist of fewer parts and will always be marked as better than their benchmarks. Some compliant designs can be constructed to be fully monolithic. The effort required to design such a part might however be notable more, taking into account more complex simulation and production processes, than a design consisting of a handful of parts. Therefore estimated workload is taken as a metric for determining complexity. Another remark to be made is that complexity will apply differently to all stakeholders. A design that is simple to design and prototype might be complex in use or require a more complex operation for implantation. The choice on design workload was taken to reasonably limit the development time for the compliant dAVF within the limits of this graduation project.
5. Cost: for this criteria the manufacturing cost of the concept will be evaluated as this is most impacted by the design choices.
   Stakeholders: Biomedical group, Nephrology group, Production Partner, Health insurances
   Evaluation method: using the CAD-model made for evaluation a quotation will requested for 100 units for each design at a manufacturer. Included in these quotes will be several design choices such as material, tolerances required and threads. In order to receive data that is comparable, these quotes will be placed at the same time.
   Reasoning: the total cost for the creation of an anastomosis involving a dAVF consists of more than just the manufacturing cost of the device. As with any technical system there will be development, manufacturing, implementation, operational and decommissioning costs. Development costs are connected to design complexity which is discussed above. The other costs will not be affected by the design choices of the dAVF-valve and are dictated by the medical treatment which for now are assumed independent of this concept selection.
6. Implantation Severity: the design for the dAVF-implant will impact the severity of the medical procedure for creation of the anastomosis and installation of the dAVF. After consultation with a vascular surgeon the most important metric was found to be the volume of the device that determines the incision size.
   Stakeholders: Biomedical group, Nephrology group, Surgeons
   Evaluation method: Estimated volume of the concept.
   Reasoning: Accounting for the implantation during the design of the dAVF can impact the

severity of the implantation operation and thus increase patient recovery. Multiple factors were considered such as implant shape, an open of closed design around the graft or rounding of sharp edges. Some research on the shape and volume of the graft has been done prior to this project [8]. According to surgeon dr. K.E.A van der Bogt, the dAVF-shape is not as relevant since the dAVF is to be placed around the graft prior to implantation. Volume will dictate the size of the required incision and thus the severity of the operation.

7. Mass: reducing the mass of the implant should result in the implant being less noticeable for the patient.
   Stakeholders: Biomedical group, Nephrology group, patient
   Evaluation method: an estimation of the concepts in made by determining the weight of the CAD-models build with the proposed material selection.
   Reasoning: currently the mass of the implant is not noted as problematic. This, in combination with the mass being partially coupled to the volume metric for the implantability criterium, places these criteria lower in the ranking (effectively lowering their weight factor).

3

Concept Design

Within this chapter on concept design, three feasible concepts will be generated that are assumed capable of fulfilling the requirements set in section 2.7. These solutions will be created from sub-solutions that are divided into various solution spaces section 3.1. A morphological overview is created in section 3.2 where all combinations of sub solutions are considered and with the help of design focusses, three concepts designs are generated and developed to a similar level showing the proposed working principles. To find the most promising concept for the posed problem, a Harris profile is set in section 3.3 to rate the concepts to the criteria that are set in section 2.8. The design methods used in throughout this paper but especially in this chapter are based on the methodology used in Space Systems Engineering [32]. These methods are developed and used for engineering complex systems. While the principles are similar to more traditional design approaches, where these differ; an explanation of the method and a motivation for its use will be given.

3.1. Solution Spaces

The solution spaces are based on the (potential) functionalities for the dAVF. This architecture is based on the functions and systems that are assumed to be required in the final system. Not all sub-functionalities will be required for the creation of a concept, as some functions could be inherently fulfilled by another selected sub-solution. Contrarily, some sub-solutions could only function with the addition of another sub-solution. The presented sub-functionalities are not directly correspond to the requirements, however, all proposed concepts will be designed to ensure satisfying these. The goal in setting these solution spaces is to be as open as possible for all plausible solutions and to allow for a varied scope of design concepts.

Figure 3.1: The architecture of solution spaces for the compliant dAVF. The interfaces between subsolutions are shown with interlocking arrows whereas the supporting systems are shown below.

3.1.1. Design Boundaries

Prior to generating solutions that fulfil the proposed sub-functionalities; a few design boundaries for this project are set. Setting boundaries on the components that can and cannot be adapted will lead to a clearer scope for the creation of design concepts but also for further developments. The impacts of these boundaries on the final design will discussed in further depth in the discussion in chapter 6.

Input

As stated in the project objective the goal of this thesis project is solely focussed on the design of a compliant valve. For the input the existing concept by Kroft as discussed in section 1.2 and shown

Figure 3.2: A dismantled bowden cable showing the inner cable (loaded on tension), an inner-sleeve to reduce friction, an outer structure (loaded on compression) and a protective coating. Source: Baran Ivo, CC BY-SA 3.0 via Wikimedia Commons

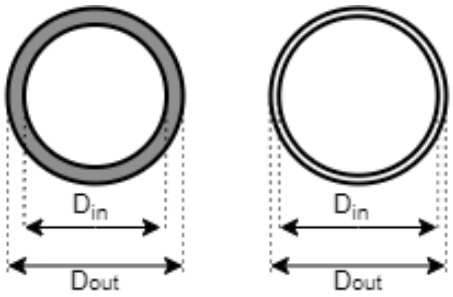

Figure 3.3: Schematic representation of the triple layered graft on the left (with the silicone layer in grey) and the double sided graft on the right.

in figure 1.3a is to be used. This actuator was optimized in further development to provide the most energy with the volume constraints. The output force generated by this actuator is transmitted to the valve using a bowden cable. This cable consists of a flexible core cable that is loaded on tension combined with an outer sleeve that is loaded in compression. An overview of the components making up a bowden cable is given in figure 3.2, the medical versions of this cable used in previous iterations lacked the protective coating and the friction reducing inner-sleeve as these materials are likely not biocompatible. A bowden cable was chosen over direct placement of the actuator on the valve to allow for flexibility in the design. This allows separate placement of the actuator close to the skin where volume is available and of the valve at the location selected for the anastomosis. In previous iterations of the dAVF, the bowden cable was already proven as a suitable transmission. What is to be kept in mind is that generally a bowden cable is preferably loaded in tension rather than compression. Thus for actuating the valve of pulling input is preferred over a pushing input motion. Alternative transmissions were considered, such as hydraulic, electric, torsion and a direct connection between actuator and valve. To reduce the added risk of changing to a new transmissions type as well as the increase of development time, the decision was made to design the new compliant valve to accept a similar type of bowden cable attached to the same actuator.

Graft

In terms of grafts selection there is a plethora of options available on the market. For this research it is opted to limit the selection to the graft types available at the LUMC. This is done for two reasons, availability of materials for testing and their selection is trusted to function as well as the LUMC surgeon's experience with these grafts. The graft brand used is the GORE®PROPATEN®Vascular Graft by GOREMedical, Flagstaff, Arizona. This family of graft comes in two variates, multiple diameters and optional ringing. The ringing is a method to prevent the graft from collapsing after placement [33]. Since the collapse of the graft is a desirable feature, all ringed options are to be discarded.

The two varieties considered are constructed differently, as shown in figure 3.3. The double layer (DL) graft is constructed of two layer of ePTFE material with a wall thickness of 0.4 mm. The triple layer (TL) graft is thicker at 1.2 mm due to the addition of a layer of silicone in-between the ePTFE material. The addition of this layer makes for a stiffer graft but more importantly is assumed to help with the complete closure of the graft.

The graft diameter is what determines the maximal flow in the open state of the dAVF. A minimal required flow is set at 600ml/min in section 2.7 with no maximum set. The selected diameter for this design is to be in line with the state of the art design, covered in section 1.2, where two grafts with internal diameter of 5mm and 6mm are considered [8]. Thus, to allow for a similar maximum flow rate, a internal diameter of 6mm was selected. The use of dual or triple layered graft depends on the

mechanisms ability to completely close the graft. The silicone layer was added to the earlier study to add a compliant layer that can be compressed to ensure closure. For concepts generated that already offer a form of compliancy in the angle of the compressors, a double layer would be favourable to reduce total stiffness.

3.1.2. Compliant Closing Mechanism

The Closing mechanism will translate the selected input type to a movement of the Graft Interface to close and open the graft at will. As stated in the project objective in section 2.6, this solution will be in the form of a compliant mechanism.
Compliant mechanisms can be defined as all types of mechanical solutions that utilizes the flexibility of a material to achieve a desired motion or force application [34]. Traditional designs consists of rigid parts with high stiffness and rely on contact surfaces as bushings or bearing to allow for movements. As defined in the problem definition in section 2.5 the fibrous tissue that is formed around the dAVF-valve severely impacted the functionality and reliability of the device. Eliminating all pin-joints in favour of compliant elements is expected to reduce the influence of tissue formation. In a monolithic compliant mechanism, there are no small cavities in which fibrous tissue can be formed. The most ideal complaint mechanisms would be those with long distributed flexures, upon deformation the load on the tissue will also be distributed reducing the high stiffness than can result from compression of this tissue. Some other, more common, advantages and disadvantages of the use of compliant mechanisms are listed below;

Advantages

Other often mentioned advantages compliant mechanisms can offer is increased performance in terms of precision due to elimination of backlash which is why compliant systems are often found in the precision industry [34]. The removal of contact surfaces will is a reason compliant mechanism can often be found in clean environments as the lack of contact results in reduced wear. Lastly the introduction of flexible elements can lead to a reduction of components. Ideally compliant mechanisms can be produced as one part, referred to as monolithic. These monolithic parts will often provide a significant weight reduction as well as lower cost as no assembly is required.

Disadvantages

The adaption to compliant mechanisms can also introduce some disadvantages like their limited range of motion and load capacity. As all elements are flexible, full rotations that bearing allow for are no longer an option. Furthermore compliant mechanisms are often more difficult to design for when compared to their rigid counterparts [34]. The integration of multiple functionalities in a single part requires the designer to account for both motion and force behaviour, the former in the desired degrees of freedom and the latter in the constraint directions. For this specific reason, the identified degrees of freedom for each mechanism are given for each concept discussed in this chapter. Ideally only the desired degrees of freedom are present in the system, as any additional degrees could lead to unexpected behaviour. Another aspect that has to be accounted for is that compliant mechanism often no longer function in the linear behaviour region of a material which leads to non-linear effects to be taken in ought. Lastly special attention is required for the fatigue load on flexible member due to their often repeated motion.

Pros	Cons
+ Reduction of effects from fibrous tissue	- Limited range of motion
+ Increased precision	- More complex in design
+ No spread of particulates due to no wear	- Material fatigue due to dynamic loads
+ Lower weight due to reduced part count	- Energy Storage within flexures
+ Lower cost due to reduced part count	

Table 3.1: Pros and cons of Compliant Mechanisms [34].

Material Selection
To allow for the desired flexibility of the mechanism, material choice is a critical part for the design of a compliant dAVF. This combined with requirement 2b of only using biocompatible material results in a select list of options, shown in section 3.1.2. These materials were found in a literature study on materials and production methods used for the creation of mechanical implants[24]. As compliant mechanisms require a material with a high yield strength and low stiffness which is shown in the fourth column. Another assessment method for a compliant material is to determine the resilience by finding the surface beneath the linear region of the stress strain curve. This results in the energy that material can handle per volume before permanent deformation occurs[34].

Table 3.2: An overview of the biocompatible materials ranked on their resilience. Source: Granta Edupack

Material	Young's Modulus E(GPa)	Yield Stress σ_y (MPa)	σ_y/E*1000	σ_y^2/2E*0.001
Nitinol 55	62	442.5	7.14	1579
Zirconia	208	800	3.85	1538
PEEK	3.85	100	26.0	1299
Cobalt alloys Co-Cr-Mo	215	487.5	2.27	552
Titanium Ti-6Al-4V	102.5	318	3.10	493
PLA	3.45	52.5	15.2	399
Stainless Steel 316L	200	205	1.03	105
Magnesium AZ31B	44.5	262.5	5.90	774

The material selection will be finalized with the parameters of the selected concept mechanism in the final design stage. In the conceptual phase the emphasis is on the working principles and motion generation for each identified compliant mechanism.

Design Synthesis
The design of a mechanism that bends requires a different approach compared to rigid systems. Several methods to design a compliant mechanisms have been described in literature [34], [35], the most suitable have been listed below;

- **Modifying an existing Rigid Body Design:** by starting of from a design build with rigid links and hinges; the functionality of an original design can be maintained with the benefits that compliant joints provide. Replacing the pin-hinges of the original dAVF-valve mechanism with compliant joints or hinges could lead to a similarly functional design as no large angles of rotation are present within the range of motion. Other existing rigid body designs with a gripping or pinching mechanism can also be researched. The benefit of this method would be the broad scope of conventional mechanisms available to study leading to a quick way to analyse a broad range of possible concepts. The results of replacing joint from a rigid mechanism is that it mostly leads to a Pseudo Rigid Body Design where large parts of the mechanism are still rigid and the compliance is lumped.
- **Modifying an existing Compliant Design:** a similar approach would be to investigate existing compliant mechanisms and extracting their working principles. The benefits of which are the complete utilization of all available flexures, both lumped and distributed. For the function of a

gripper or pliers, several existing compliant mechanisms can be identified . By grouping these concepts and extracting their working principles a complete overview of available solutions can be found. Beginning from these working principles, a design can be made were parameters are determined to achieve the required motion and force application. Several working principles can also be combined to form one design concept.

- **Generating a new Compliant Design:** when these design approaches are not an option, the only remaining option is to design and synthesize a new compliant mechanism based on the requirements. The first method suggested by the Handbook of Compliant Mechanisms [34] is to use their library of compliant 'building blocks' that can be coupled to create a mechanisms that can fulfil the desired motion path. When more control of the Degrees of Freedom (DoF) for a mechanism are required, the Freedom And Constraint Topology (FACT) method can be used. By setting the freedom space, the directions the mechanisms is free to move, and the constraint space, where the motion should be constrained, a selection of compliant members can be made from the FACT-table. This method allows for better control of the motion of the mechanism. The last method described for the synthesis of mechanisms is that of topology optimization. Here a mesh is made for the design domain and with the desired in-and output forces together with an optimization goal, an algorithm determines what nodes and links contribute to this goal. These are kept where the ones that do not contribute are removed. The use of topology optimization is rather complex and can lead to undesired results when used incorrectly. When used correctly however, it can be a powerful tool capable of synthesising mechanisms that are unlikely to be formed from the other methods.

All synthesis methods described here will lead to a compliant mechanism with the functionality for a dAVF-valve. An important aspect in determining which synthesis method to use is the amount and functionality of existing designs. As an existing rigid body design of the dAVF-valve already exists, it makes sense to investigate the possibility of replacing all joints with compliant elements. In addition to this, it was found that within te field of compliant mechanisms various research has been done in to compliant grippers, clamps, pliers or other mechanisms with a similar functionality as the dAVF-valve requires. For this reason it makes sense for this project to study the possibility of adapting the rigid link design or modifying an existing compliant design for use in the dAVF-valve. Using this approach a broad range of mechanisms can be considered in the same time span as one compliant design can be generated from scratch. If however, a clear gap in existing designs exists, a new compliant design can be generated in a later stage to fill this. [35]
To distinguish the concepts generate for the compliant closing mechanism, the different approach methods are listed below. These will be used to categorise the identified concepts based on their approach path to the graft. The identified approaches are shown in section 3.1.2 and can be described as follows;

(a) **Axial Hinge:** the planes that approach the graft share an axis of rotation that is parallel to the axis of the graft.
(b) **Radial Hinge:** the planes that approach the graft share an axis of rotation that is perpendicular to the axis of the graft.
(c) **Parallel:** the planes approaching the graft are parallel to each other.
(d) **Radial:** the graft is compressed in a radial direction towards its centre axis.

Some concepts, mainly all concepts that involve a rotation around an axis, could be placed in both directions(with their hinge parallel to the grafts axis or perpendicular). In these cases the volume requirement is taken into account to determine most logical orientation of the concept.

Axial Hinge Mechanisms

All mechanisms discussed in this section will close in the direction shown in figure 3.4b, where the rotational axis of the gripper is parallel to the central axis of the graft. The previous dAVF-valve prototypes, as discussed in section 1.2, can all be placed under this category. This is mainly due to the volume constraints are favourable for devices of this type placed in this orientation. For this reason, most of the potential compliant mechanisms can are also discussed in this section.

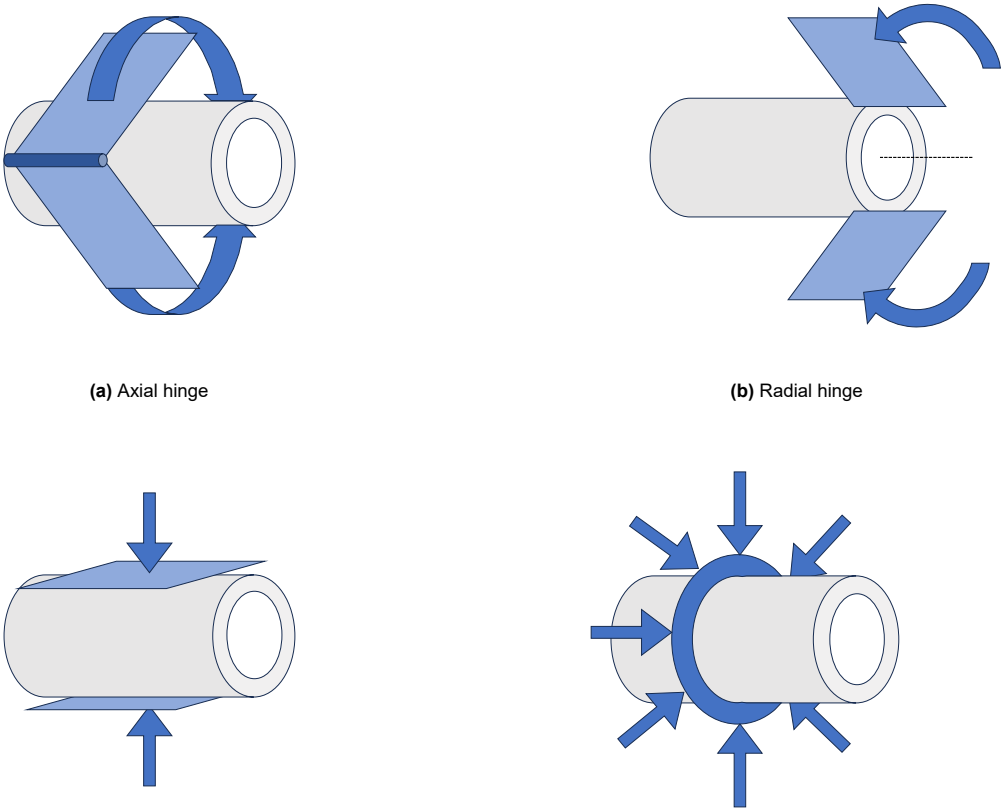

(a) Axial hinge

(b) Radial hinge

(c) Parallel

(d) Radial

Figure 3.4: All methods considered to approach the graft.

Compliant Clip The compliant clip is likely one of the simplest mechanisms found that fulfils the functionality of a gripper. The design consists of two rigid links that pivot around a compliant notched joint in the middle. This results in one degree of freedom.
The pivotpoint A in the middle of the clip allow the two rigid links to form a mechanical advantage trough leverage.

$$M_A \circlearrowleft = FinL_1 - FoutL_2 - K_A d\theta \tag{3.1a}$$

$$\frac{F_{out}}{F_{in}} \propto \frac{L_1}{L_2} \tag{3.1b}$$

By increasing the ratio of $\frac{L_1}{L_2}$, the output force on the graft will increase. Decreasing L_2 however will increase the tangent forces on the graft and will therefore negatively impact the force on the sutures.
From figure 3.5b it can be seen that all deformation occurs in the notched joint. This is a compliant element that can replace a regular joint. Upon rotation this joint will pose a counter moment by means of the rotational stiffness K;

$$K_A = 0.093Eth^2\sqrt{\frac{h}{D}} \tag{3.2}$$

As a design rule of thumb the elastic hinge parameter β, given by $\beta = \frac{h}{D}$, should be as small as possible for minimal rotational stiffness. This comes at the cost of lateral stiffness. A lower limited of this ratio is suggested at 0.01 due to manufacturing limitations [36]. In all the other directions the notched hinge is relatively stiff. All energy lost in operating the mechanism can be defined by;

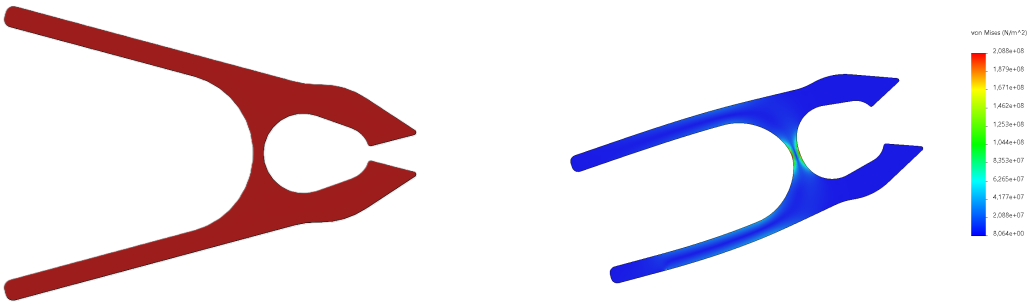

(a) A model of the compliant clip in the closed stage.

(b) Stress Analysis of the Compliant Clip deformed to the open position.

Figure 3.5: Compliant Clip.

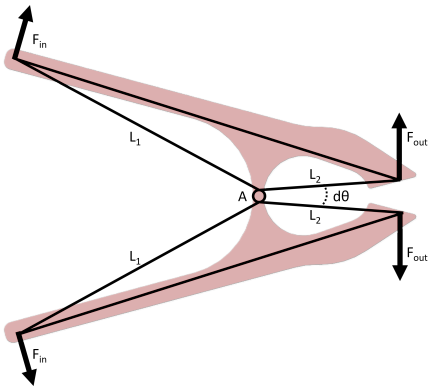

(a) FBD for the Compliant Clip

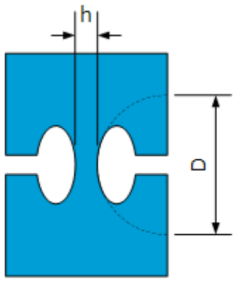

(b) Example of a notched joint [36].

$$E = \frac{1}{2} K_A d\theta^2 \tag{3.3}$$

One of the downsides of the use of a notched, or living, hinge is the limited angle of rotation which mainly leads to usecases where a small but precise displacement is required [38]. The maximum bending angle can be determined by;

$$\theta_{max} = \frac{3\pi}{4} \frac{\sigma_y}{E} \sqrt{\frac{R}{h}} \tag{3.4}$$

From this it follows that this angle is determined by the material properties in terms of the Young's Modulus, E, and the yield stress, σ_y. And furthermore by the geometry defined by the radius of the circular notch, R, and the thickness of the remaining material in between these circles, h. This typically results in angles of rotations in the range of a few degrees in both directions [38]. To counter this limitation and still find a gripping mechanism with a suitable range of motion; a longer length in arms is required. This solution can be identified in two of the found examples of a notched hinge mechanism. The use of a compliant clip with a notched hinge can be found in other designs as well. One of such a the Compliers™, a compliant set of pliers [37]. Notably are the folded leaf flexures connecting the ends of the handles and allowing for a stable position. One of the earlier dAVF prototypes designed by Hart used a notched hinge mechanism actuated by a wire [10]. In this case the design decision was made to place to hinge to the opposite side of the graft and the actuation point. This in all likelihood was done to counter the limited range of rotation that a notched hinge allows for.
For the specifications and requirements set for this study a rough dimensional estimation can be given for such a design. Using equation (3.4) with the material parameters for titanium (from section 3.1.2, which is a realistic high performance bio compatible material) and the design guide line of $\beta = h/D = 0.01$ from [36] a maximal rotational displacement of almost 3 degrees is found. This is from its resting positional to the maximal displacement. This can be optimised by placing the closed position at one of

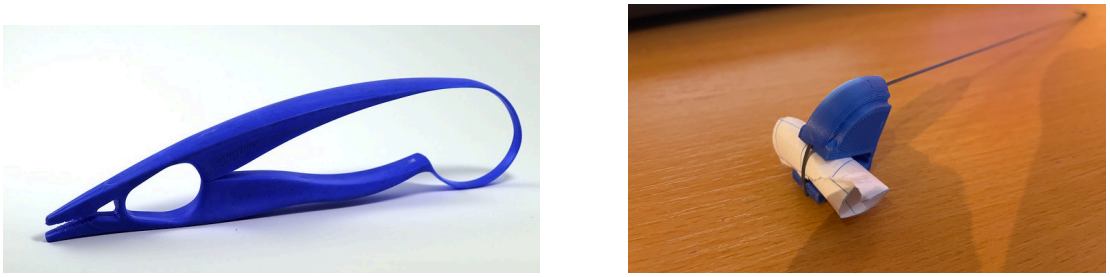

(a) Compliant Pliers [38]

(b) Compliant dAVF valve prototype by Hart [10].

Figure 3.7: Example of other usages of notched hinge mechanisms.

the extended angles and the opened position at the other. Using some simple basic trigonometry this results in an arm length of 100mm between the centre of the hinge and the graft. This is more than three times the largest dimension of the volume claim. This renders the concept of a single compliant hinge unusable for the set requirements. Multiple hinges could be stacked in series with the arms folded to find a working concept.

Compliant Clamp This compliant clip uses two pairs of parallel flexures that close the clamp when compressed [34].

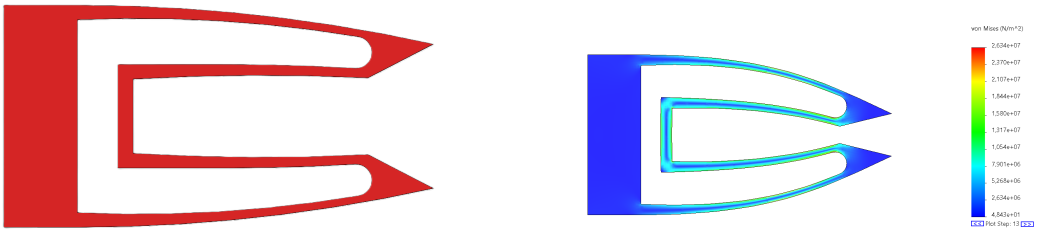

(a) A model of the compliant clamp in the opened stage.

(b) Stress Analysis of the Compliant Clip deformed to the closed position.

Figure 3.8: Compliant Clamp.

The Degrees of Freedom (DoF) for this mechanism can be determined from figure 3.9a and the Gruebler - Kutzbach - Chebychev formula in equation (3.5);

$$F = 3(n-1) - 2g = 3(8-1) - 2*8 = 5 \tag{3.5}$$

Of the five DoF, two are the motion of the end effectors, one is the compression of A towards B to actuate the mechanism. The other two result in undesired motion of member A; one translation parallel to B and one rotation of A. When the actuation force is applied evenly over the length of A these should not occur during nominal operation.

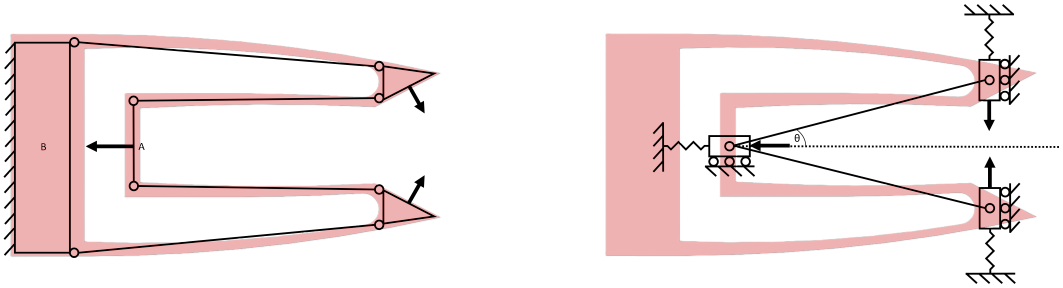

(a) PRBM-Model of the compliant elements used.

(b) Stiffness equivalent model.

Figure 3.9: Working principles of the Compliant Clamp

The compliant members making up this mechanism are two parallel sets of two leaf flexures in series. When actuated at point A, all flexures are loaded axially causing bending to closure the graft. A risk with exceeding the load on these flexure is the phenomenon of buckling. Using Eulers equation for critical load and using parameters for the model shown in figure 3.8a printed in PETG to (as to compare to a printed prototype) a critical load of around 5N was found. As the flexures are slightly pre-curved buckling could occur at an earlier stage and in a determined direction. Although buckling does not have to lead to failure, it is to be avoided due to its rapid change in deflection.

$$F_{cr} = \frac{\pi^2 EI}{(KL)^2} \tag{3.6}$$

Compliant Crimper This mechanism, although noted as a different mechanism in the *Handbook of Compliant Mechanisms* [34], shares some notable resemblances to the gripper discussed in the paragraph above. It is operated identically, by compressing the two vertical input elements (on the left in figure 3.10a) the two end effectors of the mechanism will close towards each other. The most notable difference is the change in flexural elements and the added stiffeners.

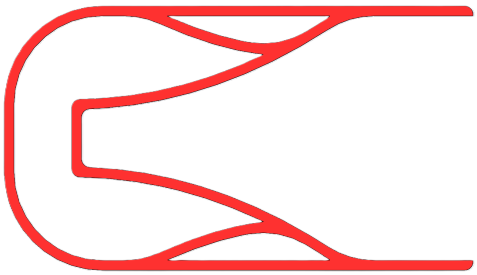

(a) A model of the crimper in the opened stage.

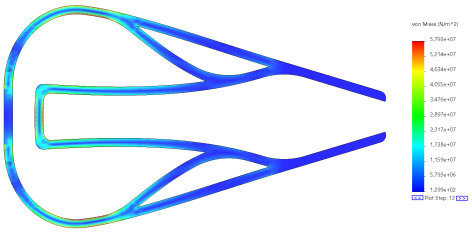

(b) Stress Analysis of the crimper deformed to the closed position.

Figure 3.10: Compliant Crimper

As can be seen in the stress analysis in figure 3.10b, all deformation occurs in the rounded flexures as opposed to along the horizontal gripper elements as in figure 3.8b. To counter flexing of the elements in the crimper, stiffening elements are added. In the stress analysis in figure 3.10b the effects of these can clearly be seen as little stress builds up in these elements.
The degrees of freedom can be determined from the elements in figure 3.11a;

$$DoF = 3(8-1) - 2*8 = 5 \tag{3.7}$$

This is the same amount of degrees of freedom as the compliant clamp discussed above. Comparing their FBDs and following earlier discussion on their similarities, the same degrees of freedom can be

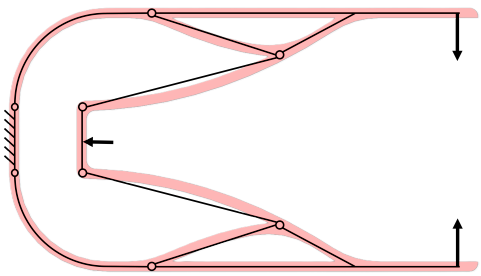

(a) FBD for the Compliant Crimper

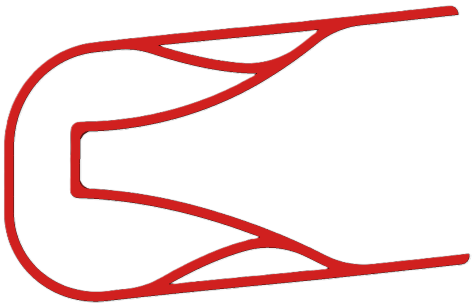

(b) Example of an undesired DoF for the Crimper mechanism

Figure 3.11: Additional analysis on the Compliant Crimper.

found. Due to different flexure elements, the extend of movement will differ. In figure 3.11b one of the undesired DoF is shown where the displacement of the end effectors is larger than that of the clamp.

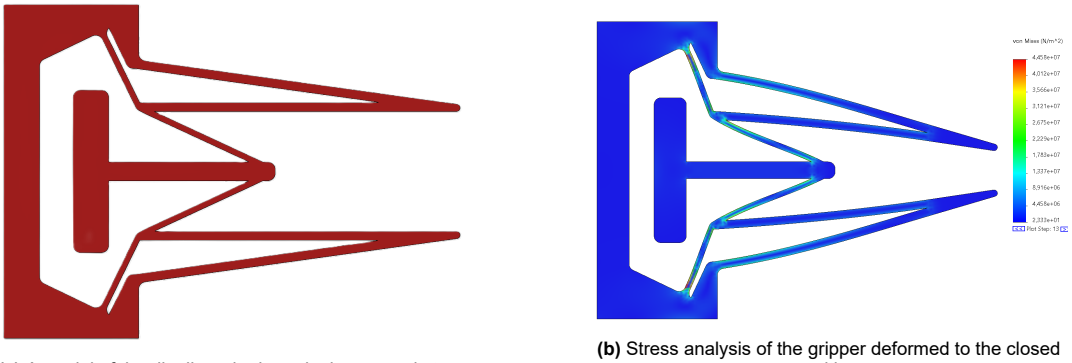

(a) A model of the distributed gripper in the opened state.

(b) Stress analysis of the gripper deformed to the closed position.

Figure 3.12: Compliant Distributed Gripper

Distributed Gripper The distributed gripper [38] has a strong resemblance to the compliant clamp discussed in section 3.1.2. However as shown in figure 3.12a additional flexures have been added to support the distributed flexure pinchers. Each pincher now forms a four-bar linkage and can move individually from one another. Each pincher is connected to the centre stage where the actuation force is applied to. As per the original design the flexures that make up the pincher elements have an increased thickness compared to the more slender elements that connect to them. This design allows for a larger output displacement for a small input displacement.

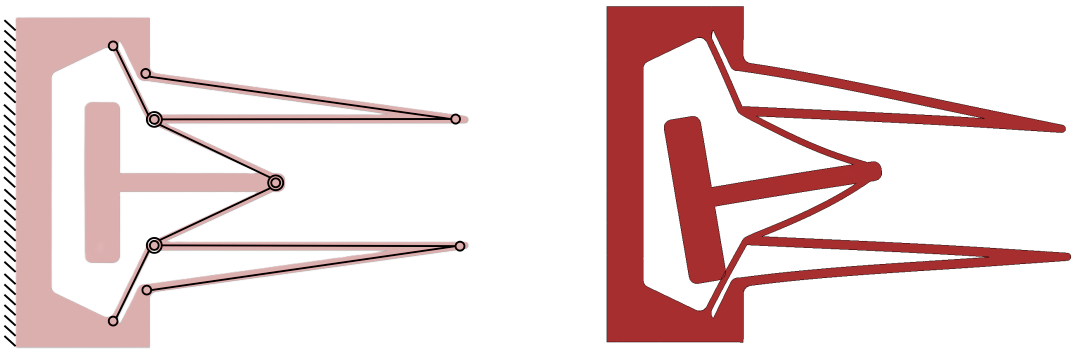

(a) A FBD of the gripper for determining the DoF.

(b) The undesired DoF for the actuator stage.

Figure 3.13: Additional analysis on the distributed gripper.

Finding the Degrees of Freedom for this mechanism, and taking into account the three double joint depicted as double circles in figure 3.13a, yields;

$$DoF = 3(10 - 1) - 2 * 12 = 3 \tag{3.8}$$

Two of these DoF are already identified to be the independent movement of each pincher element. The last however is the undesired rotation of the actuation stage around the intersection of the two slender flexures connecting it to the rest of the mechanism. This DoF is shown in figure 3.13b. If this mechanism is to be used for the Compliant dAVF-valve it would be beneficial to eliminate this DoF as it can be triggered with a minimal imbalance of the input force. Applying two (or four) collinear and, in the orientation in the images, vertical flexures to guide the actuation stage in a similar fashion as in section 3.1.2 could constrain this undesired DoF.

Howell's Handtool This handtool is designed by Howell and Midha as a case study for their paper on; "A method for the design of compliant mechanisms with small-length flexural pivots" [38]. It is used

as a demonstrator in 1994 for their Pseudo Rigid Body Design, as described earlier in section 3.1.2. This method is proposed as an alternative on the 'trial and error' approach that was common at the time due to computational time for finite element analysis being too expensive.

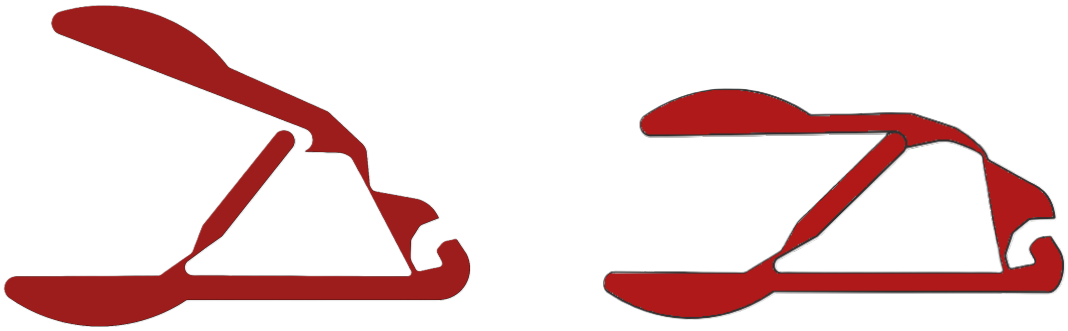

(a) A model of the gripper in the opened stage.

(b) A model of the gripper deformed to the closed position.

Figure 3.14: Howell's Handtool

The mechanism depicted here is derived from an four-bar linkage and uses three flexural pivot joints and one passive joint in the top left of figure 3.14a. For the DoF this yields;

$$DoF = 3(4-1) - 2*4 = 1 \tag{3.9}$$

The dimensions of the linkages have been optimized for mechanical advantage. With these parameters such a mechanisms would exceed the volume requirement for the Compliant dAVF-Valve. A new optimization would have to be performed to find suitable parameters without the loss of mechanical advantage this concept provides. Furthermore the model has a significant amount of empty volume in its centre. Placing the external actuators to the inside could help reduce overall volume.

Inverted L-Arm This concept is intended as an alternative to a Minimal Invasive Surgery tool. The author notes increased simplicity, performance and deflections as well as additional degrees of freedom [39].

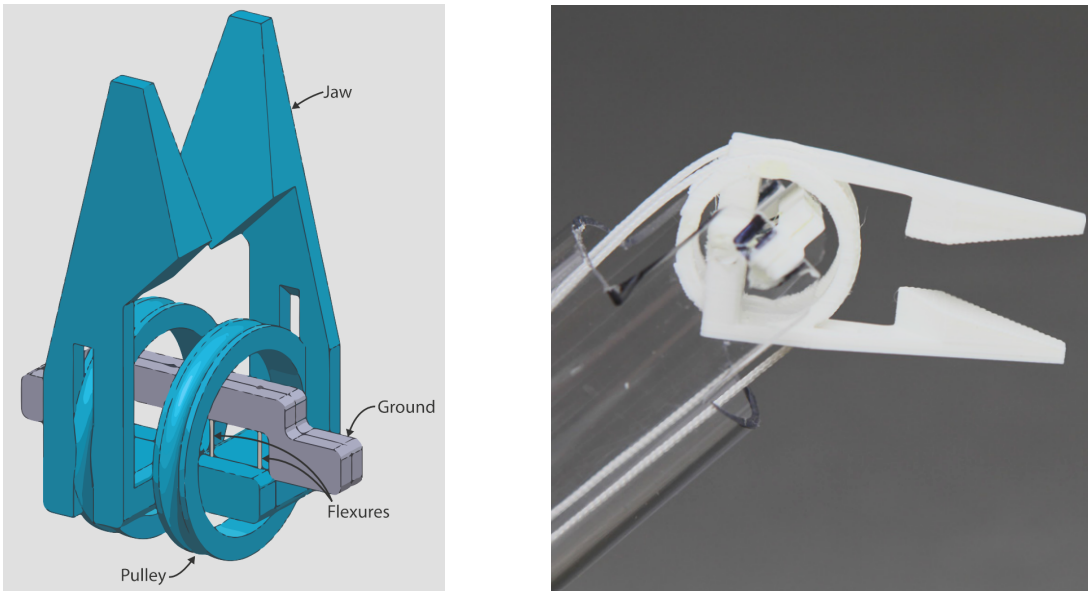

(a) An overview of the components from the Inverted L-Arm.

(b) A printed prototype of the inverted L-arm showcasing the independent degrees of freedom.

Figure 3.15: Inverted L-Arm prototype. Source: Dearden [39]

As depicted in figure 3.15a, each jaw is connected to the ground-element with two nitinol wire flexures. Following the FACT-method [38], these form a constraint plane in the 3D-space allowing the jaws to

rotate around the ground-element. However, the rotation along the vertical axis as well as the (limited) translations along the directions perpendicular to the wire flexures are unconstrained. To avoid movement in the undesired directions the input force is applied along the pulley ring placed in the middle of the two flexures. Notably the jaws are place of centre which could introduce a rotation along the jaw-axis when loaded. The author mentions that in the design the flexures are place as far apart as possible to provide torsional stability [39]. The nitinol wire flexures are chosen for their biocompatibility and their large ratio of σ_y/E. This allows the jaws to rotate more than $\pm 90^\circ$ [39]. The rotational-stiffness for a wire flexure in the direction of actuation is given by;

$$K = \frac{\pi E d^4}{64L} \tag{3.10}$$

Using the parameters for the four flexures used by Dearden for their prototype (which would be a similar scale to a compliant dAVF-Valve) gives an energy requirement of 0.0019J for an opening angle of 45°. The inverted L-Arm shape of the jaws assures that both the flexures and the cable input to the mechanisms are always loaded in tension and never in compression to avoid buckling. The mechanical advantage of the mechanism is determined by the ratio between the jaw length and the pulley radius. And whilst not mentioned in the paper, the pulley could be designed to have variable radius by giving it an oval shape. In the case of the Compliant dAVF-Valve this could help to counter the (non-linear) stiffness of the graft over compression. As each jaw is equipped with wire flexures independently from the other, this allows for rotations of the jaws (as shown in figure 3.15b). Whilst this has proven to be of use in a surgical tool, this won't benefit the functionality of the compliant dAVF-Valve.

CORE-gripper A Compliant Rolling-contact Element (CORE) is often applied as a compliant equivalent pinhole hinge replacement when a large displacement is required. The mechanism, as shown in figure 3.16a, consists of two half cylinders (a. and b.) and an multitude of flexures (c.) that are pressed between the cylinders is an S-shape[34]. The rotational point is located at the contact point (d.) and will move as the two cylinders rotate over one another. This one rotation is the only degree of freedom for this element. The allow for multiple degrees of rotation, these CORE are often seen place in series [40].
The stress in the flexures is the limiting factor in shrinking the mechanism and can be determined by adding axial stress and bending stress;

$$\sigma = \frac{T_{max}}{Rht} + \frac{Et}{2R} \tag{3.11}$$

with R as the radius of the cylinder, t as the flexure thickness and h as the flexure height. The flexures have to be placed symmetrical and both should have an equal sum of height to distribute the stress in the flexures.
An example of the use of a CORE is shown in figure 3.16b and is developed by Grames. Their chose for the CORE was based on a wish for a reduction in volume for a surgical instrument whilst maintaining a large range of motion [40]. A downside to the use of a CORE is found in section 3.1.2. Although this element allows for large displacement, it comes at the cost of a exponentially decreasing mechanical advantage. For the application of a compliant dAVF-valve where the force required to close the graft will increase over closure this behaviour is undesirable.
Another use case of a CORE is found in a laparoscopic grasper where force perception by the surgeon was crucial [41]. Here a similar joint is created, shown in figure 3.18, due to pin hinges where hysteresis occurs and other compliant hinges that produce a counter torque which negatively impacts the perception of the surgeon [41]. In a similar fashion this would be beneficial for the compliant dAVF-valve as well, however the requirement for force transmission is of greater importance due to the limited available input force. This paper does also mention a significant increase in mechanical efficiency (from 30% from old graspers to 96%). This is not to be confused with mechanical advantage.

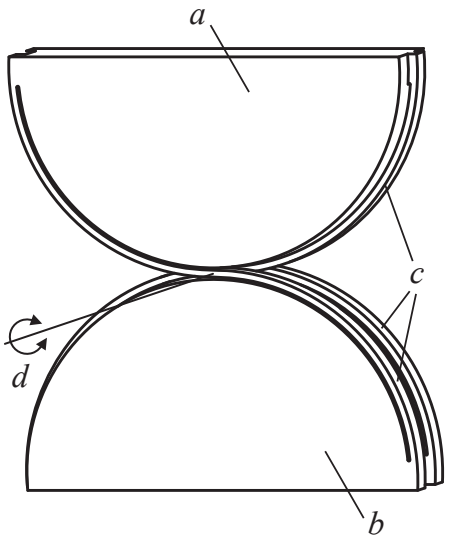

(a) A Compliant Rolling-contact Element. Source; Howell, Magleby, and Olsen [34].

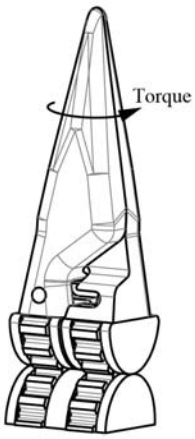

(b) Application of a CORE to a surgical instrument. Source: Grames[40].

Figure 3.16: Compliant Rolling-contact Element.

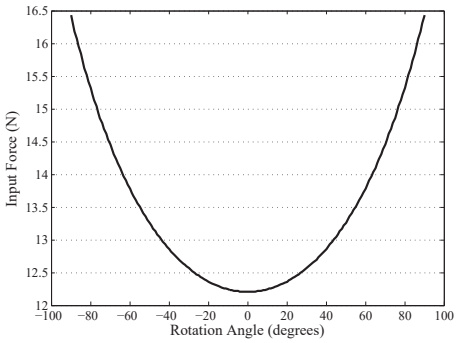

(a) Input force required to output 2N at tip over a $\pm 90^\circ$ rotation. Source; Howell, Magleby, and Olsen [34].

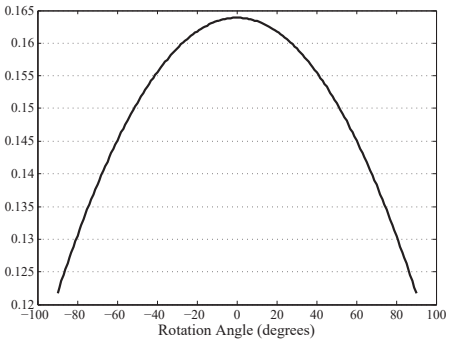

(b) Mechanical advantage over a $\pm 90^\circ$ rotation. Source: Grames[40].

Figure 3.17: Analysis on the modified CORE surgical tool in figure 3.16b.

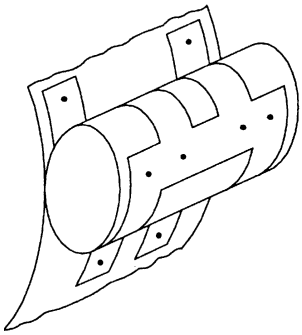

Figure 3.18: Roller assembly for a laparoscopic grasper with force perception. Source: Herder, Horward, and Sjoerdsma[41].

Radial Hinge Mechanisms

No concepts were found that could be categorized under radial hinge mechanisms. No axial mechanisms are suitable for this direction of closure due to the limited thickness available limiting the length of flexures in this direction.

Parallel Mechanisms

Parallel Anti-Buckling Grippers These grippers, as depicted in section 3.1.2, differ from the compliant clamp discussed above as counter measures are taken towards buckling behaviour. The four horizontally placed flexures assure that the actuation element (A) can only move in the desired direction, eliminating perpendicular translation and rotational degrees of freedom. The two singular flexures angled at a 45° and 135° rotation will direct the end effectors (C) in the correct direction upon loading of the actuation element (A). This will push them in a (mostly) parallel direction guide by the two sets of vertical double leaf flexures.

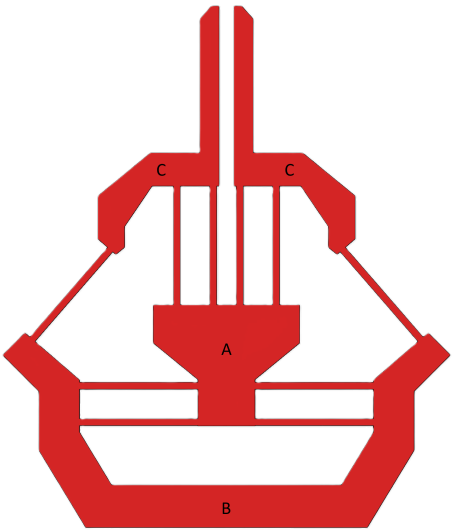

(a) A model of the gripper in the opened stage.

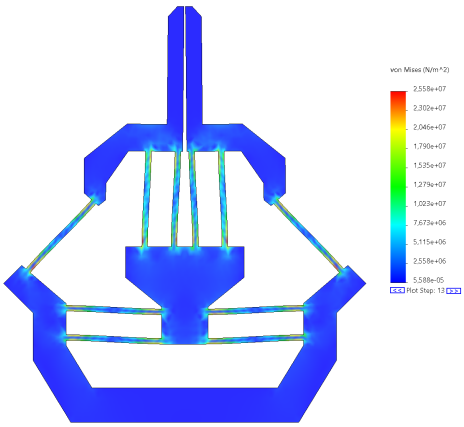

(b) Stress Analysis of the gripper deformed to the closed position.

Figure 3.19: Compliant Parallel Anti Buckling Gripper

Inputting the amount of bodies and links into the Gruebler equation (equation (3.5)) and taking into account that the four horizontal guidance flexures in figure 3.20 have a redundant set (which for small displacements should not influence the DoF) this gives;

$$DoF = 3(12 - 1) - 2 * 16 = 1 \tag{3.12}$$

Whilst the addition of extra flexures help in constraining undesired DoF, it can also be seen that these additions add a significant volume claim and a reduced range of motion. Comparing this mechanism in section 3.1.2 to the Compliant Clamp in section 3.1.2 the surface area required is roughly double with a range of motion decrease of four. Although dimensions can be altered and optimised, there is no denying that the parallel anti buckling gripper performs significantly worse on this metric.

Steerable Grippers By compressing the handles of these steerable grippers the user can close the pliers in a parallel fashion. However, by altering the force distribution over the handles, the angle of the pliers can be controlled.
The mechanism consists of two parallel sets of two parallel flexures placed in series. A single set of these allow for the flexures to contract and remain parallel. As there are two of these sets, this allows for the angle of the end effectors to be altered as well.
Determining the degrees of freedom with the help of figure 3.22a gives (accounting for the sets flexures mounted in parallel);

$$DoF = 3(8 - 1) - 2 * 8 = 5 \tag{3.13}$$

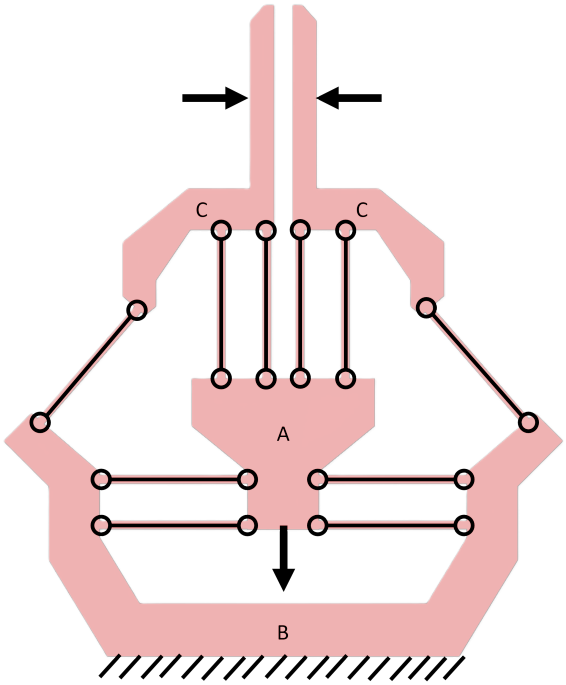

Figure 3.20: FBD for the Compliant Parallel Anti Buckling Gripper.

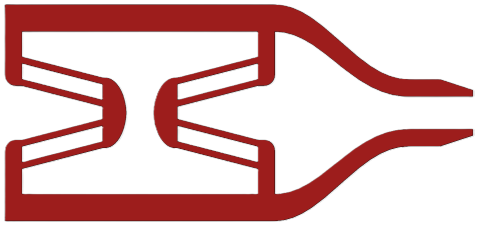

(a) A model of the gripper in the opened stage.

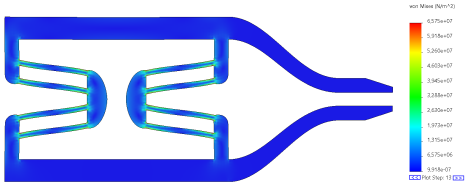

(b) Stress Analysis of the gripper deformed to the closed position.

Figure 3.21: Compliant Steerable Gripper

The five DoF are a translational and rotational constraint for each gripper and a undesired DoF in translation for the intermediary stages.
To determine the energy required to close the gripper, it is assumed that all flexures are of similar stiffness; k. For a compression of the grippers of dx this gives;

$$E = \frac{1}{2} * 2(\frac{4k^2}{2k}) * dx^2 = 2kdx^2 \tag{3.14}$$

The main differentiating feature of this mechanism is its ability to not only control translation between the grippers but also the rotation between the two of them. However, for the purpose of the compliant dAVF-valve this extra degree of freedom can lead to complications in closing the graft. At which point the attachment point for the input from the actuator would have to be place closer towards the flexures near the grippers. At this point the additional degree of freedom, and its increased volume claim, do not add anything useful to the functionality of the dAVF. An adaption of this design where the grippers and the graft are not place externally but internally could aid the balancing issue as this would make the rotational degree of freedom self correcting. Two concepts of what these adaptations could look like are shown in section 3.1.2.

Embedded Linear Motion developable mechanism A developable mechanism can be defined as a mechanism where the linkages that fold outwards are embedded in a plane. These planes can be flat, cylindrical, conical or other shapes as long as the bend line in tangent to the surface. These

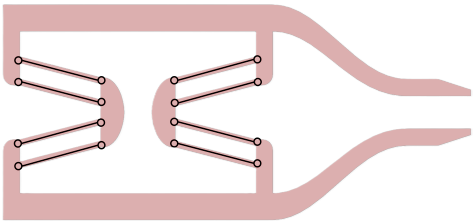

(a) FBD for the steerable gripper.

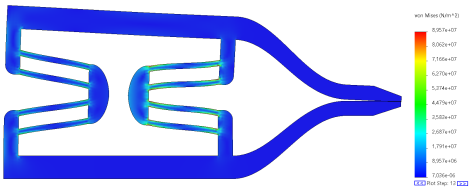

(b) Stress Analysis of the gripper deformed by undistributed load to the closed position.

Figure 3.22: Analysis on the Steerable Gripper

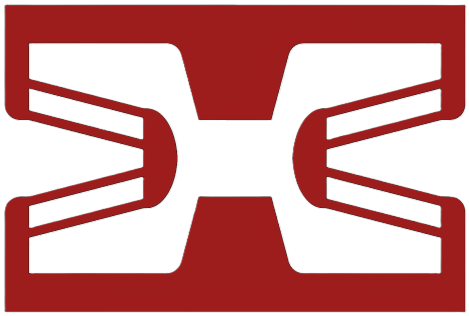

(a) A variation on the steerable gripper design where the graft is placed internally.

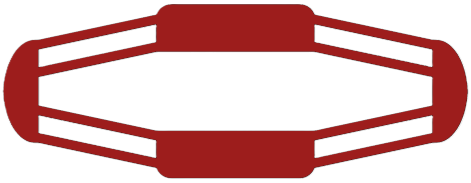

(b) A similar configuration with the flexures mirrored to allow for a smaller volume claim.

Figure 3.23: Alternative variations on the steerable gripper design

mechanisms are often combined with compliant mechanisms as this allows for monolithic production options but a developable mechanisms can also make use of traditional joints. In their paper “Embedded Linear-Motion Developable Mechanisms on Cylindrical Surfaces” the authors Sheffield, Sargent, and Howell describe multiple options for developable mechanisms place on cylindrical surface capable of achieving a linear motion. After explaining their methods for the design of a developable mechanism on a cylindrical surface, they show the implementation of various straight line linkages. These linkages are shown in section 3.1.2.

The mechanisms above have all been modified from flat linkage configurations to versions that can be embedded onto a cylinder wall. All are able to follow a (mostly) linear motion path, however each arrangement places this path on a different position relative to the cylinder. Of these different motion paths, the path of the kite-linkage seems the most applicable to a compliant dAVF-valve where the graft could be place inside of the cylinder. A side note is that this mechanism is under-constrained.

Another characteristic of importance in regard to the compliant dAVF-valve is the range of motion for each of the linkages. As depicted in figure 3.25, where on the left a mechanism is shown where over the compression of the middle element, all linkages will remain within the boundaries of the cylinder. This is referred to as intramobility. The opposite of this, transmobility, is demonstrated on the right mechanisms where linkages exceed the outer circumference of the cylinder[43]. All mechanisms shown in section 3.1.2 are transmobile.

As with the other mechanisms, two methods of adding compliance are available; lumped or distributed compliance. In their paper, Sheffield, Sargent, and Howell, provide an exemplary application for a linear motion developable mechanism on a cylindrical surface in the form of a wiper mechanisms to be attached to a laparoscopic camera probe [42]. A similar mechanism to figure 3.26.c was applied. The application of a developable mechanism allowed for a small packaging around existing bodies and lead to a successful prototype [42]. For similar reasons the incorporation of a developable mechanism for the compliant dAVF-Valve could reduce the volume claim of the device and optimize packaging around the graft. An additional benefit would be better protection of the anastomosis.

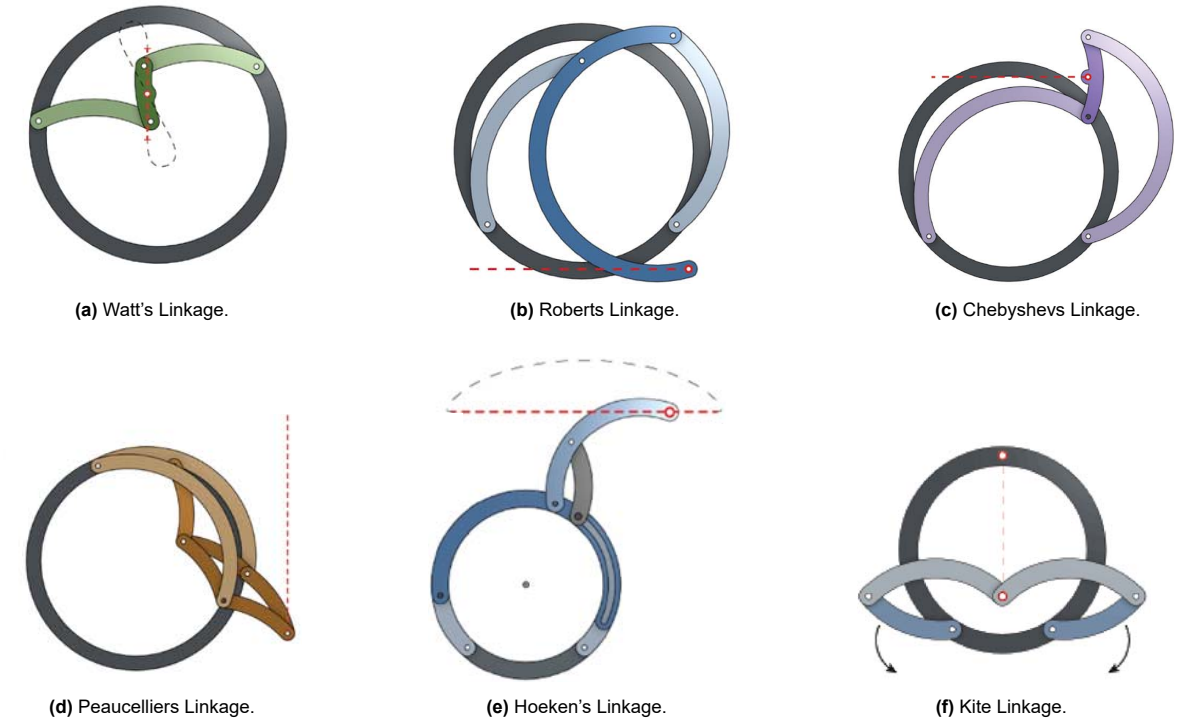

(a) Watt's Linkage. **(b)** Roberts Linkage. **(c)** Chebyshevs Linkage.

(d) Peaucelliers Linkage. **(e)** Hoeken's Linkage. **(f)** Kite Linkage.

Figure 3.24: Multiple linear motion developable mechanisms for cylindrical surfaces. Source: Sheffield, Sargent, and Howell [42]

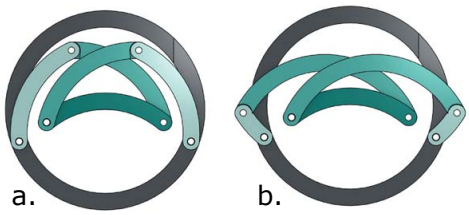

Figure 3.25: Intramobility and transmobility of Developable Mechanisms. Source: Sheffield, Sargent, and Howell [42]

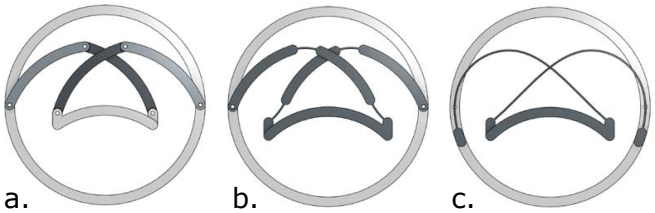

Figure 3.26: Multiple joint options for the developable mechanisms. A. Rigid links, B. Lumped compliance, C. Distributed Compliance. Source: Sheffield, Sargent, and Howell [42]

Radial Mechanisms

This category of compliant mechanisms is defined as any mechanism that uses multiple elements contracting to the centre where the graft is to positioned.

Loop A simple solution would be to tie a loop around the graft such that upon tensioning it, constricts the graft. However, as the circumference of the graft remains a constant, the walls of the graft will have to fold over itself to accommodate with the reducing diameter. This will lead to large deformations and a small orifice that remains stiff and requires more actuation force to be fully closed.
A solution that alleviates this would be to introduce some guidance to the contracting of the graft. The goal of which would be to fold the graft in to a flat state to ensure closure of the graft and a minimal energy state. Some potential solutions are shown in section 3.1.2 with an increasing number of contact-points to guide the graft to a flat position.

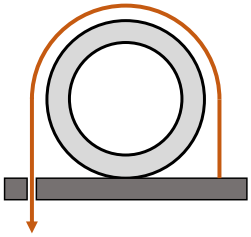

(a) A looped graft that is constrained by a single element.

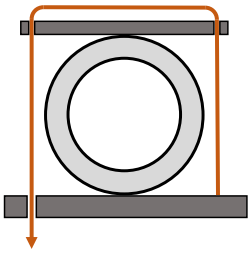

(b) A looped graft that is constrained on two sides by parallel elements.

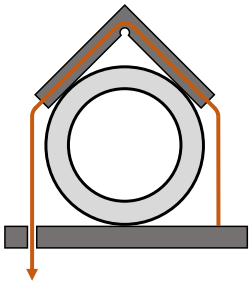

(c) A looped graft that is constrained by base element and a compliant element that folds at one point.

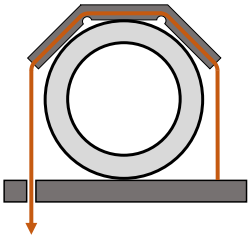

(d) A looped graft that is constrained by base element and a compliant element that folds at two points.

Figure 3.27: Concepts for a looped graft where a section-cut of the graft is shown and the tensioning element is depicted in orange.

The addition of folds in to the top element as is the case in figures 3.27c and 3.27d, will store an amount of energy in the flexure, causing these options to require a large amount of energy overall. Notches can be added to these bends to reduce their stiffness. As the position of the guidance elements is not determined, it is likely that over repeated actuation their position relative to the bottom plate will shift. Sutures connecting the graft to these elements could be added to fix these in place. Alternatively a set of guiding flexures could be added to control their position.

3D-Grippers This concept can be directly linked to the compliant clamp discussed in the gripper category in section 3.1.2. The flexure elements used are near identical but not placed in a plane but multiplied around a concentric axis. This allows for each individual element to contract inwards.
Similarly to the Compliant Clamp in 2D, this mechanism has several unconstrained degrees of freedom. The input stage in the middle, besides being free to move up and down to actuate the mechanism, can rotated along a point located above the grippers. Such a degrees of freedom is shown in figure 3.29a.

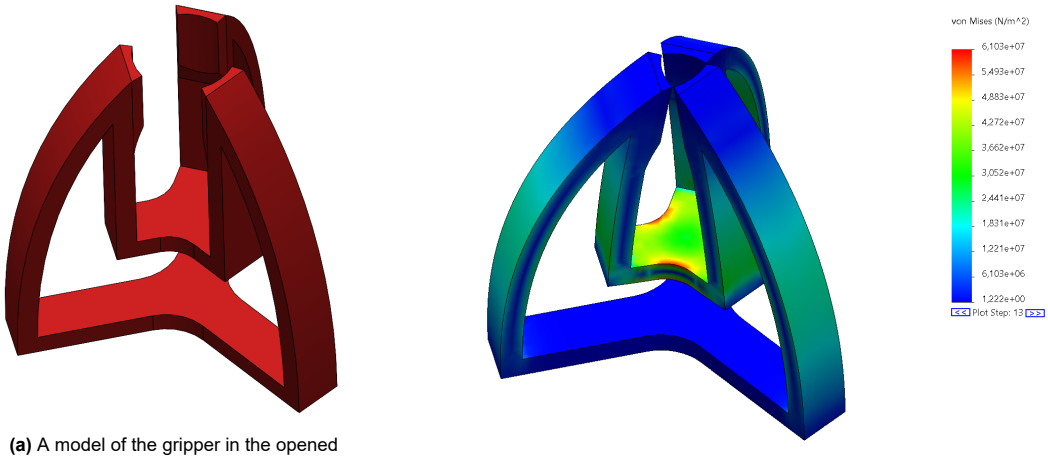

(a) A model of the gripper in the opened stage.

(b) Stress Analysis of the gripper deformed to the closed position.

Figure 3.28: 3D Compliant Gripper

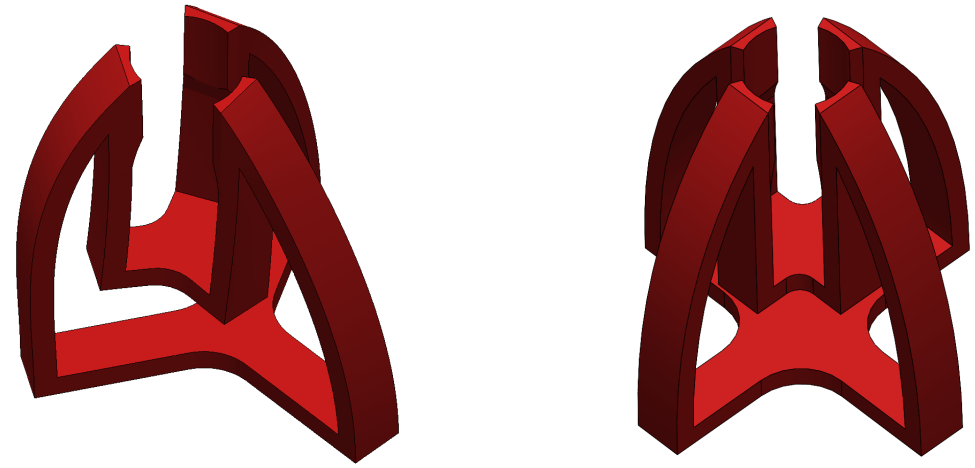

(a) An underconstrained DoF of the input stage of the 3D-Gripper.

(b) A 3D-Gripper design using four elements.

Figure 3.29: Additional analysis on the 3D Compliant Gripper

Other variations with an increased number of flexures can also be considered such as the one shown in figure 3.29b. However, as more elements are added, the required force and energy required to close the graft will increase linearly.
There is only one orientation the mechanism can be placed relatively to the graft which is coaxially. Which brings considerable challenges in forming the mechanism around the graft whilst maintaining within the allowed volume claim. Another result from closing the graft in this direction is the difficulty in closing the graft with three contact point. This will be discussed in more detail in section 3.1.3.
Considering this concept does not add anything beneficial and comes at the cost of increased volume- and energy claims it seems unviable to pursue further.

Compliant Iris This mechanism is the compliant counterpart of a traditional aperture like mechanism found in not only camera but also in some iris-valves [44]. For these applications a iris-like mechanism is chosen for its ability to maintain a somewhat round opening that can vary in diameter. In the case of the compliant iris this is done with a set of pre-curved distributed flexures connecting the two independent outer rings to pins in the centre of the iris. Multiplied, in this case six times, and intertwined this results in six of such pins that will be placed along the circumference of the circular opening.
Upon rotating the rings relatively from each others, the flexures will deform and the aperture of the iris will open, as can be seen in figure 3.30b. This deformation all happens within the plane of the iris which

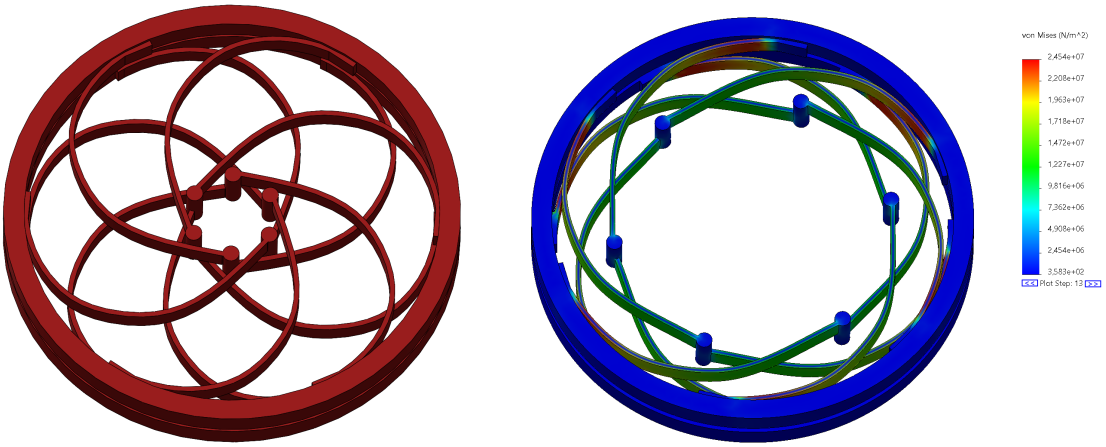

(a) A model of the compliant iris in the closed stage.

(b) Stress Analysis of the compliant iris deformed to the open position.

Figure 3.30: Compliant Iris

results in a more favourable volume claim when compared to the 3D-gripper. The amount of flexures required for this mechanism, twelve for six pairs, will lead to a large energy requirement for actuating the iris when compared to other mechanisms. Furthermore each pin will have two degrees of freedom in translation and one in rotation, of which the rotational and translational movement tangential to the graft are undesired.
Two designs mimicking the iris mechanism were identified; the pipe-gripper and a compliant Hobberman Ring. Both are shown in section 3.1.2. The first uses a similar mechanism to the compliant iris as discussed above, by rotating the rings relatively from one another and tensioning the flexures the contact pads move inwards. This deformation allows for a significantly reduced range of movement and makes this variation unsuitable for the application of a compliant dAVF-valve [45]. The contact pads are mounted to the flexure in series with a second set of smaller flexures that aid alignment, this will be discussed in more detail in section 3.1.2. The Hobberman Ring shown in figure 3.31b is a compliant variant of the original Hobberman ring. The most important feature of this compliant ring is its ability to maintain its circular shape for 99% throughout its range of movement. A compliant variant utilizing leaf flexures over notched joints was chosen for their extended range of motion. The model used in this study uses 16 leaf flexures. This will, similarly to the compliant iris discussed earlier, required a large sum of energy to accommodate for this amount of deflection.

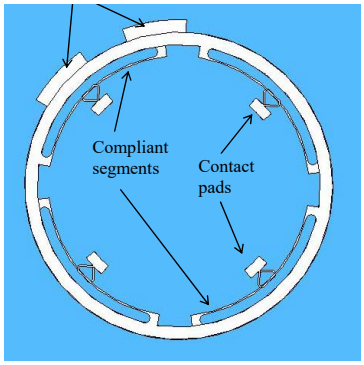

(a) Axial view of the pipe crawler mechanism. Source: Kumar, Badige, Hegde, *et al.*[45].

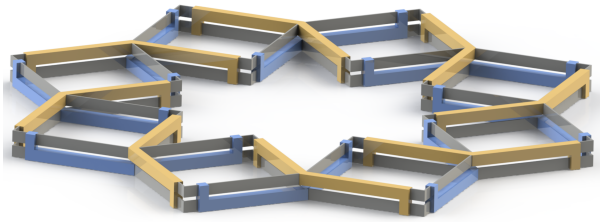

(b) 3D-render of the compliant Hobberman Ring with each individual links in either yellow or blue and the flexures depicted in grey. Source:Schreurs[46].

Figure 3.31: Other applications of iris-like mechanisms

Protection against Tissue Formation

Following the problem definition, an important sub-functionality is to protect the selected closure mechanism. The possible options are shown in section 3.1.2 for an arbitrary shape with a graft positioned in the middle.

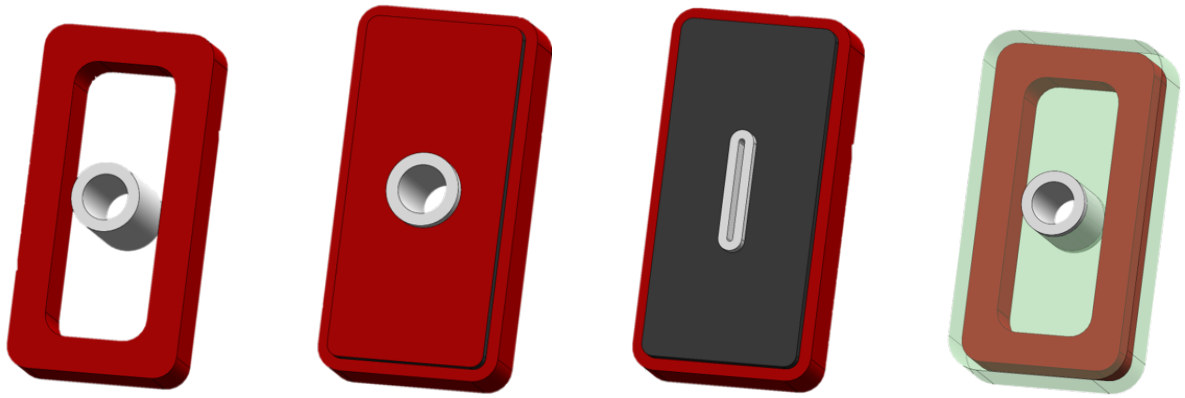

(a) No Protection

(b) A rigid seal.

(c) A flexible seal that can deform over closure.

(d) A stiff mechanism encased in a softer material.

Figure 3.32: Considered sub-solutions to protect the mechanism. The red hollow rectangle represent a mechanism with a graft place in the centre.

No Protection Without any protection, whatever mechanism selected will certainly encounter inrush of collagen that will commence the forming of fibrous tissue. This leaves the mechanism to overcome the added resistance from this tissue. Although some mechanisms might be able to do so, no material properties of fibrous tissue could be found. Therefore the added stiffness caused by the ingrowth of this tissue is hard to determine with current knowledge and would require additional investigations. Furthermore, the tissue stiffness (and other material properties) might differ from patient to patient and it is unlikely that an identical isotropic volume of tissue is formed. A benefit of choosing to let ingrowth occur, is that no additional material is required (reducing the risk of introducing a new foreign material and the effects this could cause). This approach could also be utilized in parts to design an anchoring point for the tissue to grow in to. Although a compliant mechanism with distributed flexures will see reduced resistance compared to the state of the art concept that relied on fixed hinges. Nonetheless, this option does come with an added risk making it unfavourable compared to the other options. Reducing this risk would require more significant research into the material properties and effects of tissue ingrowth.

Fixed Seal A simple to implement form of protection would be to extend parts of the mechanisms outer casing to shield the internals from collagen inrush. The would result in a rigid casing made from the same stiff material as the mechanism. The interface where this casing connects to the graft is crucial. To protect the open internals, the graft has to be fixated to the casing preventing any fluid from entering. Doing so will decrease traction on the sutures connecting the graft to the arteriovenous system. However, this does result in an open volume in the part of the graft that is not compressed. In these space stagnation of flow is likely in close position, which has high risk of resulting thrombus formation [8].

Flexible Seal A flexible seal, consisting of a soft outer-layer and an open internal space, would reduce the aforementioned risk of thrombus formation. Upon closure of the graft, the seal will deform with the graft to reduce open volumes. The flexible seal will add less overall stiffness to the concept compared to complete encapsulation due to the open inner volume. This does come with the risk that, upon leakage, the risk of failure is high. Therefore, additional efforts in the design of the interface between the seal and the mechanism and the seal and the graft have to be put in place. If leakage, resulting in failure, occur it will likely be at the interfaces of the different materials.

Encapsulated For this solution it is proposed to fill the entire mechanism (and potentially the outsides) with a known soft material. In essence the result in comparable to what would happen without any protection method where fibrous tissue formation would occur. However, in this case a known material is placed on the insides. This reduces the uncertainties mentioned involving the behaviour of the fibrous tissue that forms without any protection. And without any open spaces internally, there will be no risk of leakage. Compared to the other seal concepts, this option does add more stiffness due to more material being deformed.

Traction Reduction

This category of sub-solutions can be seen as optional as some compliant mechanisms already approach the graft parallel or have some form of alignment build in. Others however have the tendency to approach the graft at a varying angle due to the bending of their flexures. An example of this is the Compliant Crimper as seen in figure 3.10b. One approach to mitigate this could be to angle to end effectors so that when the mechanisms closes, the difference in angle between them reduces to near zero. This is implemented in the Compliant Clamp, seen in figure 3.8b.However this will introduce an axial force on the graft, resulting in additional stresses on the sutures.
Another solution would be to introduce a new DoF between the closing mechanism and the end effectors. In this section a few options to add these DoF will be discussed. All of these will add a rotational degree of freedom to aid alignment of the end effectors with the graft.

Living Hinge The living hinge, also known as a notched hinge, has already been discussed in detail in section 3.1.2. In section 3.1.2 this hinge is shown with its centre of rotation.

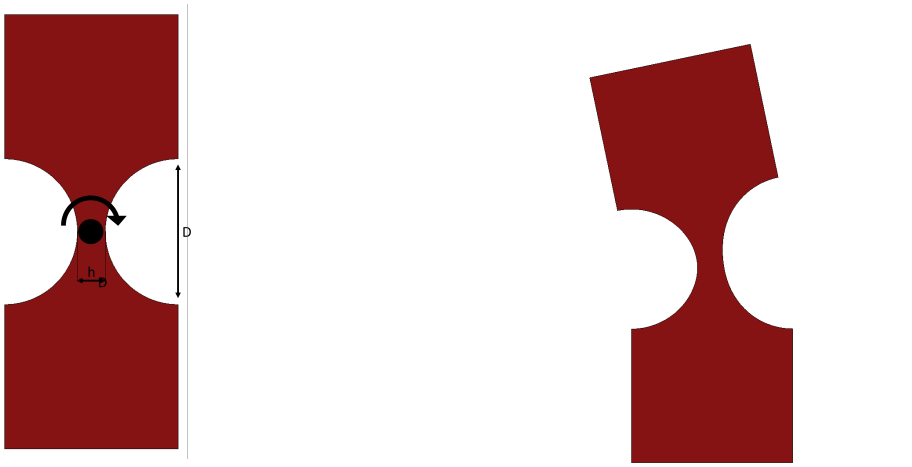

(a) A model of the living hinge with the centre of rotation shown.

(b) Deformed living hinge by introduction of a torque.

Figure 3.33: Compliant Living Hinge

As found earlier, the living hinge is only capable of small but precise deformations. These deformations will be in the order of magnitude of a few degrees. When these small angles of rotation are usable to correct the angle introduced by the mechanism, these hinges have two notable benefits. Their simplicity in design; they can simply be added by removing two half circles of material and their stiffness is tunable by selection in parameters D and h, as found in equation (3.2).

Double Blade Rotary Flexure This compliant end effectors makes use of leaf flexures rather than the notched hinge. Due to the orientation of these flexures, the axis of rotation is placed on their intersection. This is shown in figure 3.34a. This allows the angle of rotation to be placed on the surface of the end effector or in front or behind them.
Compared to the other solutions, this rotary flexure does require more space due to the leaf flexures. The simple adaptability of the mechanism to change to position of the rotation point can be seen as a differentiating factor over its alternatives [34].

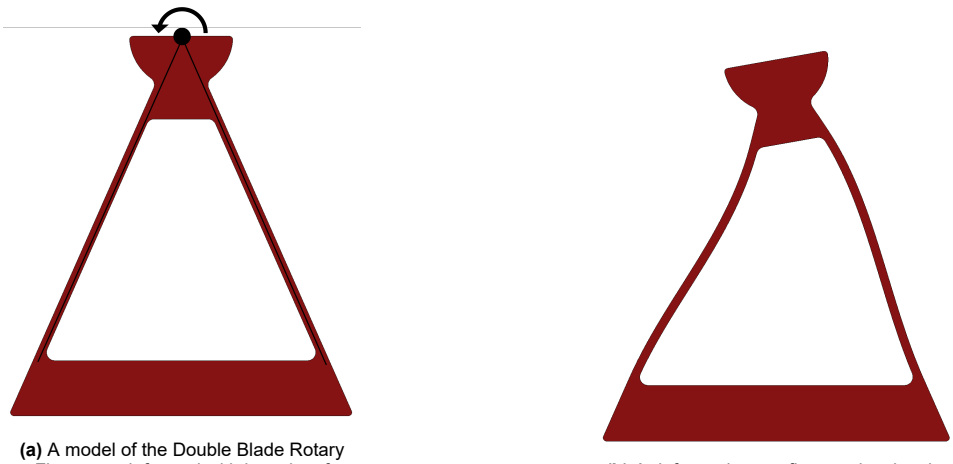

(a) A model of the Double Blade Rotary Flexure undeformed with its point of rotation at the intersection of the flexures.

(b) A deformed rotary flexure showing the pure rotation of the end effector.

Figure 3.34: Double Blade Rotary Flexure

Cross-Axis Flexural Pivot This pivot has two leaf flexures that cross over in its centre. This point becomes its centre of rotation, as indicated in figure 3.35a.

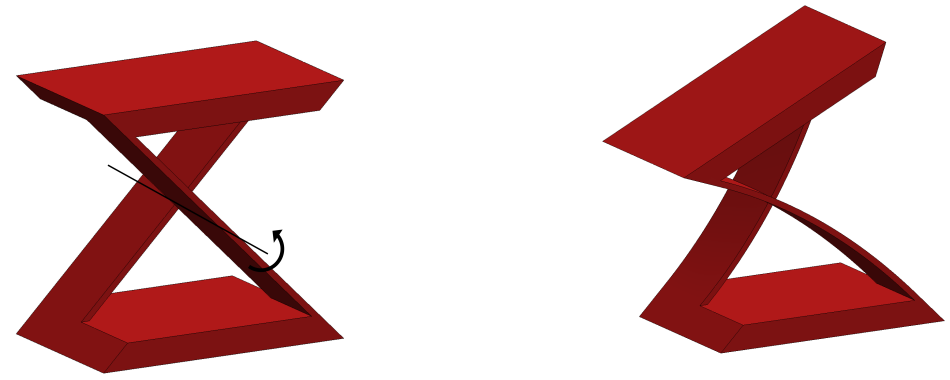

(a) A model of the cross-axis pivot Flexure undeformed with its point of rotation at the intersection of the flexures.

(b) A deformed cross-axis pivot flexure showing the rotation around its centre of rotation and the translational effects this has on the end effectors.

Figure 3.35: Cross Axis Flexural Pivot

Due to the orientation of the flexures their length can be maximised for a limited frontal-area claim, resulting in large rotational displacements for its size [34]. As a trade-off, the depth of the flexure will likely increase due to the cross over of the flexures and the required open space in between.
The centre of rotation can be changed by altering the angles of the flexures and thus the height of their intersection. Finding a specific configuration of the flexure angles will lead to a cross-axis flexural pivot with a constant stiffness when the following condition is met [34];

$$cos^2(\alpha) = \frac{-2(9\lambda^2 - 9\lambda + 1)}{15\lambda} \tag{3.15}$$

Control over Closure

All compliant mechanisms discussed so far all share a single similarity; upon actuation from its resting stage the flexures will all store potential energy. Upon release the mechanism will return to its minimal energy state. This state is determined by the shape in where the least stress is present in the flexures which in most cases is the shape in which it is produced. As discussed in requirement 1.8 on fail safety this position would logically be placed in the open state such that dialysis sessions can continue in case of implant failure. With the addition of new (local)minimal energy states, multiple opening states

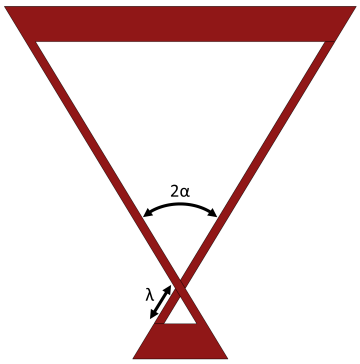

Figure 3.36: Example of a constant stiffness variant of the flexural pivot.

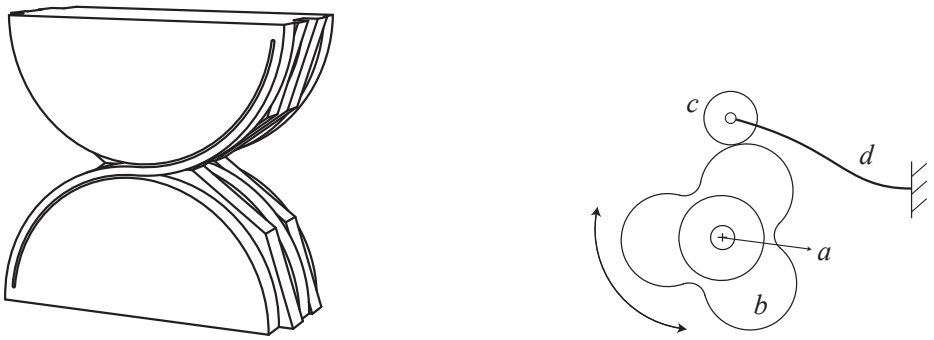

(a) A CORE mechanism with added multi-stability.

(b) A detent mechanism capable of multiple stable positions on a rotational element.

Figure 3.37: Examples of multi-stability elements that can be added or incorporated to concepts. Source: Howell, Magleby, and Olsen[34].

can be achieved with the addition of bi(or multi-)stable mechanisms. As their name suggests, these mechanisms add one or more stable positions to the mechanisms path of motion. The addition of multi-stability to a concept can either be incorporated into the elements of those mechanisms or it can be an additional set of elements added to the input. Two examples found in the *Handbook of Compliant Mechanisms* [34] are the multi-stable CORE mechanism as shown in figure 3.37a where the cylindrical rollers have altered geometry that results in multiple stable positions. The leaf flexures that bend in the S-shape are in contact with a cylindrical surface as in the concept discussed in section 3.1.2, and in between these flexures the notched multi-stable surfaces are added. The other concept in section 3.1.2 is that of a rolling detent mechanism. A rolling contact between follower (c) over the rotation body (b) is enforced by the flexure (d) [34]. It should be noted that this concept does add a rolling contact which is deemed less favourable for the prevention of and resistance to fibrous tissue formation. Such a solution could best be added to the actuator or alternatively on the input of the valve.
An alternative for creating multi-stable mechanisms is to add flexures with negative stiffness. Two simple methods for creating such a flexure are identified. Soemers provided a detailed explanation, a short overview of which is shown in figure 3.38, where a regular flexure (A) clamped at both ends, is compressed to causing the flexure to buckle (B). In doing so, energy is stored in the flexure and by moving the midpoint of the flexure in the direction indicated in A & B in figure 3.38, a part of this energy is released moving the midpoint in between two stable points, the one indicated in B and the symmetrical point. In this motion, indicated in C, the mid point of the flexure experiences negative stiffness.
For configuration C in figure 3.38 the force-displacement curve is given in figure 3.39. As can been seen in this figure; within the working range defined by v_{max} and $-v_{max}$, the spring constant is negative causing the flexure to be bistable at these points. The work domain of v_{max} caused by the buckling of the flexure can be determined by;

$$v_{max} = (1 - \frac{1}{4}\frac{\Delta L}{L})\sqrt{\frac{\Delta L}{3L}} \tag{3.16}$$

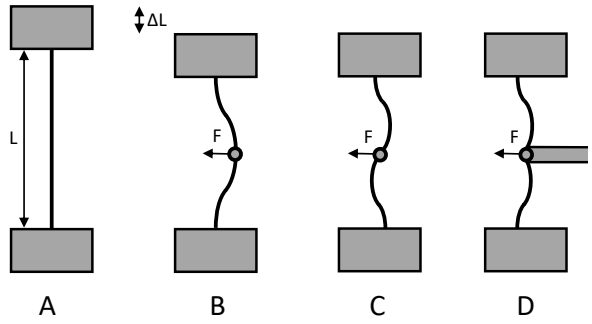

Figure 3.38: A. original straight flexure

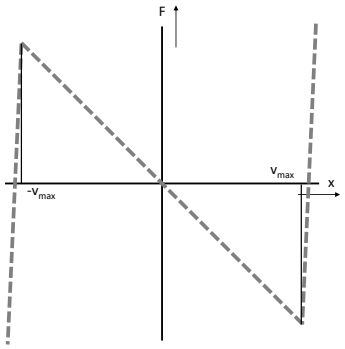

Figure 3.39: Force-displacement curve of a bistable spring. Based on a figure made by Soemers[47].

The stiffness and maximum bending stress of this flexure blade C for ($\Delta L/L < 0.25$) are respectively given by;

$$c_x = -210\frac{EI}{L^3} \tag{3.17a}$$

$$\sigma_{b,max} = 8.9Eh\sqrt{\frac{\Delta L}{L^3}} \tag{3.17b}$$

In the configuration shown B and C the midpoint of the flexure is unconstrained in rotation. This results in a slight rotation of this point over its translation between stable positions. To counter this, configuration D is proposed where this rotation is constrained, which results in a different, stiffer, bending profile as seen in figure 3.38. Whilst the working range remains identical to equation (3.16), the stiffness and maximum bending stress are now determined by;

$$c_x = -64\pi^2\frac{EI}{L^3} \tag{3.18a}$$

$$\sigma_{b,max} = 4\pi Eh\sqrt{\frac{\Delta L}{L^3}} \tag{3.18b}$$

So in order to maintain a parallel motion on the midpoint as in configuration D, a three times stiffer mechanism results compared to configuration C.
These bistable flexure configuration with their negative stiffness domains can be placed in parallel with a regular positive stiffness flexure to result in an overall lower stiffness mechanism. These bistable flexures can be placed at either the input of a mechanism or, where feasible, existing flexures can be adapted to introduce multi-stability. An example of which is given in figure 3.40 where by placing

the parallel flexures at an angle, multi-stable properties can be added without the need for additional flexures and maintaining original functionality.

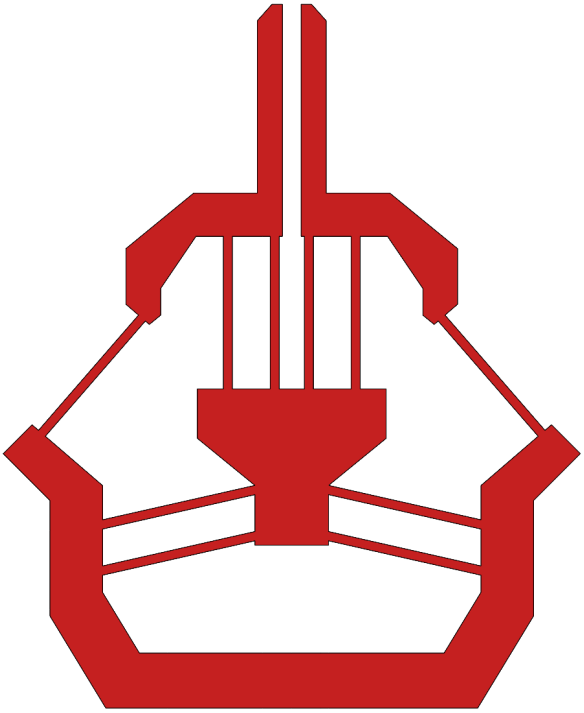

Figure 3.40: Example a modified mechanism (discussed in section 3.1.2) to include multi-stable properties without adding new flexures.

3.1.3. Graft Contact

The graft interface is where the end effectors of the dAVF come in contact with the graft. In this section the conceptual design of these elements will be discussed per number of elements used. In these sections element shape and flexible properties will be discussed. A distinction is made between one, two, three or more than three elements.
The most important criterium for selection of a closing mechanism would be force required for complete closure of the graft. As compatibility with the selected other solution spaces will also impact the selection of such a graft interface this can not be the sole influence in its selection. Assuming a set graft type and diameter it can be reasoned that the compression that requires the least graft displacement will lead to the least force required.

One Element

A singular element, although limited in applications, can be used when the element is flexible and it is formed around the graft. This can only be applied in combination with the radial loop concept in section 3.1.2. A depiction of this single element is given in figure 3.41a. As discussed in section 3.1.2, this would cause the graft to contract in a non-controllable way that lead to increased deformation and a small opening remaining in the centre. To mitigate this one could add irregularities to the surface of the loop as is done in figure 3.41b. This however will introduce a torque to the graft that is undesirable. Also, it could be argued that these are multiple elements connected with living hinges. It can therefore be concluded that options utilizing singular elements are unviable for the compliant dAVF-Valve.

Two Elements

From the state of the art in section 1.2 it can be found that all valves since the first prototype by the LUMC utilize two elements to compress the graft. This decision is likely taken to minimize traction on the graft. All elements interfacing with the graft are flat planes with a width of a few millimetres. By introducing new element types, a more efficient (less force required for complete closure) methods of graft compression

(a) A single element looped around the graft. **(b)** A modified geometry of the loop.

Figure 3.41: One element

might be found. In table 3.3 an overview of these elements and the possible combinations is given where combinations for the four possible elements are given. The graft orientation is such that it is approached by the elements radially. Obvious non-viable combinations such as any 'inverse triangular' option other than the combination with the 'triangular element' can be discarded as complete closure of the graft is not possible.

Top / Bottom	Flat	Rounded	Triangular	Triangular Inverse
Flat				
Rounded				
Triangular				
Triangular Inverse				

Graft Orientation

Table 3.3: An overview of possible dual element configurations for radial compression. All options below the diagonal are left out as these merely result in rotated versions of the other configurations. Options indicated in green are considered for further experiments. Options in red will not be able to close the graft.

The elements considered in table 3.3(flat, rounded and triangular) provide a decreasing amount of contact with the graft. Where the flat surface will provide the large area of contact which remains constant. The rounded edges will slowly increase this area. And with the triangular element contact with the graft initiates with a line contact and will linearly increase. The inverse triangular option introduces a negative of the triangular option. In combination with this, the area of contact is larger compared to the combination of two flat elements.
Other options include rotating the elements to face the axial plane (whilst still compressing the graft radially), one of the options is illustrated in figure 3.42. Although it is expected that this setup is capable

of complete collapse of the graft, closing the graft in such a manner requires an extra fold of the graft which leads to a larger deformation and will lead to a increased closing force.

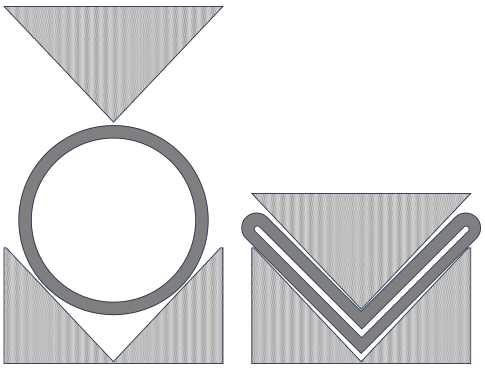

Figure 3.42: Example of graft closure by a set of elements facing the graft axially. With on the left the open position and closed on the right.

Three or more Elements

For compressing the graft with three or more elements, the options are limited considering all elements are to be placed in the same plane. Not doing so will complicate complete closure as the elements won't be in contact, which also introduces unnecessary shear forces on the graft. Thus to ensure complete graft closure n-amount of elements with a corner of $360°/n$ are to be translated evenly towards the centre of the graft. In section 3.1.3 an example is given of a configuration with three such elements. In figure 3.43b an approximation is given for the closed position. This results in n-amount of folds of 180 degrees and n-amount of $360°/n$ folds. Each of these folds put extra strain on the graft and as more deformation occurs, requires more energy to close the graft.

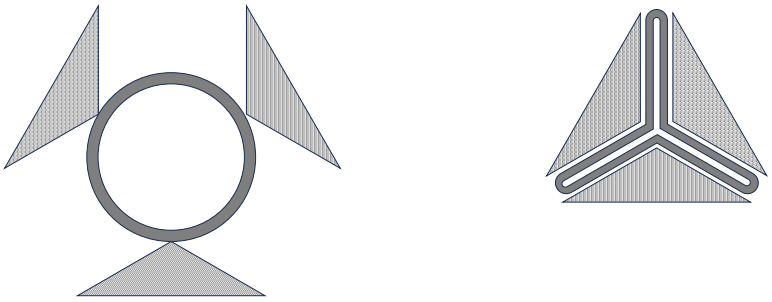

(a) Three triangular elements in the open position. **(b)** Three triangular elements in the closed position.

Figure 3.43: Three triangular elements

Furthermore, the increased number of moving elements will result in a more complex and larger mechanism. As of such it can be concluded that the use of more than two elements will likely not benefit the dAVF-Valve.

3.2. Concept Generation

In this section three of concepts will be created and developed further in order to compare them relatively as well as to the state of the art.

3.2.1. Morphological Overview

In order to create a clear overview of all sub-concepts found in their relative solution spaces and to generate feasible concepts from these for the compliant dAVF-valve, a morphological overview is created in figure 3.44 on page 48. Each row represents the identified solution spaces with the sub-solutions. To create some order in this chart, the Compliant Mechanisms and Graft options are divided into subcategories following the structure used throughout this report. As discussed in their relative sections (3.1.2 and 3.1.2) there is an option to not include compliant end effectors and/or multi-stable elements. Multiplying the amount of concepts within each sub-solution results in a total of 8.100 possible concepts. As it is not feasible to investigate each and every concept, a selection of concepts most likely to succeed is made. To do so each concept is created by selecting sub-solutions based on a focus. This approach will help to find options that score well on the criteria (discussed in section 2.8 in page 16) in the Harris profile as well as a good variation within these selected concepts. As all concepts are rated to the same criteria, this approach can be seen as a sensitivity analysis; what effect does the focus on one criteria have on the performance on the others. The selected focusses are; Robustness, Compactness and Traction Reduction and will be discussed below. These concepts were selected on the aspects deemed challenging at this stage of development.

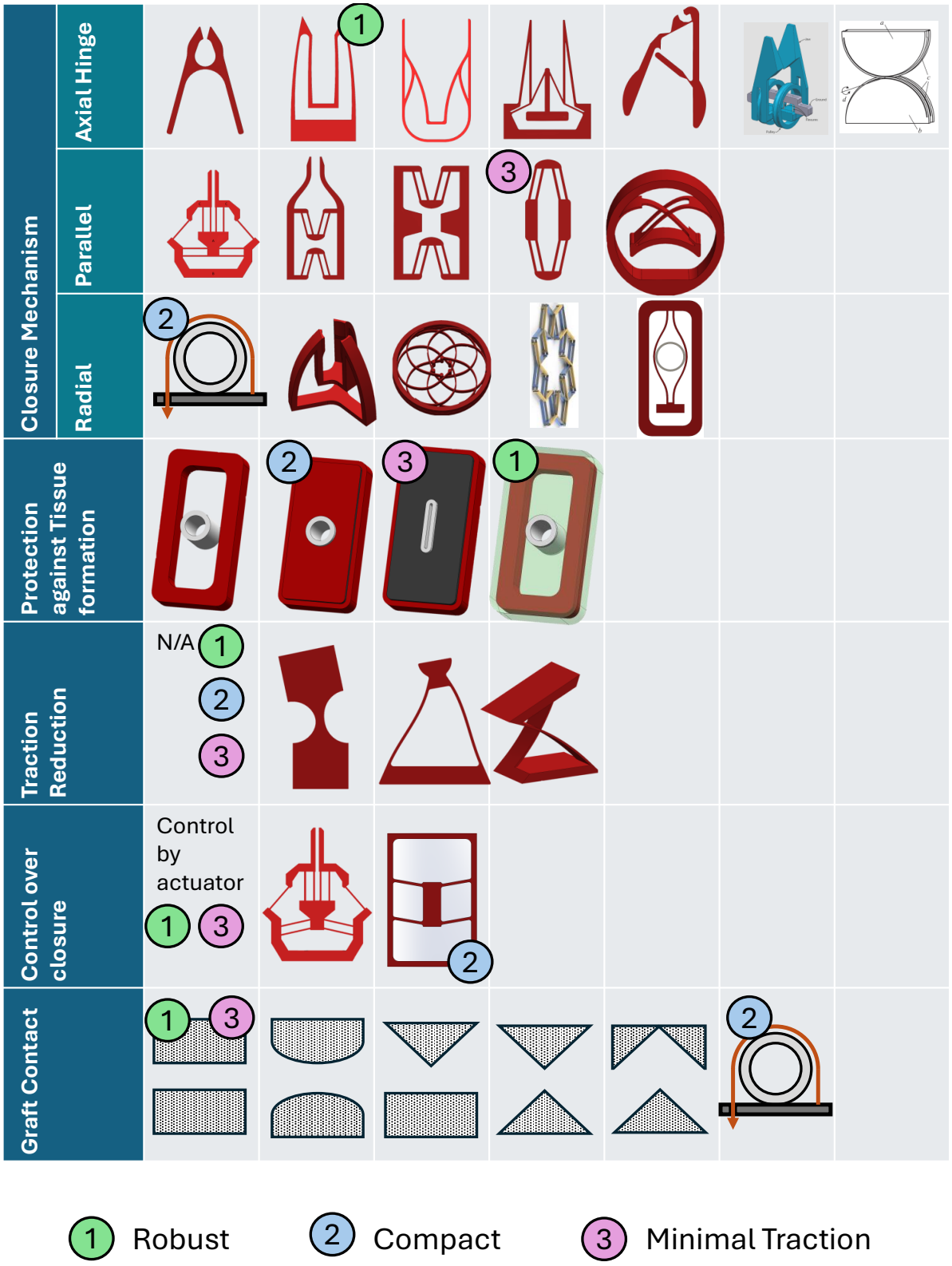

Figure 3.44: Morphological overview for the compliant dAVF-Valve. The identified sub-solutions for each functionality are given per row. For the Closure Mechanism functionality, three sub categories are defined to indicate the motion of closure as shown in section 3.1.2. For the creation of concepts, one sub-solution of each main category is selected. This is indicated with the coloured numbers for the concepts considered in this project.

3.2.2. Concept I: Robust

As specified in the project objective, the goal of this project is to develop a compliant variant of the dAVF-valve that is more resistant to fibrous tissue formation and the effects this has on performance and durability. It makes sense to have this as one of the focusses for an concept; a robust dAVF-Valve.

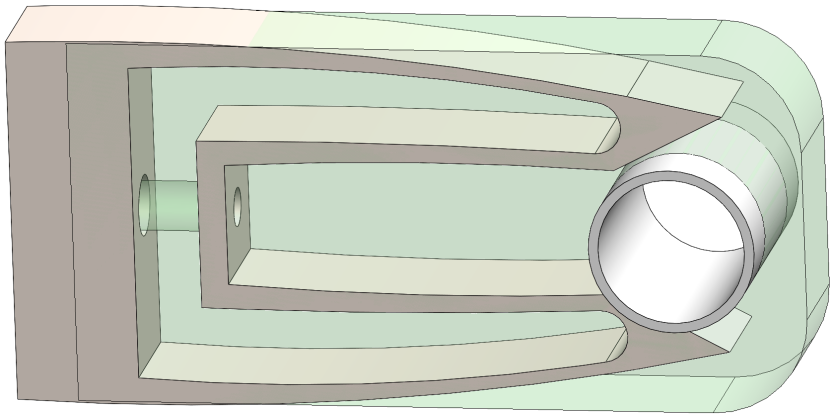

Figure 3.45: Simplified model for the Robust concept

The robustness of this concept, of which a simplified model is given in figure 3.45, could be reasoned to be based on a bio-inspired design. Where the compliant mechanism acts as a bone like structure that provides the motion path. To prevent all forms of tissue formation in or around this mechanism, as softer bio-compatible material is cast around it. The compliant mechanism chosen to base this concept on is the compliant clamp, discussed in detail in section 3.1.2 on page 26. Although other, similar options were considered. The distributed gripper, section 3.1.2 page 28, was discarded due to its increased number of flexures that not only increase complexity but reduces volume for the soft material which will likely increase overall stiffness. The compliant crimper concept, section 3.1.2 on 27, as discussed in its relative section, shares multiple similarities with the compliant clamp with the main difference being the bending of the curve leaf flexures of the crimper rather than the buckling behaviour in the clamp. For now the clamp is chosen for its simplicity, however, a combination of both concepts should be considered if this concept is to be further developed upon. All other enhancements are omitted as it is assumed that all additional flexures reduce the space where the soft material can compact and expand. Considering the soft material is low in stiffness enough, the overall stiffness of the concept would not require the use of a bistable mechanism. This material is likely to be a silicone elastomer due to their low stiffness, elongation and most importantly biocompatibility [48]. To ensure traction on the anastomosis remains minimal, the geometry of the compliant mechanism has to be optimized as to reduce the angle at which the end effectors approach the graft. Another optimization that will be required is to limit small gaps between the flexures as well as between actuation stages. The point of optimization is a downside for this concept. It is estimated that development time would overall be longer compared to the other concepts due to two different factors. On the one hand due to the complexity involved with buckling leaf flexures over a relative large deformation making an analytical approach non-feasible. On the other hand due two the involvement of two materials that interact with one-another. The estimated approach would be to simulate the model to optimize parameters and start testing soon to allow for multiple iterations. This is feasible as the manufacturing process of this concept is relatively simple involving three steps without assembly. First the 2D-profile of the mechanism is to be cut using a EDM-machine, as milling is not feasible due to the slender and delicate flexures and lasercutting will struggle to reach the desired precision at this thickness. After the mechanism is cut, two holes have to be drilled and tapped to attach the input to. After this the mechanism is to be placed in a mould to cast the silicone.

3.2.3. Concept II: Compact

Due to the limited volume available and the tendency of the mechanisms found in the sub-solutions to require a larger are, the focus for this concept will be compactness. The foundation of this concept will be the looped mechanism, as discussed in section 3.1.2 on 36, due to its simplicity and limited

footprint. In line with the goal for compactness, the smallest possible graft is chosen and any non-essential enhancements are omitted where they are not required. As the loop tightens around the graft, no compliant end effectors are required, saving space.

Iteration I

For the first iteration of this concept is was assumed that a bistable mechanism is required to actuate the mechanism as specifically the opening of the graft is assumed to require this push. A simplified model of the compact concept is given in section 3.2.3.

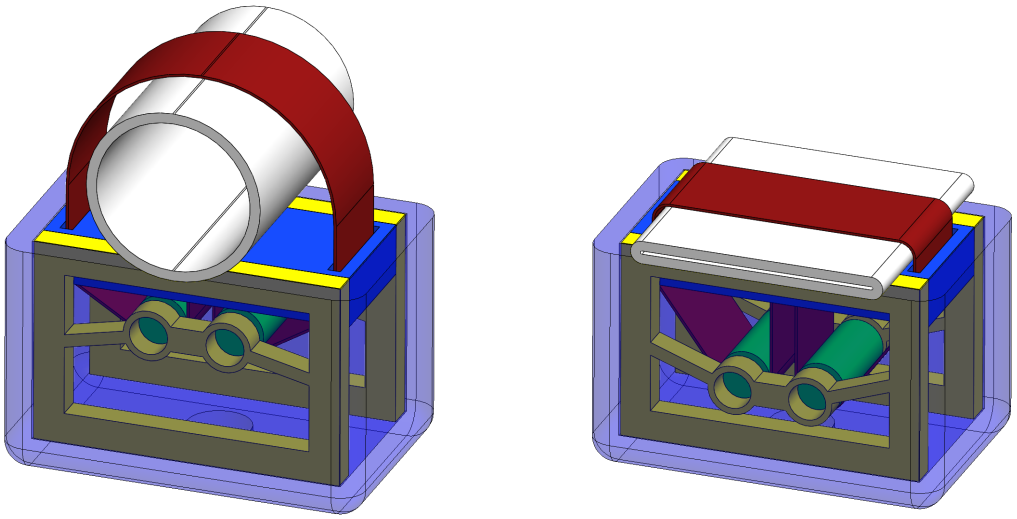

(a) A simplified model of the compact concept in the opened state.

(b) A simplified model of the compact concept in the closed state.

Figure 3.46: Compact Concept

In red the compliant loop is shown which is to be cut from a thin sheet of material to allow for its flexibility. The actuation length of the loop can be determined by first determining the internal width of the closed graft and substituting this into the ;

$$2\pi(r_{in} + t) = 2t\pi + 2w \tag{3.19a}$$

$$w = \frac{2\pi r_{in}}{2} \tag{3.19b}$$

$$dL = L_{open} - Lclosed = (\pi r + 2r) - (w + 2t + \pi t) \tag{3.19c}$$

For a double layered graft with $D_{in} = 6mm$ and $t = 0.44mm$, this results in a retraction of 7.5mm of the loop. As this is more than the maximal actuation distance of 4.5mm from the actuator, the loop will be closed from both sides. This would also be beneficial as a retraction from the one side would cause a shear force introduced on the graft which introduces a torque on the anastomosis. The red loop is to be pulled through the blue block of soft material that acts as a seal to protect the internals of the mechanism from ingrowth. A seal was chosen over filling the frame similar to the robust concept, as the volume reduction here is much more significant. The materials is to be soft enough that as the loop is retracted, it is wiped clean, and yet it has to withstand the compressive force from the closure of the graft. For this purpose it will be supported by the yellow frame. The green roller are internalized in the frame, and guided by the flexures cut out of the yellow frame, guide the loop. The flexures in this frame can be configured in thickness and angle to tune the stiffness and bi-stability. As it is shown in section 3.2.3, the flexures will have a bistable effect. Due to the limited length available in this direction and the large displacement required, these flexure will either be to stiff or will be overloaded leading to failure. This is to be dealt with in the next iteration.

Iteration II
With the lessons learned from the first iteration, this version removes the bi-stability and places the flexures in an optimal orientation. With a lengthwise orientation, the flexure can be as long as reasonably can be. As shown in figure 3.47b, the loop is fixated between the green flexures and the yellow actuation block. The outer sheath of the bowden cable is attached to the blue shell and the inner cable to the actuation block. Upon actuation, the block is pulled down, guided by the flexures that are attached on the other end to the white seal allowing only for the desired sliding direction.

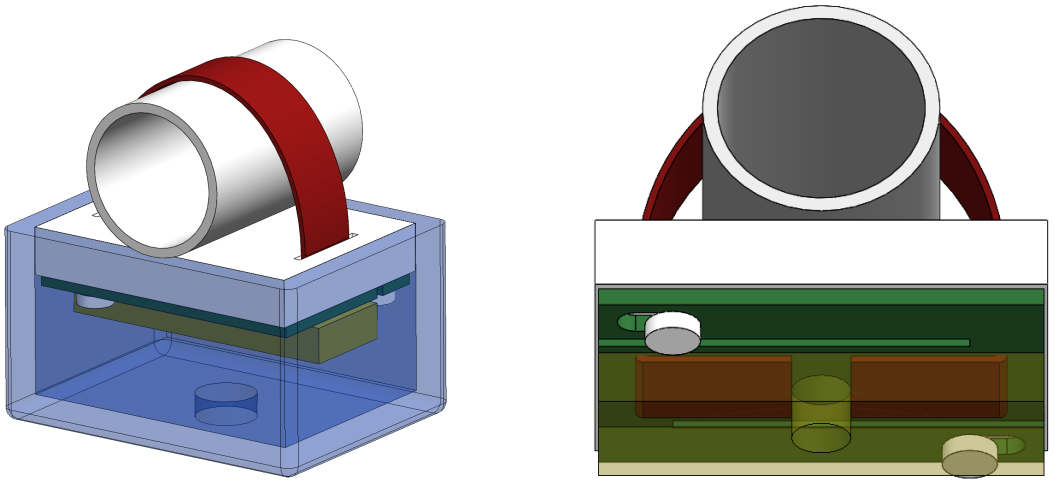

(a) A simplified model of the second iteration compact concept in the opened state.

(b) A detailed view of the internals in second iteration of the compact concept.

Figure 3.47: Second Iteration Compact Concept

The optimized flexures should bring a significant reduction in stiffness. Furthermore, this concept allows for a simpler assembly with a reduced part count. However, upon consultation, it was found that the direction of actuation, present in this and the previous iteration, is not favourable. Upon exiting the mechanism the cable would have to bend a sharp 90 degrees towards the intended placement of the actuator. Upon this revelation, it was decided to take the proceedings of this iteration, onwards to a new version where this mishap is addressed.

Iteration III
Developed upon the previous iteration, this proposal for the compact concept should meet basic functionality. The issue of input orientation is addressed with the introduction of a rocker, as seen internally in section 3.2.3, to introduced an input perpendicular to the output direction. As seen in the figure, this rocker rotates around a pin connection. A compliant alternative was considered in a configuration where the virtual intersection of both flexures forms the rotation point. The relation in lengths of these two flexures would determine the transmission ratio. However, it was found that for a displacement for ΔL, as found in equation (3.19), a flexure length large than the volume requirement prescribes was required. Thus, a hinged rocker was introduced with dimensions selected to provide a transmission ratio required to couple the loop retract length to actuator input displacement. A double rocker setup was considered to ease the traction on the graft, but as the thickness requirement was limited, this idea was dropped. Due the to omission of a flexure, other than the loop around the graft, a conventional spiral spring was added between the rocker and bowden cable input. This spring should ensure the anastomosis to return to a safe open state in case of failure in the actuator or cable.

3.2.4. Concept III: Reduced Traction

As was the case in the first iteration of a dAVF by the LUMC and described in further detail in item 1f, the forces the systems exerts on the anastomosis are to be minimized due to fragility in the interface between graft and arteriovenous system. To achieve this a parallel motion type mechanism was selected, specifically are derivative of the steerable gripper mechanism due to their, compared to the other parallel mechanisms, frontal surface area.

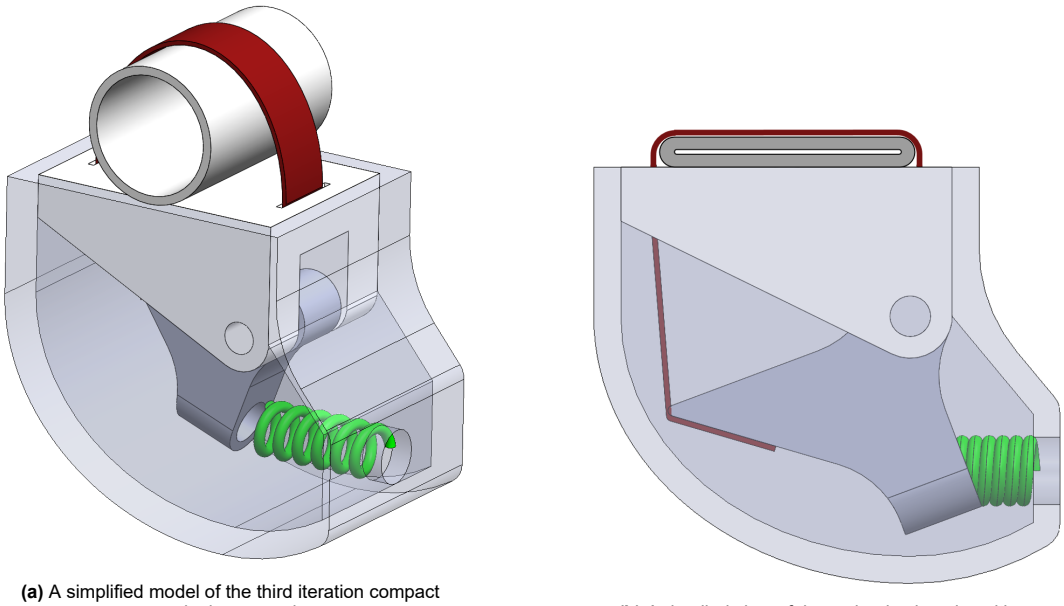

(a) A simplified model of the third iteration compact concept in the opened state.

(b) A detailed view of the rocker in closed position.

Figure 3.48: Third Iteration Compact Concept

Iteration I

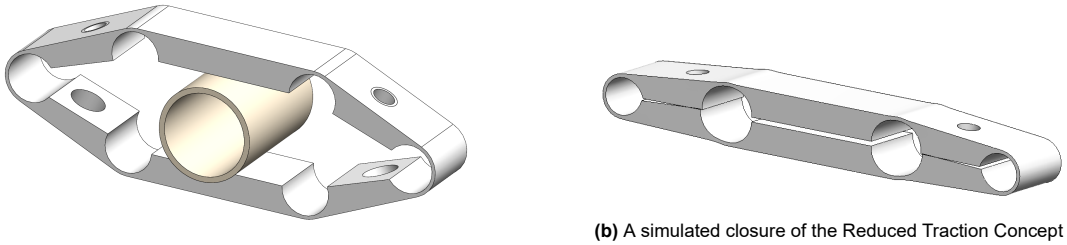

(a) A simplified model of the first iteration Reduced Traction concept in the opened state.

(b) A simulated closure of the Reduced Traction Concept in closed position. The closure of the graft was not simulated and is left out of this image.

Figure 3.49: First iteration of the Reduced Traction Concept.

The first iteration of this concept is mechanically identical to the compacted concept discussed in section 3.1.2 other than the leaf flexures are replaced with notched joints at the hinge points. This decision was made due to their proclaimed greater flexibility [38]. A simple non-linear simulation for a PEEK model with flexure-width of 0.3mm showed a required input of 6N for complete closure of solely the mechanism. The actuation is performed again by a Bowden cable, or in this instance a cable that splits from one two two inputs. This due to the inputs being attached to the threaded holes the angled arms of the mechanism, as can be seen in figure 3.49a. The position of the input points was chosen to facilitate the correct transmission-ratio between the input-and output displacement. For the protection of the mechanism against tissue formation, a seal placed on the front and back is proposed. However, before this could be implemented, an external consult pointed out that, in a similar fashion to the second iteration of the compact concept (section 3.2.3), this actuation direction inline with that of closure, is unfavourable. In response to this a second iteration was developed.

Iteration II

In search of a new actuation direction, perpendicular to the direction of closure, an additional two layers were added to the mechanism discussed in the previous iteration. The function of these extra members, as can be seen in section 3.2.4, is to achieve a in-plane perpendicular transmission between the cable input and the output on the graft. By applying a tension force between the two stage visible on the left-hand side, this causes the two flexures on this side to contract and initiate a closure. Due to the

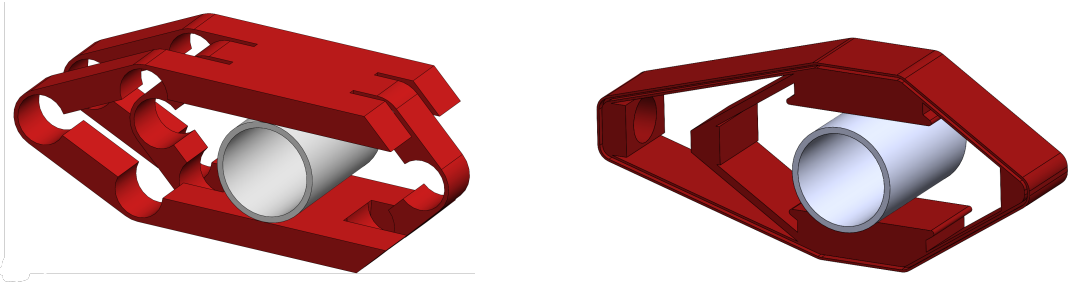

(a) A simplified model of the low traction concept with added members to facilitate side actuation.

(b) A model of a version utilizing leaf flexures instead of notched flexures.

Figure 3.50: Reiterations on a side actuation of a reduced traction concept.

lateral non-symmetry, the flexure thickness of the flexures on the opposite side have to be adapted to provide an equal stiffness in order for the end effectors of the mechanism to remain parallel.

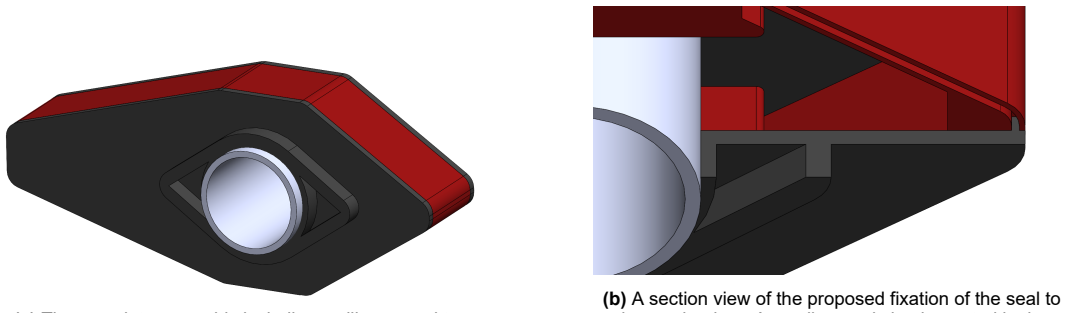

(a) The complete assembly including a silicone seal to protect the mechanism against intrusion of tissue.

(b) A section view of the proposed fixation of the seal to the mechanism. A small grove is implemented in the compliant mechanism in which the silicone seal is fixated.

Figure 3.51

For protection against tissue formation, a seal was chosen over a complete silicone encasing as used in the robust concept. This is due to the volume reduction over closure of this mechanism is orders of magnitude larger compared to the robust concept. As silicone is non compressible this would result in an increased stiffness compared to the alternatives. For this reason a silicone seal is chosen fixated along the outer contours of the mechanism. To ensure the seal remains attached to the mechanism over closure, the seal is form closed in a grove which can be seen in the cross-section of the seal in figure 3.51b. Also visible in this image is a proposed extended contact area formed to aid contact over closure and prevent inrush cells. The risk of a failure in the seals is not taken lightly as a failure of this system will likely result in a failure of the system. Thus, in further development of this system a thorough investigation in the mitigation of leaks of any kind will have to be performed.

3.3. Concept Selection

To converge towards the design concept with the most potential, the concepts as discussed above are to be evaluated using a Harris Profile. Multiple interpretations of this method exist and are applied throughout various projects. For this selection the graphical approach [49] was applied in favour of the weighted scoring method. The primary reason is that where the concepts are well developed enough for a relative comparison to each other and the state of the art, none of the designs can realistically be scored on a scale from 1 to 10. For this score to be confidently attributed for each criteria and each design a significantly longer design period would be required. Secondary, the weighing score with which each score is multiplied with a weight factor that quantifies the importance of the criterium. As both the scoring and the weight factor are highly uncertain at this point in the design, this would introduce a non realistic image of confidence to the selection. The graphical method [49] focusses on the comparison of criteria between the concepts where a (as much as possible) the concepts are compared to an existing state of the art, in this case the pinjoint-dAVF as discussed in section 1.2. For each criterium a concept can score significantly bad (- -), moderately worse (-), moderately better (+) or

significantly better (++). As the Delft Design describes; it can be tempting to see a Harris Profile as an objectively true comparison . However at this stage a truly objective examination of the concepts is not realistic nor desirable. To ensure a certain level of repeatability; for each criterium a short motivation for each score will be given in this section. The Harris Profile that results of this comparison is given in figure 3.53.
The justification for the scoring of each criterium is given in the following section.

3.3.1. Resistance to Fibrous Tissue

For the scoring of this criterium a risk assessment of the formation of fibrous tissue and its influence on the dAVF-valve. This can be based of three factors; open volume, surfaces for the tissue to attach to and the ability of the mechanism to deal with this tissue. Based on these factors, a score of + or - is given based on the concepts ability to prevent tissue formation. The mechanisms ability to cope with potential ingrowth will determine the other part of the score which is then combined to result in a final score within the Harris profile. For the robust concept where the entire mechanism is surrounded by a protective layer of silicone preventing any intrusion resulting in the formation of fibrous tissue. Seeing there is no point of entry and thus no open volume or surface on which tissue can grow and disrupt the functioning of the mechanism, this results in a ++ scoring. The Compact concept is only partially protected against the inflow of collagen. The internal mechanism is sealed (assuming the barrier through which the loop is fed holds), leaving only the loop surrounding the graft vulnerable for fibrous tissue. Especially upon closure the volume outside of the graft can fill with tissue, causing a resistance to opening of the valve. In terms of protection this is similar to the state of the art. However, the flexible loop is likely less resistant against tissue formation than the stiff compactors featured in the state of the art. In this comparison, a score of - is applied. The reduced traction concept is scored with a single +. The seal offer protection for the entirety of the design resulting in a +. However, as the empty space internal to the mechanisms is not protected, any inrush of collagen will cause to tissue formation. This results in a similar risk as is the case for the current state of the art dAVF. Therefore, it is rated equally on the factor of mitigation leading to a score of + on resistance to fibrous tissue.

3.3.2. Traction on Anastomosis

The final loads that the concepts exert on the mechanism in non-trivial to predict at this stage in development. For the comparison of the proposed concepts and the state of the art design, the focus was on the motion path followed by the end effectors. For the state of the art mechanism attention was paid to reducing extra loads on the graft during closure [8].
The compliant clamp mechanism considered for the robust concept has a similar type of closure path as the state of the art. A distinction is the length of the arms, that can have a greater length for the compliant mechanism as can be concluded from figure 3.9a. What is uncertain is how the mechanism will anchor in the body, ideally it would anchor to fixate relative to the graft. The silicone surrounding should help in this aspect. For these reasons the robust concept is rated with a 0 as similar performance to the state of the art is expected.
Earlier iterations of the compact concept would reduce traction on the graft due to their retraction of the loop on both sides. However, the version that meets all the requirements is only capable of retracting the loop at the one side. In attempts to resolve this, it was found that the hinged rocker mechanism can not reasonably be stacked within the volume constraints. This leaves a mechanism that upon closure of the graft will introduce a torque on the anastomosis leading to an undesired load of the sutures. At the high risk of torquing the sutures , the compact concept is score with a - -.
With a focus on parallel closure the reduced traction concept is estimated to perform the best on this criterium. The only introduction of an additional tractive force on the graft would be if the mechanism is not anchored as intended. This however is deemed unlikely due to the majority of contact-surface is keeping the mechanism in the intended location. Therefore a score of + is inputted in the Harris profile.

3.3.3. Energy Storage

The potential energy stored in the mechanism upon actuation ideally is minimized to reduce operating force for the user. At most it is not to exceed the limit set in requirement 1.5. As the storage of energy does not occur in conventional pin-hinges as the state of the art, and all concepts are to be compared relatively to the state of the art; all mechanisms involving flexures will inherently score lower. The storage of energy within the flexures is one of the disadvantages discussed in section 3.1.2.

The robust concept mechanism as depicted in figure 3.45 has been simulated in a non-linear FEA which indicated a rough 20N is required for closure of the mechanism over an input distance of 1.4mm. For this mechanism (which is not optimized other than on not exceeding the yield stress), assuming constant stiffness, this would result in 0.014J required to close the mechanism. Assuming that the silicone does not more than double the stiffness, this still leaves margin of 50% for the estimated energy budget. This places this concept in the middle at a score of -.
The compact concept is harder to predict, but as pin-hinges are utilized to achieve the internal motion, the only energy stored is within the loop and the small coil spring. The coil spring is to be dimensioned to provide enough force to ensure correct opening of the loop. The required force to do so is, at this point in development, hard to predict as the effects of FBR on this specific type of mechanism are unknown. Compared to the state of the art however, it can be argued that due to the control over stiffness of the spring and with the deformation of the loop considered insignificant , this concept scores a 0.
A preliminary simulation of the mechanism shown in figure 3.50b revealed that to close the mechanism, 3mm input was required at 40N of force. Again, as is the case for the robust concept; these values derived from a non optimized model and should be interpreted as a range rather than exact. The increased stiffness however does make sense due to the added number of flexures (dimensioned similarly to the robust concept). Assuming similar linearity in stiffness this results in around 0.06 J spend on solely the mechanism. While the seals will likely add less stiffness compared to the silicone filling, this is still rather close to the maximum budget available of 0.072J. For this reason the reduced traction concept scores - - for the Harris profile.

3.3.4. Design Complexity

As discussed in section 2.8, the complexity of design is expressed in an estimation of the workload to turn the proposed concept into an optimized design that can be validated. An important note is that at the time of scoring each concept is at the same stage of development. This is important for all criteria but noted especially for this criterium. Furthermore, it should be noted that a zero rating set by the state of the art would take into account the work done in that study on which this research is build upon.
Based on the conceptual design, there are two uncertainties that are identified for the robust concept. The first being optimization of the mechanism in order to reduce stiffness and increase input/output ratio. This will likely require multiple iterations utilizing FEA and testing prototypes to ensure the outcomes. Secondly, the behaviour of a silicone encasing of the mechanism is largely unknown. No relevant literature could be found on compliant mechanisms operating in a softer medium. Consultation with several experts pointed out that this behaviour is complex to model in software and is best to iterate on by experimentation. This leads to a complexity score of -.
The compact concept won't require much optimization. The use of conventional pin joints internally leads to a relatively simple transmission. In further work on this concept this transmission can be improved upon by creating a variable contact point between rocker and loop over rotation of the rocker. Most work will be understanding the dynamics of the loop over closure of the graft and the effects FBR will pose on the mechanism. This complexity relative to the other concepts is rated at +.
Finalizing the design of the reduced traction concept would take approximately a similar amount of development time compared to the robust concept. Based on the design of these two concepts, it can be estimated that the parallel closure mechanism proposed will take more time to optimized base on the current state and the larger amount of parameters to optimize for. The seal on the other hand is likely less influential on the functioning of the concept. Therefore these two concepts are rated the same.

3.3.5. Manufacturing Cost

The cost of manufacturing is dependent on several aspects; material selection, manufacturing method, required tolerance, part count, volume and mass to name a few. For each part of each mechanism the desired method of manufacturing was selected, largely dependent on material choice and geometry of the part. To gain a realistic cost estimation, for each concept a quote was requested. Multiple companies offer instant quoting such as Shapeways, Xeometry, Onshape, 247TailorSteel etc. For this estimation Xeometry was selected for their broad range of materials and manufacturing techniques. In order to account for economies of scale, a quote was requested for 50 prototypes, the maximum quantity, to limit the effect of mould costs as would realistically be the case. The quotes were requested at the same time to limited the effects in demand. This resulted in an estimated cost of €46.50 for the

robust concept and €67.70 and €60.70 for the compact and reduced traction concepts respectively. These results are in line with expectations, the increased part count of the Compact Concept will have influenced its cost. Where the tolerance required on the slender flexure of the reduced traction concept as the doubled amount of silicone seals will have increased its price relative to the robust concept. As these instant quotations do not offer a clear insight in the cost breakdown and due to the influence of order quantity, these estimates are solely used as a comparison between concepts. Therefore, the robust concept is scored with a + and the small difference between the other two is interpreted to be within the margin of error, and as a result are both score 0.

3.3.6. Volume

As describe in the criterium description, the volume of the concepts is determined by the dimensions a bounding box containing the model. The dimensions for each of these volumes was determined using the concept models in CAD. The results of which are depicted here;

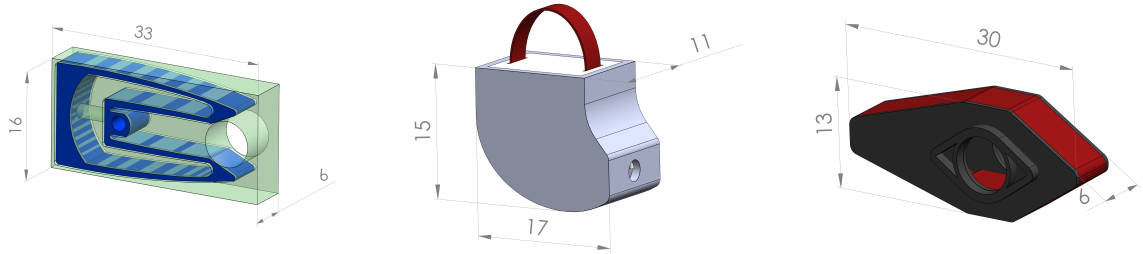

(a) Robust Concept **(b)** Compact Concept **(c)** Reduced Traction Concept.

Figure 3.52: Volume of the boundary boxes.

The volumes as shown above are taken from the conceptual designs, although these designs were build with the volume constraints in consideration, they are yet to be optimized. All measurements are taken without the Bowdencable or graft attached as was the case for the state of the art [8]. This design had the final dimensions of 30mm in length, 15mm in height and a thickness of 7mm [8]. The robust concept has a similar volume, with the length being 3mm over. This dimension is likely to be reduced without major consequences, therefore a score of 0 submitted for the robust concept. The compact concept delivers an interesting result. With a form factor different from the other concepts. The width is slightly over with 11mm, but considering this is a conceptual design this can easily be reduced to be back into requirements. Especially in length this concept offers a reduction of almost half of the state of the art. Compared to the other concepts, the graft is located outside of the design. The effects of this are unknown, however were it to be included the height would be 6mm bringing it over the initial requirement. As this is currently a large unknown, the concept is rated with a single +. The Reduced traction concept is similar in volume to the robust concept and the state of the art and scores 0.

3.3.7. Mass

The mass of the concepts is found by evaluating the models (with the proposed materials applied) in CAD. This is referenced to the mass found of the state of the art concept. The state of the art is 8 grams [8].
The total mass of the robust concept is 5.5 grams. This is a 30% reduction, resulting in a + score on mass.
For the compact concept, a mass of 2.5 grams is calculated, a 63% reduction.
The total estimated mass for the Reduced Traction Concept amounts to 2.2 grams which would amount to a 72% reduction.
A few notes should be made on this criterium, the most noteworthy is the effect of material selection on the total mass. The state of the art concept consisted largely of parts milled from 316L stainless steel, likely due to the required stiffness for this concept operate safely. Another being that, similar to this design study, mass is not a top priority for the dAVF. In between the concepts evaluated here, the outlier is unsurprisingly the robust concept where all of the empty space is filled with silicone, adding to the overall mass. In a similar fashion to the evaluation of the state of the art, the Bowden cable and graft were not included.

Table 3.4: Robust Concept

Part	Material	Mass (g)
Clamp Mechanism	PEEK	1
2 Seals	Silicone	1.2

Table 3.5: Compact Concept

Part	Material	Mass (g)
Loop	Nylon	0.1
Seal	Silicone	0.3
Bracket	PEEK	0.5
Rocker	PEEK	0.5
Spring	316L	0.1
Encasing	PEEK	1

Table 3.6: Reduced Traction Concept

Part	Material	Mass (g)
Clamp Mechanism	PEEK	1
2 Seals	Silicone	1.2

Compared to the state of the art design this is due to materials with lower densities (and larger performance indexes) are utilized.

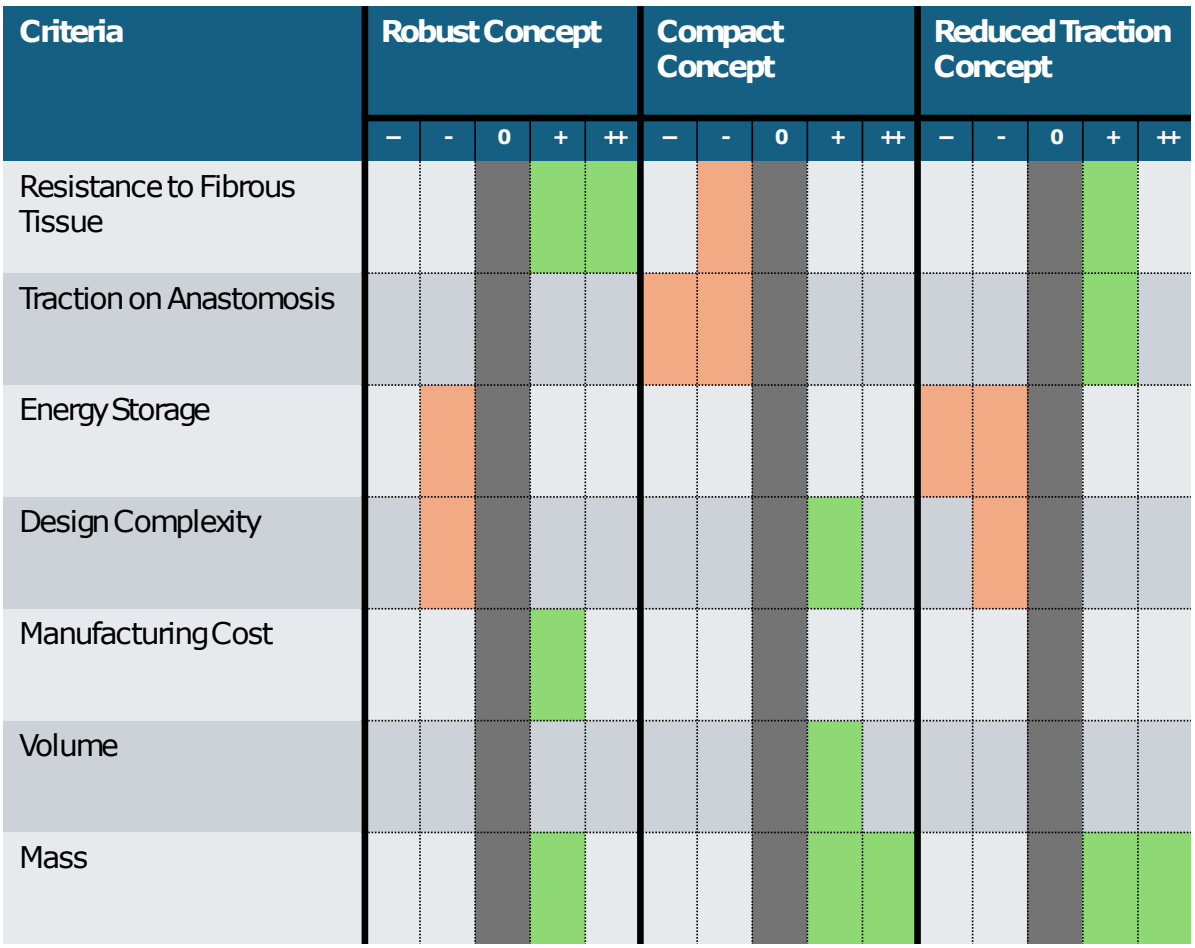

Figure 3.53: Harris Profile with a visual focus to select the best performing concept design based on criteria. The criteria are sorted on importance from top to bottom. Each concept is scored with a - - , -, 0, + or ++ relative to the state of the art. Justification of each score is given in this section.

3.3.8. Selected Concept

The Harris profile used in this study, as explained in to further detail on 53, does not make use of multiplication of scores by weighing factors. Rather, a graphical approach was applied [49]. The weight factors used to express importance of the criteria in other methods, are replaced by the order of these criteria. The criteria placed at the top of the Harris profile are of greater importance than those place below. This method of ranking allows a differentiation in importance of criteria without putting a mostly arbitrary number to it. Each criteria is scored as discussed in the previous sub-sections. For each criteria a method of scoring was explained, allowing for potential new concepts to be scored in a similar fashion. Starting at the top of the Harris profile, it can be found that both the robust and the reduced

traction concept score well on resistance to fibrous tissue (a key criteria for this research) and traction on the anastomosis (a focus of earlier study on the dAVF [8]). The reduced traction concept however does score unfavourable on the energy stored due to the short flexures in the compliant mechanism. On design complexity, a criteria placed in the middle and thus deemed medium important, the compact concept appears to score preferably to the others, however for the both resistance to tissue formation and traction on the anastomosis it is expected to perform no better than the state of the art and therefore not considered for further development. Further down the ranking of the criteria no shocking differentiation of scoring was found. Out of the Robust-and the Low Traction Concept, the decision was made to continue work on the Robust concept with the main differentiator between the two the aforementioned energy storage.
As described in the Design Guide [49] followed for this selection process, a Harris profile does not portray true and final performance for each concepts best version but rather, it is a performance assessment of the concepts in the design state at the time of selection. Knowing this, specific care was put into ensuring all concepts discussed are at an equal level of development to ensure the concept with the best potential was selected. This concept of the Robust dAVF will be developed and optimized further in the next chapter.

4

Detailed Design

After a concept was selected in the conclusion of chapter 3, this chapter will describe the improvements and optimization of this concept to a detailed design that is to be verified and validated in chapter 5. The structure of this chapter is split in to two sections covering the two iterations that were performed for the development of the compliant DAS-valve. Below a graphical overview is given of this process that will form the contents of this chapter;

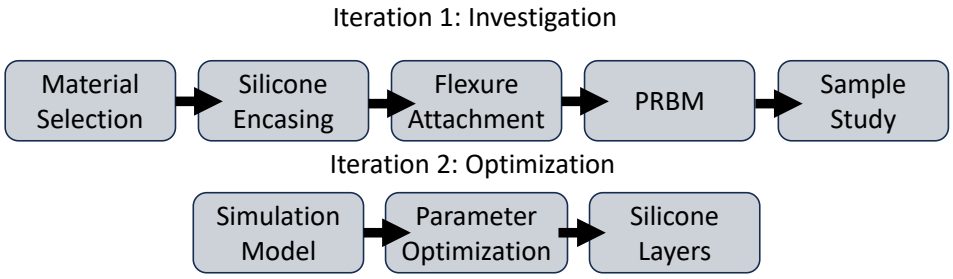

Figure 4.1: Graphical overview of the design steps for the detailed design.

4.1. Design Iteration I: Investigation

The goal of this iteration cycle is to investigate the fundamental questions for this design. Topics covered will be the material selection, casting of silicone and the shape and parameter relevant to the performance of the compliant mechanism.

4.1.1. Material Selection

This design consists of two materials; the stiff material used for the flexure and the softer material used to fill and protect the mechanism. An in-depth study on biocompatible materials and associated manufacturing techniques is performed in a literature study prior to this thesis project [24]. The use of biocompatible materials on various applications was studied and a list of suitable and often used materials produced. An overview of materials is given in figure 4.2 where from the Level 2 BioEngineering material database, the metallic and polymeric materials were filtered and the materials identified in the material literature study are labelled. To find the best material an optimization line is to be plotted in the Ashby plot in figure 4.2. Two goals were considered, resulting in different indexes;

1. **Flexibility:** With a goal to find the material capable of bending the furthest without failure [50]. First the stress in a flexure with thickness t bent in radius R can be found with;

$$\sigma = E\frac{t}{2R} \tag{4.1}$$

Rewriting this to the goal of minimizing the radius (to achieve the largest bent);

$$R_{min} = \frac{t}{2}\frac{E}{\sigma_y} \tag{4.2}$$

By separating the design parameter from the material parameters the following index is found;

$$M = \frac{E}{\sigma_y} \tag{4.3}$$

Thus, as the ashby plot is logarithmic, the slope of the index in this figure would be 1, as seen in the line labelled with 1. Flexibility.

2. **Elastic Energy:** Another goal could be to minimize the energy stored within the flexures. The energy stored can be written as the work per unit volume which can be written as;

$$dW = \sigma d\epsilon \tag{4.4}$$

Knowing that for plastic and metallic materials the stiffness is linear in the elastic domain, this can be written as the area underneath the stress strain curve;

$$w = \int_0^{\sigma_y} \sigma d\epsilon = \int_0^{\sigma_y} \frac{\sigma d\sigma}{E} = \frac{1}{2}\frac{\sigma_y^2}{E} \tag{4.5}$$

Hence a line with a slope of 2 is plotted in the Ashby plot.

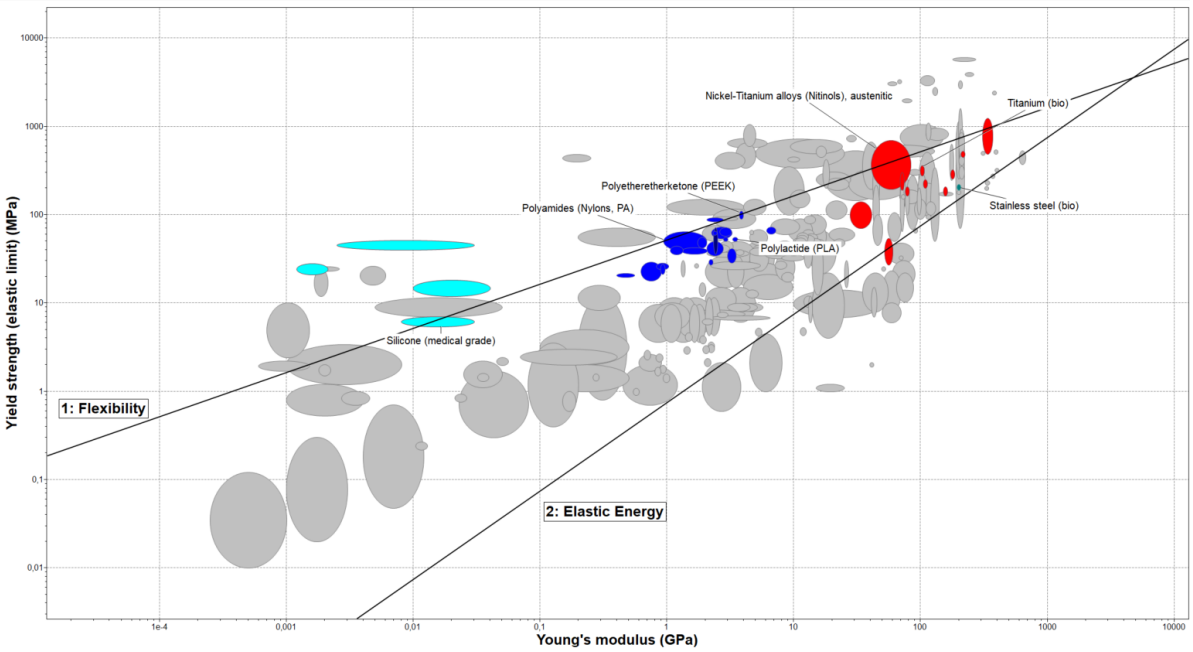

Figure 4.2: Plot of Yield Strength vs Youngs Modulus of various biocompatible materials and two performance indeces; 1. for optimizing flexibility, 2. for optimizing spring stiffness. Source: CES-Edupack.

Considering the challenge of fitting a compliant mechanism the decision was made to utilize the first index focussed on flexibility. Maximizing this for the materials for the compliant mechanism resulted in a slight favour for polymeric materials with PEEK and Nylon among the top contenders. From the metals nitinol would also have been an option but was discarded for its cost and difficulty to machine (this would especially introduced complexities further considering the slender flexures required).
For the selection of the material for the protective encasing of the mechanism, the second index minimizing stored energy was applied on the elastomeric materials (light blue in the figure). This family of materials was chosen for their reduced stiffness compared to the material of the compliant mechanism, around an order of one hundred times less stiff. Minimizing the second index with a slope of 2, silicone was found as the most favourable material.

4.1.2. Silicone Casting

The effects of the silicone encasing on the compliant mechanism was one of the uncertainties following the conceptual design in chapter 3. Consulting with two experts in the field of modelling of compliant mechanisms and construction with silicone, both individually advised to not pursue simulation of the compliant mechanism within silicone due to the complex interfaces. Rather they advised to evaluate and quantify this effect by constructing a prototype and test for its stiffness. For the compliant mechanism the conceptual design as seen in figure 3.45 was printed in PLA (slightly less performance in terms of flexibility compared to PEEK but near equal in stiffness).

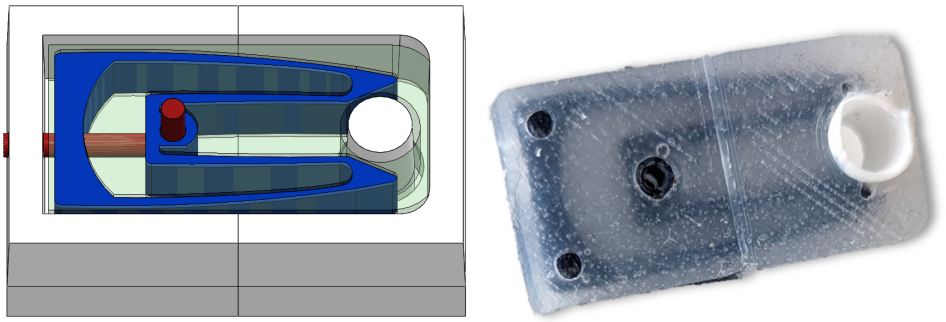

(a) CAD-model of the white castinng mould for the Silicone Encasing. In blue the compliant mechanism, fixated with locating pins in red.

(b) The result of silicone casting. Noteworthy are the open volumes were the locating pins were located and the small bubbles within the silicone material.

Figure 4.3: Study into Silicone casting around the conceptual compliant mechanism.

A casting mould was designed to pour the test silicone into, this design is shown in figure 4.3a. Notable considerations applied to this mould are the release angles of 2 degrees and the construction of two parts split in the middle to aid the release of the poured product. On the bottom of the mould stand-offs are added to lift the compliant mechanism 1mm to ensure a complete enclosure by the silicone material. The compliant mechanism is fixed in place with two locating pins (indicated in red in figure 4.3a). The horizontal pin also ensures a cavity is included in the silicone were the Bowden cable is to be attached in the final design. Finally a conical locating feature is added to hold the graft in place during casting. The specific silicone selected was based on availability and consultation, the Platsil Gel-00 with a Shore hardness of 00-30 [51], the softest material available. A point of notice is that this specific material is suited for life casting and prosthetic appliances, no mention is made of biocompatibility within the body. This is in all likelihood not the intended purpose of the manufacturer (Polytek Development Corp), thus the prototypes developed here, although similar in mechanical performance, are not suitable for implantation. Ensuring a mix of 1:1, the silicone was poured using a syringe. First ensuring the base of the mould was covered, after which the mechanism was fixed into place using the afore mentioned locating pins and the silicone was poured over the mechanism to surround it and left to dry. The result of this can be seen in figure 4.3b. In this image, the small air pockets within the material can be seen. This likely occurred either during mixing of the two components or during pouring using a syringe. To reduce this effect, in the following silicone production, the mixed silicone is to be place in a vacuum for 1 minute to remove all of the air within the material. Other noteworthy observation, as mentioned by the staff, silicone does not bond with the other material but simply forms around it. Pulling on the silicone reveals that no bond was created between the mechanism and the silicone other than it being form closed. Also the graft, although place in the mould during pouring, is poorly attached to the silicone.
The prototype depicted in figure 4.3b was fixated at the input stage and pushed closed on the usually fixated side by a PI Linear stage with a Futek 45N Loadcell attached. This was done using two identical mechanisms, one encased in silicone and one not. The still frame taken from a video of the actuation of the mechanism are shown in figure 4.4 where the stage actuates the mechanism from the right.
Important to note again, is that this mechanism is taken from the conceptual design and in no way optimized. The sole purpose was to test the effects of the silicone. In the closed state of the silicone prototype it can be seen that the (unpressurised) graft does not completely closed as the contact surfaces are lacking in size. The point of contact could still be seen in testing, the dimensions of the mechanism will be iterated upon at at later stage.

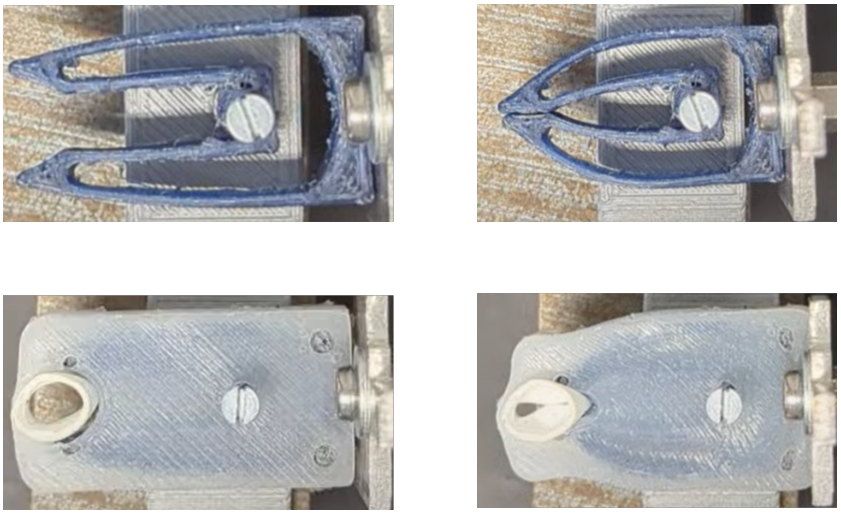

Figure 4.4: Still frames of the stiffness tests for both only the mechanism and the mechanism encased in silicone, in opened state on the left and closed on the right.

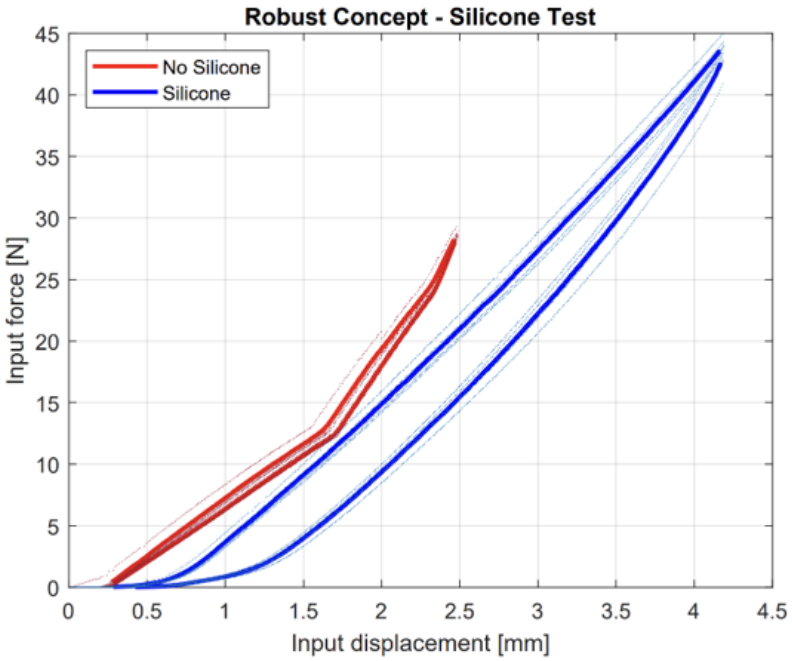

Figure 4.5: Result of the Siliconetests in the linear stage.

During testing, the mechanism was actuated 5 times (where one actuation is both opening and closing of the graft) at a speed of 0.1mm/s sampling the input force at 10Hz. This data was accumulated in Matlab where the data at standstill was remove and the remaining data sorted in opening and closing movements. These data sets were combined and using a moving average the stiffness response in figure 4.5 was found.
For the red line, only the mechanism, multiple stiffness coefficients were found over closure, a characteristic that will also be seen in later iterations. The first coefficient is the closure of the mechanism until the contact points start touching at 1.7mm of actuation. From this point where contact is established, the stiffness will increase as the contact surfaces are pushed towards each other until at 2.3mm of actuation the mechanism is closed. For the blue line, mechanism in silicone, a slower increase in force response is noticed. This can be attributed to the actuation of the mechanism in this setup. By pushing on the back of the mechanism, a 1mm layer of silicone is compressed before the mechanism starts to close. This can clearly be seen in figure 4.5. Furthermore a slightly increased stiffness is found over

closure and the contact points, discussed for the mechanism, are less pronounced. This is attributed due to the silicone between the contact surfaces that is compressed during closure. From this test it can be concluded that the added stiffness by the silicone layer for the conceptual design, increases the force required to close the graft from 28.5N to 42.2N (an increase of 48%). This results in a mechanism that can be closed with the actuator (with a max of 45N), however in section 4.2.4 the silicone encasing will be improved upon to increase the margin. Reducing the stiffness in the mechanism will be discussed in the following sections.

4.1.3. Flexure Placement

The design of the compliant mechanism was started with a short but fundamental study into the placement of the flexures. For this purpose a rudimentary version of the compliant mechanism was drafted in CAD and parametrized for a design study optimization. The model used is shown in figure 4.6. This model was applied to a two dimensional non-linear FEA coupled to a design study with the free variables, fixed parameters and goals noted in table 4.1.

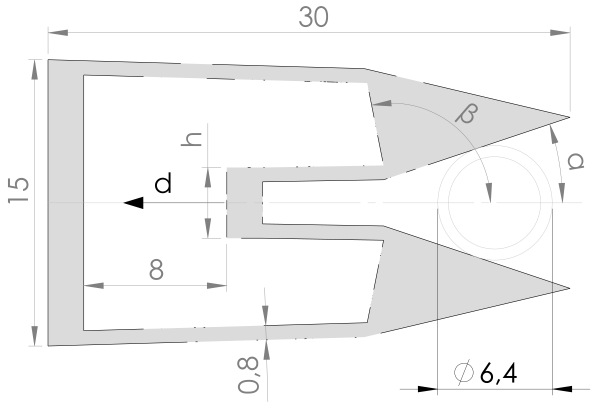

Figure 4.6: Parametric model for flexure placement study

Table 4.1: Optimization Settings - Attachment Point

Free Variables	Values	**Fixed Parameters**	Values
α- Contact Angle Gripper	12°- 18°	Input Displacement	4.5mm
β- Angle to Top Flexure	25°- 150°	Outer Dimensions (LxHxW)	30mmx15mmx5mm
h - Input Stage Height	2mm-5mm	Flexure Thickness	0.8mm
		Distance Input-Output	8mm
		Outer Diameter Graft	6.4mm

Goals	Target
Y-displacement Gripper	Close to 3.2mm
X-displacement Gripper	minimize

The free variable of interest in this study is the angle β(the angle to the top flexure). In conceptual versions so far this was assumed at around 90°. Decreasing the angle however could lead to a longer top flexure which in turn would decrease stiffness lead to a better closure. However, by moving the attachment point to the contact surfaces, the mechanism will change its closing motion. The other free variables; the angle αand h, were added to help the optimizer to find a correct closure.
A few iterations of the optimization are shown in section 4.1.3
The optimizer for the design study found an optimum for the given fixed parameters, a closure in Y-direction of 3.2 and a minimal displacement in X-direction at angle βabout 120°, angle αat 18°and h at 5mm. This results in geometry similar to the model shown in figure 4.7c. Analysing the simulations, it

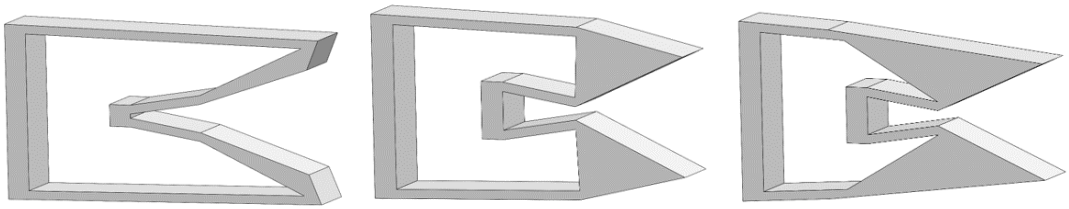

(a) Model with β= 25°. **(b)** Model with β= 90°. **(c)** Model with β= 150°.

Figure 4.7: Flexure placement models at different angles of β.

was found that for models similar to figure 4.7a, the rotation was too little to allow for complete closure of the graft as well as a large displacement in the direction of the graft which would introduce undesired traction of the anastomosis. The models ranging between the ones depicted in figures 4.7b and 4.7c showed similar closure in Y-direction, however, due to the increased rotation of the contact surfaces (and the free variable of angle αallowing for this increased rotation) the model with a sharper angle βwas favoured by the optimizer. As stiffness or the accompanied stresses in the members were not given as a constraint, the effects of a shorter flexure were omitted by the optimization. Which is why a the resulting shorter top flexure is not punished. Seeing that as all angles of βbetween 90 °and 150 °were capable of closing the graft, a decision was made to favour the longer flexure and implement an angle of β90°. The height of h was not of much influence on the closure motion and angle αwas found to be a useful free variable as it allowed the optimizer to analyse multiple motions.

4.1.4. PRBM-study

With the goal of gaining more insight in the effects of the parameters of the flexures, a Pseudo Rigid Body Model (PRBM) was made. For this model the flexures are replaced with rigid linkages to simplify modelling of the motion of the mechanism. This method was chosen for its simplicity in order to extract usable values for the length of the flexures and the influence these lengths have on the motion of the mechanism. A graphical representation of this model is given in figure 4.8.

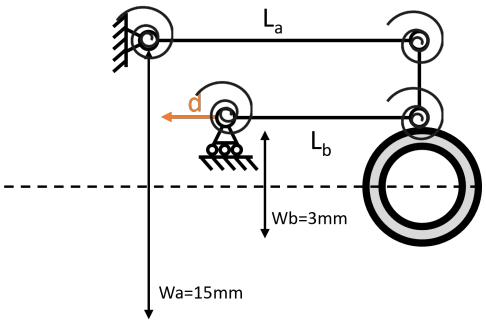

Figure 4.8: Pseudo Rigid Body Model with parameter indications for the analysis of the compliant mechanism.

As the model is symmetric only one half was modelled. Torsional springs with a stiffness equivalent of a C-shape leaf flexure loaded in similar fashion were added to the member to which the contact angles are attached to coupled their rotation and reduce the degrees of freedom so the model is constrained. From the equation for this stiffness found;

$$K_y = \frac{EI}{L} \tag{4.6}$$

it was found that the torsional stiffness is linearly inverse to the length of the flexure considering the materials and cross-section remain the same.
This results in the following equations of motion;

$$\sum X \rightarrow^{+} = L_A cos(\theta_0) - L_C sin(\theta_1) - L_B cos(\theta_2) - L_A - L_B - d = 0 \tag{4.7a}$$

$$\sum Y \uparrow^{+} = -L_A sin(\theta_0) - L_C cos(\theta_1) + L_B sin(\theta_2) + L_C = 0 \tag{4.7b}$$

$$\sum M \circlearrowleft^{+} = \frac{\theta_0 + \theta_1}{L_A} - \frac{2\theta_2}{L_B} = 0 \tag{4.7c}$$

Solving these equations of motion for a input displacement d=4.5mm and the following lengths of flexure A and flexure B;

$$15mm < L_A < 30mm \tag{4.8a}$$

$$5mm < L_B < 15mm \tag{4.8b}$$

Plotting the Y-displacement of element C (where the contact surfaces are located) and the rotation of this element at 4.5mm actuation gives the figures shown in section 4.1.4.

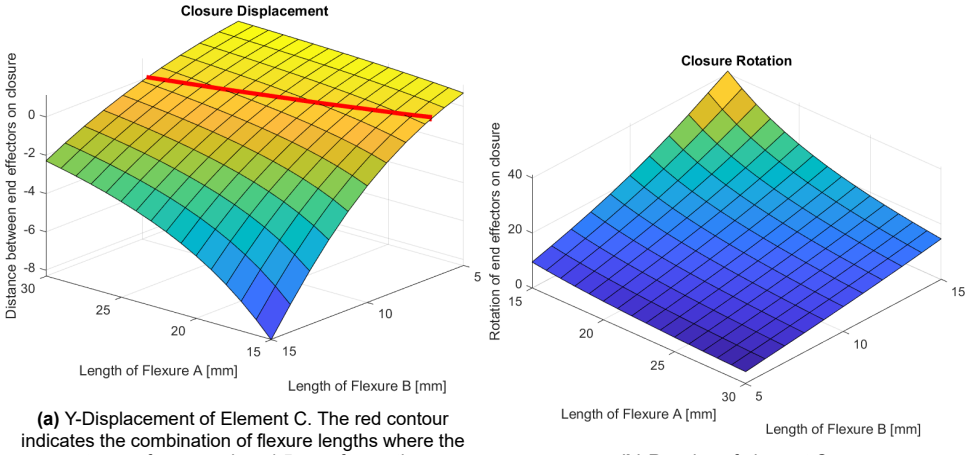

(a) Y-Displacement of Element C. The red contour indicates the combination of flexure lengths where the contact surfaces touch at 4.5mm of actuation.

(b) Rotation of element C.

Figure 4.9: Surface plots for the design variations of the compliant mechanism evaluated using the PRBM-method.

From the surface plot for displacement in figure 4.9a, the combinations of flexure lengths can be found for which the mechanism will be closed at 4.5mm of actuation. Any combination along the red contour should accomplish this. However, in figure 4.9b where the effective rotation of the contact surfaces is given upon actuation (ergo, the angle these surfaces are to be modelled at in the open state), it can be concluded that large lengths of flexure A will reduce the rotation. And thus, as the more parallel the closure, the less traction will be present on the graft, longer lengths of flexure A are favourable. From the displacement plots it can be concluded that flexure B has a larger influence on the rotation of the contact element than on its displacement. Some limitations of this method are to be noted. The main concern is that for these large displacements relative to the flexure lengths, there is a doubt on the accuracy of the predicted motion of the mechanism due to the non-linearities not taken into account. At the time the decision was made to continue with the results found due to time limitations. This study has served its purpose of gaining more insight in the working of the mechanism and the effect of the flexure lengths upon the motion. Instead of further optimization of this model, a sample of design candidates are to be prototyped and tested as measurement will always provide a more accurate result than models. These tests will be discussed in section 4.1.5.

4.1.5. Variation Testing

Based on the results from the PRBM study, a selection of prototypes of varying combination of lengths was created. An overview of the selected length combinations is given in figure 4.10. This selection is based on three lengths for the outer flexure (referred to as A), being 20mm, 25mm and 30mm and the accompanying lengths of the inner flexure (referred to as B) based on the the findings in figure 4.9a. Models A20B9, A25B10 and A30B11 are place along the red contour (where the mechanism should be closed at an actuation of 4.5mm). From the findings in the silicone study (see section 4.1.2) it was concluded that the added silicone will require additional input actuation. With this in mind, concepts A20B11, A25B12, A25B15 and A30B14 were chosen for their position beneath the red contour in figure 4.9a and therefore expected reduced input displacement required for closure. The contact angles

of mechanism to the 6mm DL graft were derived from the same PRBM-study from the results in figure figure 4.9b. Other than the length of the flexures and the contact angles, the mechanisms are all identical in terms of width, height, compressor width and input stage. Furthermore, all flexures have a similar thickness of 0.8mm which was selected as this is two times the nozzle diameter for a standard FDM-printer and early prototypes showed no failure for this dimension. All flexures were also pre-curved by placing the attachment-points 1mm vertically from one another. This is done to allow for initiation of bending.

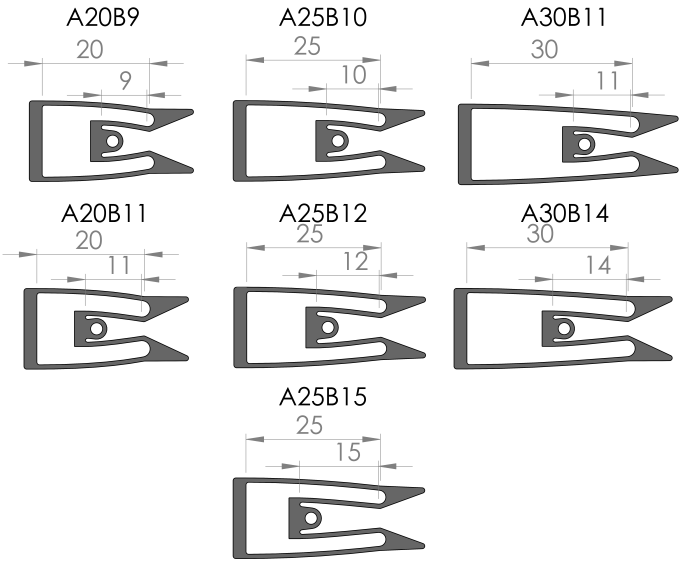

Figure 4.10: Selection of models for testing.

All concepts shown in figure 4.10 were printed on a Ultimaker 2 printer using Real Filament PLA material using identical slicer settings. These prototypes were mounted by fixing the input stage with a press fitted pin. Using a PI linear stage with a Futek 45N Loadcell the flat side was actuated. Each mechanism was actuated (opened and closed) for 5 times. The data gathered from these runs was combined using Matlab and the results are plotted in figure 4.11.
The following observations were made from this plot. First of all, the input length required to close these mechanisms was significantly less than predicted by the PRBM. In hindsight this can be attributed to the simplification of the model, specifically the contact point between the mechanism and the graft. Where for the PRBM the attachment point of the inner flexure is attached at the height corresponding to the radius of the graft, in the models in figure 4.10 this point is placed lower due to the actual length of the compressors. Unrelated to this error, multiple results from the PRBM can be confirmed by these tests. Firstly, an increased length of the outer flexure A does lead to a increased actuation distance to close the graft and a decreased stiffness. Likewise, increasing the length of the inner flexures B does decreased stiffness, however also reduces input displacement required for closure. Thus for increasing the input distance to be near the specifications of the actuator a shorter inner flexure would be beneficial combined with a longer outer flexure.

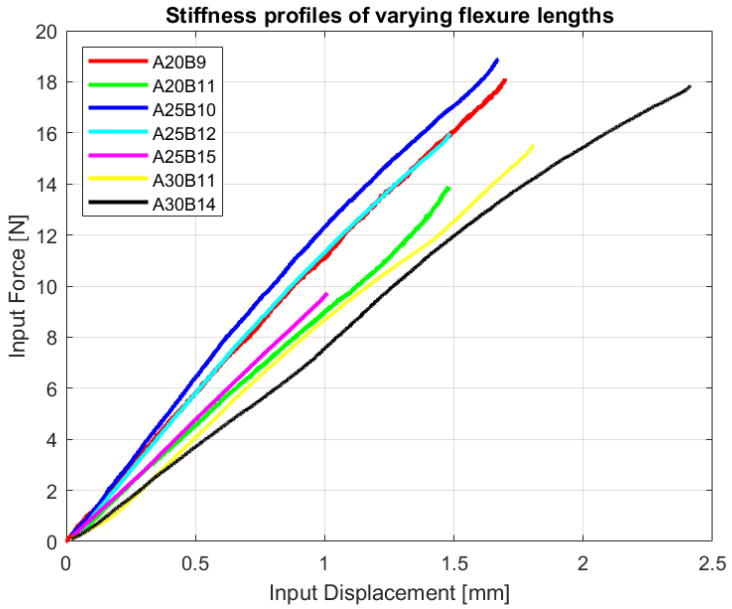

Figure 4.11: Result of stiffness tests for varying prototypes.

4.2. Design Iteration II: Optimization

Although the PRBM provided meaningful insight in the effects of the parameters for the compliant mechanism, the decision was made to discontinue further development due to the uncertainty of gaining realistic results within the allocated timespan. Therefore, this iteration will focus on the application of Finite Element Analysis.

4.2.1. Simulation Model

Before any simulations or optimizations were set up, a new CAD-model was drafted with the goal to be flexible and robust for all parameters.

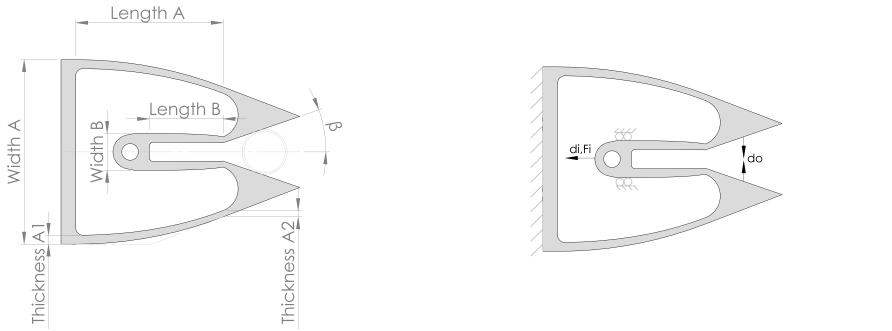

(a) Overview of the model used in FEA and optimization with all possible variables.

(b) Overview of the fixtures and inputs used in the FEA

Figure 4.12: View of the model used for FEA and optimization.

The parameters that define the model and can be adapted within optimization are;

1. **Length A;** length of outer flexure A
2. **Length B;** length of inner flexure B
3. **Width A;** width of fixed side (also determines the overall width of the mechanism)
4. **Width B;** width of the input stage
5. **Angle** β**;** opening angle of the compressors to the centre line

6. **Thickness A1;** thickness of the outer flexure at the fixed side.
7. **Thickness A2;** thickness of the outer flexure at the compressor side.
8. **Thickness B1;** thickness of the inner flexure at the input side (*Not shown in figure 4.12a*).
9. **Thickness B2;** thickness of the inner flexure at the compressor side (*Not shown in figure 4.12a*).

The flexures are defined with 3rd degree B-splines with guide lines of equal length. The model is also build to be adaptable for different grafts supporting their diameters and required compactor lengths. To reduces possible variables however, these were set constant for a 6mm DL graft. It is not feasible to optimize for all the parameters at once. Not only because the implications on computing time this will have, but having a plethora of parameters to optimize for will lose the overview of the effects of the parameters. With this in mind the optimization of the mechanism is to be done in two steps; first the overall parameters (i.e. lengths and widths) are optimized and discussed in section 4.2.2. After which the flexures of the resulting mechanisms will be optimized to reduce their stiffness.
Before this can be done, a FEA-model is required. For this a non-linear 2D simulation was created to account for the large deflections but also keep computing time to a reasonable level for optimization purposes. The left side of the model, where the outer sleeve of the Bowden cable will be attached to, is fixated. As the inner cable will always pull the mechanism towards the fixated side, rolling supports are added to the inner input-stage to prevent vertical movement of this stage caused by computational errors. Finally a contact set was created for the nodes along the surfaces of the compressor to ensure contact can be simulated and the mechanism is capable of closing properly.
Various inputs were considered, all of them are shown in figure 4.12b. These are; an input force (**Fi**) upon the input-stage (set to the maximal force of the actuator), a prescribed displacement (**di**) on the input stage (set to the maximal displacement of the actuator)or a prescribed displacement (**do**) on the compressors(set to the radius of the graft). Per optimization study an assessment is made on which input to use.
For the material settings the material properties of PLA set as a standard in the CAD software are utilized. However, FDM-printed PLA will likely have slightly different material properties compared to homogeneous material [52]. Based on the findings of Travieso-Rodriguez, Jerez-Mesa, Llumà, *et al.* the standard settings for PLA are adjusted to a Young's modulus of 2.4GPa and a Yield Strength of 31MPa [52]. To verify these properties, a test flexure was printed of similar dimensions using the same PLA-material, FDM-Printer and slicer settings. This model was both simulated in FEA, using the material properties discussed above, and tested on a linear stage. The results of this test is shown in figure 4.13b. Based on these findings the Young's Modulus was adjusted to 2.5GPa, plotted in the orange line, to better resemble to measured values.

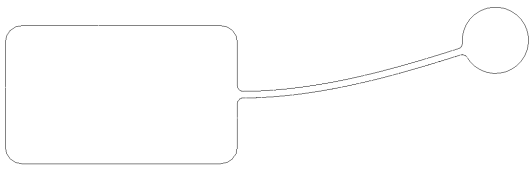

(a) The model used for material validation, simulated at a 10mm displacement.

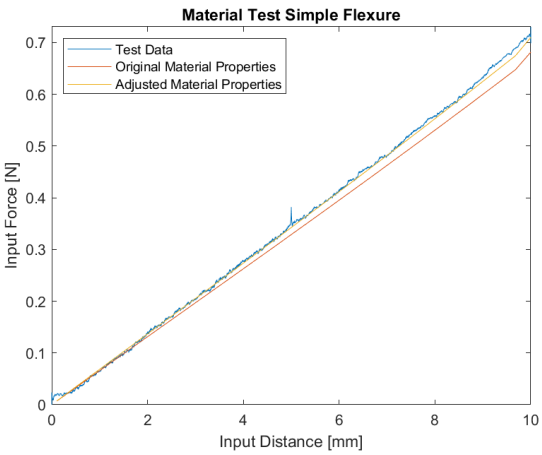

(b) Plot of the measured stiffness compared to the simulated stiffness for the material properties found in literature, and material properties adjusted to follow the stiffness of the measured data.

Figure 4.13: Validation of the material properties

Following these material tests on a simple flexure, a simulation study on the A30B14 model from the variation test in section 4.1.5 was build and compared to the data collected on the stiffness testing. The

results of this are shown in section 4.2.1. Upon iteration it was found that for a Young's Modulus of 2.52GPa seemed to match the behaviour of the printed prototypes. With these adjusted factors it is crucial that the same printer, filament and slicer settings are used throughout this project.

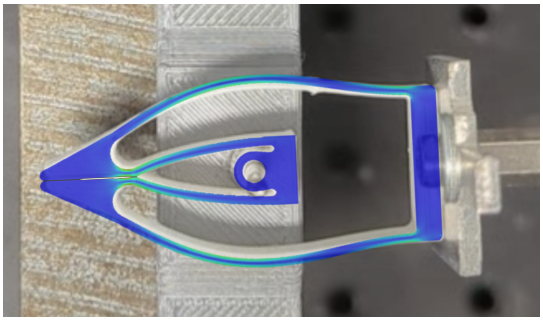

(a) A still frame of closed mechanism A30B14 with an overlay of the simulated result.

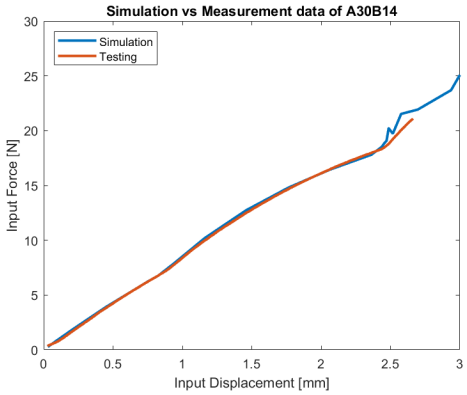

(b) Plot of the simulated stiffness compared to the measured stiffness for mechanism A30B14

Figure 4.14: Validation of the simulation

In section 4.2.1 a comparison is made for the simulation model applied to one of the prototypes of the variation study in section 4.1.5 and the test results. In figure 4.14a it can be seen that the simulation overlaps rather well with real sample. A small mismatch is seen where in the simulation the outer flexure appears to buckle more compared to the tested sample. This can either be accredited to a simulation error, a mismatch in material properties or alignment of the camera. The result in end effectors and inner flexures do overlap. Therefore the decision was made to keep the material properties as found. With the simulation results plotted against the measured data a good overlap is found. Besides the near identical stiffness (found by tuning the Young's Modulus for the print settings), the contact points where the compressor surfaces first touch and close are also matching. It can be seen that the simulation struggles at further loads after the mechanism is closed. However, as this is of no concern for the optimization, where the focus is on the closure of the mechanism, this behaviour is ignored.

4.2.2. Parameter Optimization

With the parametric CAD-model created and the FEA-simulation set up and validated, the design can be further optimized. As discussed in the parametrization of the model (section 4.2.1) optimizing for all available parameters all at once will result in an increase of computing time and a loss of overview on the influence of each free variable. Therefore a exploratory search was done on the most influential parameter on the performance of the design. As one of the conclusion points of the variation study (section 4.1.5) following the results of the PRBM-study (in section 4.1.4) was that for all resulting models the input displacement was to be increase to utilize the actuator to its fullest potential. More on this will be discussed later in setting the optimization goals . Another conclusion drawn from the previous results was that the length of the outer flexure has a greater impact on the stiffness and input displacement compared to the length of the inner flexures. From several exploratory quick studies, the greatest variation of resulting input displacement was found for free variables of the L_A, the length of the outer flexure, and W_A, the width of the fixed side (see figure 4.12a for reference). As this width was already set at 15mm (the maximal width specified by the requirements), the decision was made to allow for a larger value to determine its impact. The effects of this will be discussed. Furthermore, as found in the Flexure Placement study in section 4.1.3, to accommodate for the effects these changes have on the motion path of the mechanism, the angle $\beta$of the compressor was added as a third free variable. The other parameters were fixed based on previous results . The inner flexure is dimensioned at 10mm in length, at 5mm apart for width B. The thickness of the flexures is set evenly at 0.8mm as this has not resulted in material failure of the flexure so far. After this study is completed, the thickness for each resulting mechanism will be determined in the next section. The prototyping will still be done using the same FDM as described in the previous paragraph, thus similar material properties are applied with a total thickness of 4mm.

The goals of this study were, after multiple iterations, set in twofold. Based on the results of the variation study, seen in figure 4.11, it can be argued that the mechanism with the least force required for the largest input displacement is desired, thus a mechanism with a low stiffness over closure. This was one of the potential goals. Upon further consideration, with the unknown added stiffness of the silicone encasing in mind. The mechanism with the largest available energy budget to accommodate for the deformation of the silicone material is desirable. A representation of this goal is given in figure 4.15. This energy budget can be defined by the energy the actuator can deliver over the input distance (more on which insection 1.2), minus the energy required to close the mechanism (indicated in red). This leaves the remaining energy as indicated in green in figure 4.15. By placing the actuation at the end of the stroke of the actuator, this total energy budget can be maximized.

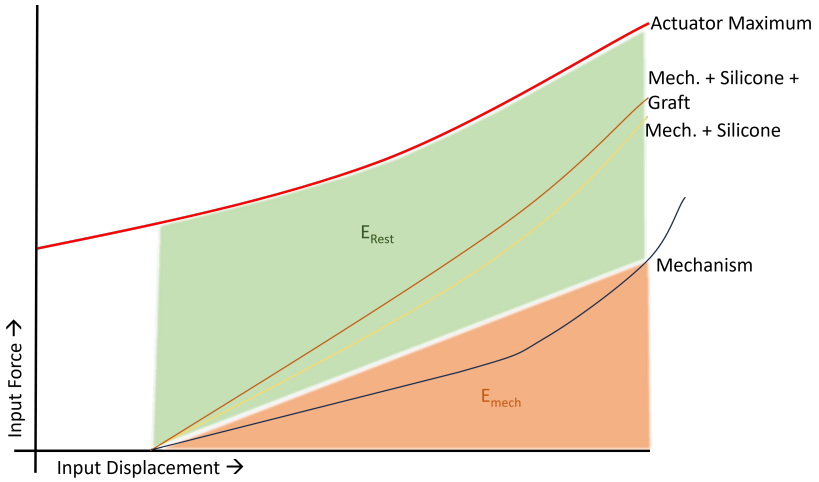

Figure 4.15: A diagram of the expected energy budgets of the system.

Due to the goal of optimizing for maximum remaining energy in the system approaches the problem at its core, it was favoured over optimizing for stiffness. However, as both strategies seemed viable, in the end both were considered for the optimization process. With an additional third goal of maximizing the remaining energy within the volume constraints.

Table 4.2: Optimization Settings - Parameter Optimization

Free Variables	Values	**Fixed Parameters**	Values
L_A - Outer Flexure Length	15mm-30mm	L_B - Inner Flexure Length	10mm
W_A - Width input stage	15mm-25mm	W_B - Width input stage	5mm
β- Contact Angle Gripper	18°- 21°	Flexure Thickness	0.8mm
		Mechanism Thickness	4mm
		Material	FDM PLA

Goals *optimized for individually*	Target
Remaining Energy	Maximize
Remaining Energy within original volume constraint	Maximize
Stiffness	Minimize

Running the optimization, several caveats were found. No sensor in the software was capable of determining the point of closure confidently. This resulted in a manual determination of the closure point. The forced introduction of manual determination of this point changed the optimization process to a brute-force approach rather than with the use of the build in optimization algorithm. The contact point was determined at the first contact made between the compressors. The input displacements at which these occur are noted in table 4.3. Mechanisms capable of good closure are marked with green. Good closure is defined as either parallel contact, or first contact on the near side of the compressor which upon further actuation will result in complete closure. An example of good closure is given in

Table 4.3: Displacements from optimization. Cells colours green provided correct closure, where red combinations did not.

d18deg				
Wa\La	15	20	25	30
15	1.8	1.8	1.8	1.8
20	2.2	2.2	2.2	2.2
25	3.0	2.6	2.6	2.6

d19deg				
Wa\La	15	20	25	30
15	1.8	1.8	1.8	1.8
20	2.2	2.2	2.2	2.2
25	3.0	2.8	2.6	2.6

d20deg				
Wa\La	15	20	25	30
15	1.8	1.8	1.8	1.8
20	2.2	2.2	2.2	2.2
25	3.0	2.6	2.6	2.6

d21deg				
Wa\La	15	20	25	30
15	1.8	1.8	1.8	1.8
20	2.6	2.6	2.4	2.4
25	3.4	3.0	3.0	3.0

Table 4.4: Forces from parameter optimization.

F18deg				
Wa\La	15	20	25	30
15	43.824	36.768	29.136	22.704
20	14.688	19.968	19.056	16.416
25	19.392	8.976	11.76	11.712

F19deg				
Wa\La	15	20	25	30
15	36	31.44	25.536	20.112
20	11.184	15.6	15.888	13.968
25	13.968	8.496	8.976	9.696

F20deg				
Wa\La	15	20	25	30
15	28.512	26.112	21.648	17.472
20	10.752	8.112	11.712	11.568
25	9.12	8.304	8.784	9.024

F21deg				
Wa\La	15	20	25	30
15	17.904	19.584	16.992	13.632
20	23.52	24.24	15.072	13.44
25	22.512	10.128	13.056	12.624

figure 4.16a. In contrast, when the first contact occurs at the far end of the compressors (as shown in figure 4.16b), upon further actuation this will results in further rotation and no complete closure. Mechanisms with this behaviour are marked red and were excluded from further consideration.

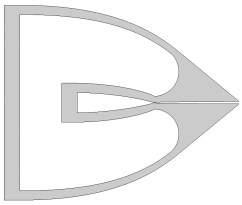

(a) Closure of mechanism La=20mm, Wa=25mm and β=19°, for which good closure is achieved.

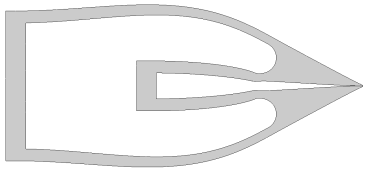

(b) Closure of mechanism La=25mm, Wa=15mm and β=18°, which results in first contact occuring at the far end of the compressor. Following this, no complete closure will be achieved.

Figure 4.16: Definition of good closure of the mechanism

At these points of closure, the simulated input forces are noted in table 4.4. Assuming the stiffness up to the first contact point is linear, based on earlier test results in the variation study in section 4.1.5, the stiffness of the first stage of closure is determined in table 4.5. Finally the remaining energy in the system is determined as discussed for the goals and given in table 4.6.
From these results the following mechanisms were selected based on the different goals;

4.2.3. Flexure Optimization

With the global parameters of the mechanism set, the flexure thickness for each design is to be optimized. This is done with the same non-linear 2D simulation as setup in section 4.2.1 and the thickness of the two flexure at the start and end point, defined in section 4.2.1, as the free variables. These free variables were set at multiples of 0.4mm as this is the standard nozzle diameter on the Ultimaker 2 FDM printer. For slender members like these it is best practice to keep to multiples as there is no space for infill. The constraints for this optimization were set to be the yield strength of FDM-printed PLA, which was found to be at 60Mpa [52], monitored by a sensor along the edges of the flexure where the most

Table 4.5: Stiffness from parameter optimization. Conditional formatting is applied, the minimal stiffness is indicated with the greenest cell shade.

k18deg	(N/m)			
Wa\La	15	20	25	30
15	24346.667	20426.67	16186.67	12613.33
20	6676.3636	9076.364	8661.818	7461.818
25	6464	3452.308	4523.077	4504.615

k19deg				
Wa\La	15	20	25	30
15	20000	17466.67	14186.67	11173.33
20	5083.6364	7090.909	7221.818	6349.091
25	4656	3034.286	3452.308	3729.231

k20deg				
Wa\La	15	20	25	30
15	15840	14506.67	12026.67	9706.667
20	4887.272727	3687.273	5323.636	5258.182
25	3040	3193.846	3378.462	3470.769

k21deg				
Wa\La	15	20	25	30
15	9946.6667	10880	9440	7573.333
20	9046.1538	9323.077	6280	5600
25	6621.1765	3376	4352	4208

Table 4.6: Remaining Energy from parameter optimization. Conditional formatting is applied, the most remaining energy is indicated with the greenest cell shade.

Eres18deg				
Wa\La	15	20	25	30
15	0.0197196	0.025364	0.03147	0.036616
20	0.0467337	0.049943	0.049463	0.049559
25	0.055679	0.054805	0.054811	0.054581

Eres19deg				
Wa\La	15	20	25	30
15	0.0406768	0.040475	0.04061	0.041282
20	0.0505881	0.050567	0.050087	0.050327
25	0.0480351	0.055429	0.054805	0.053869

Eres20deg				
Wa\La	15	20	25	30
15	0.043642837	0.041214	0.04145	0.041954
20	0.051063274	0.053967	0.050007	0.050166
25	0.05530708	0.055679	0.054812	0.05439

Eres21deg				
Wa\La	15	20	25	30
15	0.0467777	0.048002	0.048237	0.048741
20	0.054647	0.057551	0.053591	0.053749
25	0.0553071	0.058192	0.060909	0.060486

stress in to be expected.

Table 4.7: Optimization Settings - Flexure Optimization

Free Variables	Values
T_{A1} - Outer Flexure Start Thickness	0.4mm-1.2mm
T_{A2} - Outer Flexure End Thickness	0.4mm-1.2mm
T_{B1} - Inner Flexure Start Thickness	0.4mm-1.2mm
T_{B2} - Inner Flexure End Thickness	0.4mm-1.2mm

Fixed Parameters	Values
Mechanism Overall Parameters	set per optimized design
Mechanism Thickness	4mm
Input displacement	determined in table 4.3
Material	FDM PLA

Constraints	Target	**Goals**	Target
Max Von Mises Stress Outer Flexure	Less than 60Mpa	Force at input stage	minimize
Max Von Mises Stress Inner Flexure	Less than 60Mpa	Factor of safety	close to 2

Applying these parameter to a design study yielded the following results;

- **Most Remaining Energy:** Both Flexures starting at 1.2mm, ending at 0.8mm.
- **Most Remaining Energy within Volume:** Outer Flexure starting at 1.2mm, ending at 0.8mm. Inner flexure constant thickness of 0.8mm.
- **Lowest Stiffness:** Both Flexures starting at 1.2mm, ending at 0.8mm.

4.2.4. Improvements to Silicone Casting

Based on the performance and the conclusions from the first iteration of silicone and mould, a second design iteration was performed. The split mould consisting of two parts did ease the release of the product, however a line where the seam is located was left on the silicone. Thus the second mould consists of one main mould with a small removable plug to create a cavity in the silicone for the graft. The plug is removable to ease separation of the silicone product. Furthermore the wall thickness of

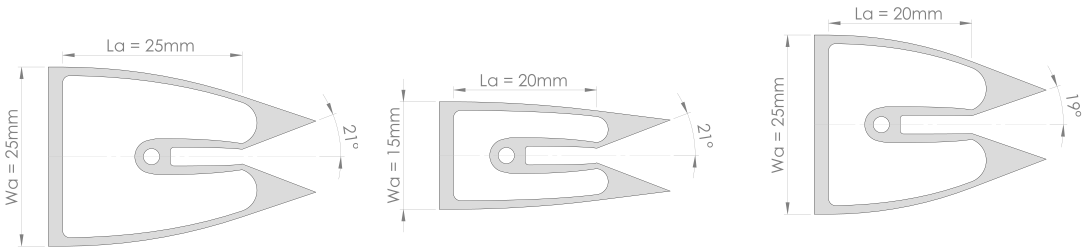

(a) Optimization result for most remaining energy goal.

(b) Optimization result for most remaining energy within volume constraint goal.

(c) Closure of mechanism La=25mm, Wa=15mm and β=18°, which results in first contact occurring at the far end of the compressor. Following this, no complete closure will be achieved.

Figure 4.17: Results of the parameter optimization study per goal

the main-mould was reduced to 0.8mm to help ejecting the product. The CAD model of the mould was designed to be parametric to the mechanism. The result of this is a mould that is self adapting to the mechanism design allowing for quicker iterations. To reduce the increased stiffness by the added silicone, the walls around the mechanism are reduced in thickness from 1.5mm to 0.8mm. The compression of silicone situated inside of the mechanism is suspected to have a large impact of the overall stiffness when compressed. To reduce this a softer silicone is created by adding deadener to the original silicone (which already was the softest available material). Deadener is based on sulphur based and limits the forming of elastomeric bonds when the two components of the silicone are mixed. Adding deadener to the mix in a ratio of 1A:1B:1D should reduce the shore-hardness of the silicone from OO-30 to OOO-50 [51]. A few drops of blue dye are added to allow differentiation between the two silicones. At the deadened stage, the material is more gel-like than elastic. For this reason the deadened silicone is only used in the internals of the mechanism with the bottom, top and sides constructed of the original OO-30 hardness silicone. The steps of the pouring process to achieve this layered structure is shown in section 4.2.4.

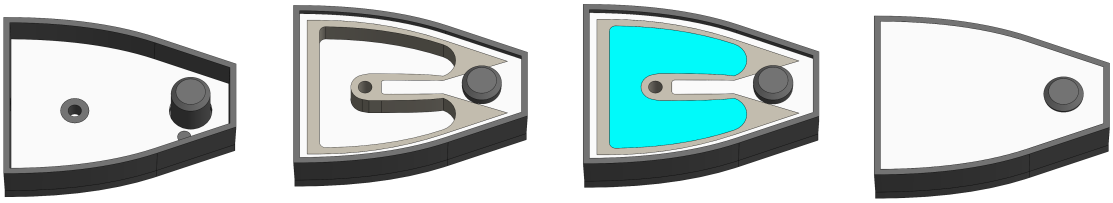

(a) Step 1: Pouring the bottom layer.

(b) Step 2: Placing and fixing the mechanism and pouring the walls.

(c) Step 3: Pouring the deadened silicone coloured blue.

(d) Step 4: Pouring the top layer.

Figure 4.18: Moulding process for the silicone encasing

The results of this moulding process is shown in section 4.2.4.

(a) Prototype Most remaining energy

(b) Prototype most remaining energy within volume claim

(c) Prototype lowest Stiffness

Figure 4.19: Prototypes resulting from the moulding process.

5

Validation and Verification

In this chapter all of the experiments that were performed on the final designs of the compliant DAS are described. These test will serve either to verify the design to the requirement or to validate the usage of the mechanism and the design choices made.

5.1. Volume

Requirement: in section 2.7, requirement 1.1 the maximum volume was defined with a boxshape of 30mm in length, 15mm in width and a thickness of 10mm.
Method: The three prototypes created as a result of the design process in chapter 4 were measured using a digital calipers. With the soft silicone layer, minimal force was applied whilst measuring the outer dimensions.
Result: The dimensions found for each mechanism is given in table 5.1.
Discussion: during the design process the conscious decision was made to exceed the volume requirement. The reasoning here was the unfavourable transmission ratio for mechanisms fitting this requirement leading to a reduced input displacement. This in its place would decrease the energy available from the actuator to deform the mechanism. The volume concept was created to examine the performance of a mechanism within the volume claim. The addition of the silicone layer did however also exceed the volume claim by a small margin. The performance of the mechanisms is discussed further in this chapter. After this a more elaborate discussion will be given in section 6.2.1.

5.2. Mass

Requirement: the mass of the DAS-Valve was set to be less than 20 grams.
Method: the three prototypes were weighed using a digital scale with an accuracy of . *Result:* the mass found for each design is given in table 5.1.
Discussion: all three designs pass the mass criterium. As predicted in the conceptual design, the use of lightweight materials compared to the state of the art is what resulted in a weight reduction of at most 50% compared to the state of the art. As Peek is similar to PLA in density and the majority of mass determined by the silicone, no large change of mass is to be expected.

Table 5.1: Measured volumes and mass for the three considered designs.

	Most Energy	Most Energy within Volume	Lowest Stiffness
Length [mm]	38	32	32
Width [mm]	26	16	16
Height [mm]	6.5	6.5	6.5
Mass [g]	5.96	4.56	5.38

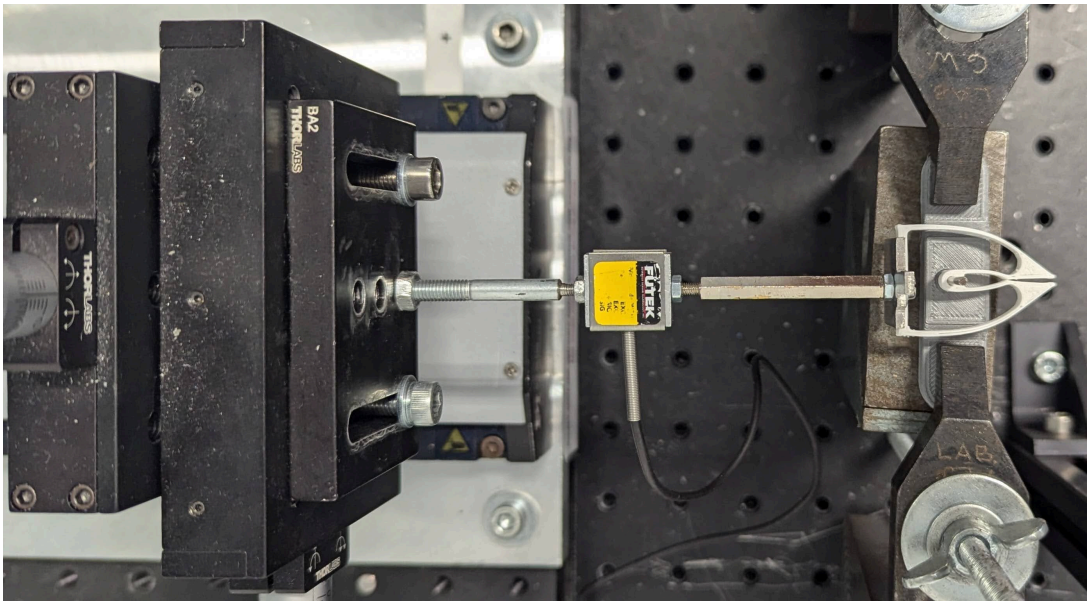

Figure 5.1: Overview of the linear stage test setup. From left to right; the linear stage, the Futek 45N Loadcell, flat pusher interface to the mechanism mounted on the fixation base.

5.3. Stiffness Contribution of Components

A linear stage was used measuring the input displacement and corresponding input force to determine and compare the stiffness and stiffness compositions of the different designs.
Requirements: Pressure resistance: graft must be capable of closing a graft at 180mmHg.
Input work: must be compatible with the existing DAS-Actuator using no more than 0.12J over closure.
Fail safe: must have a safe state where the graft is opened.
Multiple stages: must be capable of controlling the degree of opening and thus controlling the flow.
Control of opening speed: the actuation speed of the graft should be controlled and at least be more than 10 seconds.
Method: The prototypes were printed and mounted using a custom mount to a PI Linear Stage with a 45N Futek Loadcell. The interface of a pin was used to allow for swapping of samples with a repeatable result. The print is iterated on to ensure the pin fits the actuation point without presence of play.
The test setup is controlled and monitored using Labview. At the start of each set of measurements the load-cell is zeroed and the pusher interface is positioned in front of the mechanism so it is just touching (this can be checked with the load cell). For each new mechanism an exploration run is done, slowly advancing the mechanism until the mechanism reaches a closed state. With this pint found the mechanisms is opened and the measurements are started. The stage is actuated at 0.1mm/s with a sampling frequency for the load-cell of 10Hz resulting in roughly one hundred force and position samples per millimetre. Each mechanisms is actuated, opened and closed, five times. After this the gathered data is exported to Matlab for further processing. Here the 5 runs are combined and a moving average is applied to reduce the noise. To gain an in-depth insight in the contribution of individual factors, three tests were performed for each design; mechanism only, mechanism in silicone and mechanism in silicone with a pressurized graft.

Mechanisms Only:
Research Question: What is the stiffness of each individual compliant mechanism over closure and do they perform as expected? *Method:* The mechanisms, as seen in section 4.2.2, without silicone or a graft were tested for their stiffness to find their contribution to overall stiffness. The result of these tests are plotted in figure 5.2.
Discussion: with the mechanisms isolated from the silicone, the characteristic stiffness of these mechanisms can be seen. Where the stiffness first increases when the compressors make contact (this moment is shown in figure 5.3a). This increased stiffness continues until the mechanism is completely closed (shown in figure 5.3b) at which point the stiffness is increase a last time and the outer-flexures

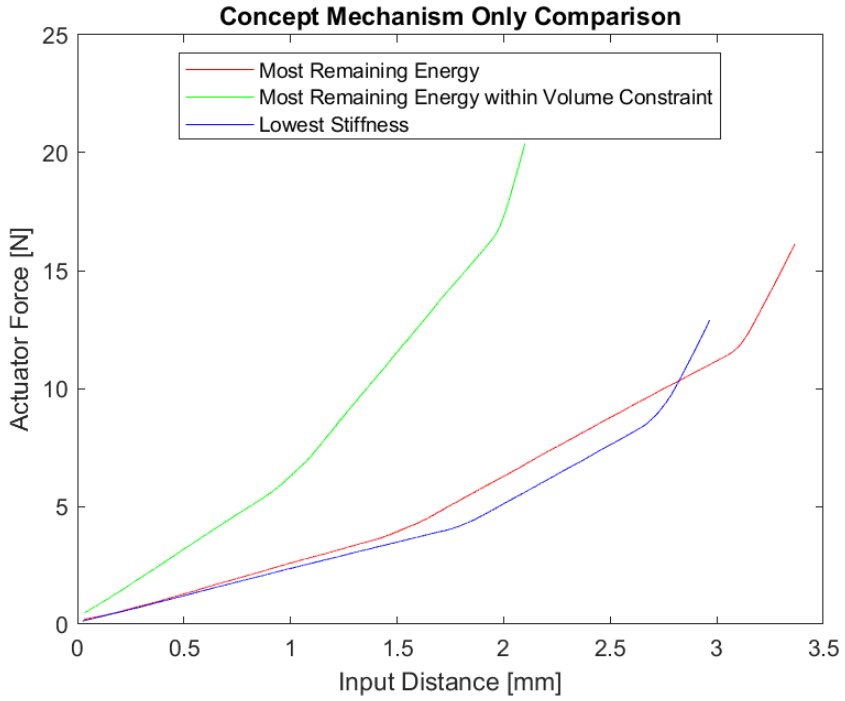

Figure 5.2: The mechanism stiffness found for each design.

start buckling. This last point is a clear indication that the mechanism is closed.

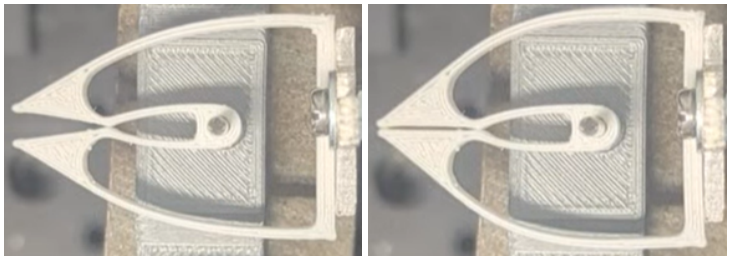

(a) First Contact point

(b) Prototype most remaining energy within volume claim

Figure 5.3: Still frames of the point at which the stiffness increases.

In figure 5.2 the results of the different optimization goals applied in section 4.2.2 can be seen. The blue line for lowest stiffness does indeed have the lowest stiffness of the three, although the difference with the Most Remaining Energy concept is negligible. What differentiates this concept is that, following an optimization on extracting the most energy from the actuator, the input distance is the greatest of the three. Lastly, due to adherence to the requirements, the concept with the most remaining energy within the volume constraint does significantly increase the stiffness.

Mechanisms in Silicone:
Research Question: what is the influence on each mechanisms stiffness on the introduction of silicone?
Method: the method as described in the previous section was repeated in a similar fashion to find the stiffness of the mechanisms encased in silicone. The results of which are shown in figure 5.4a.
Discussion: from the results the first observation is that the changes in stiffness are less pronounced compared to only the mechanisms. A more noticeable difference is the more pronounced increase in stiffness for the low stiffness concepts. This can be explained by the smaller volume of silicone, thus compression is relatively increased. The input displacement required to close the graft has also increased. Which is notable, this can at least partly be attributed to the added silicone between the graft and the compressors adding stiffness.

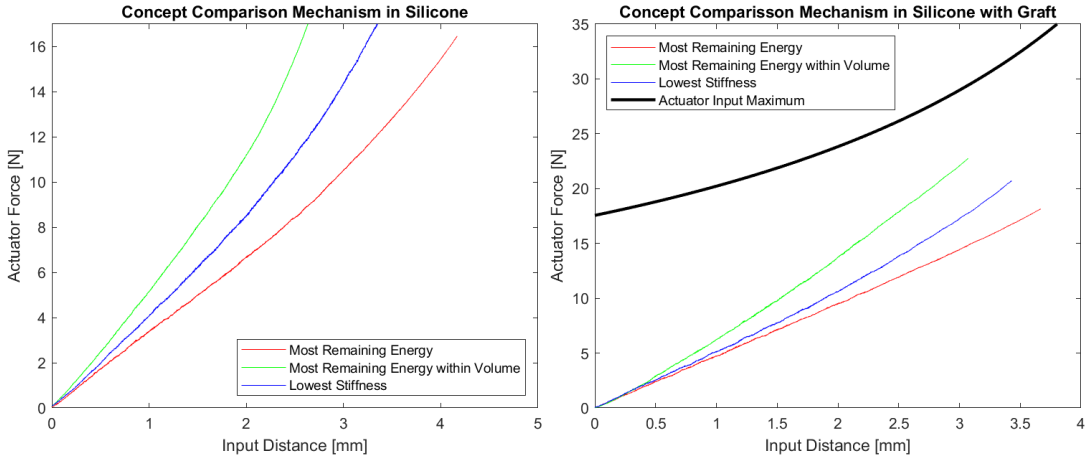

(a) The mechanism stiffness in silicone found for each design. **(b)** The mechanism stiffness in silicone found for each design.

Figure 5.4

Mechanisms in Silicone with pressurized Graft:
Research Question: how do the mechanisms encased in silicone perform over the closure of a 180mmHg pressurized graft? *Method:* to investigated the added stiffness from a pressurized graft and determine the mechanisms ability to close the graft the following changes were made. The fixation plate for the mechanism was adapted to accommodate for the graft. The graft is filled with water and pressurized by compression of a syringe which is, monitored by a manometer, set at 180mmHg. Similar procedures as in the other stiffness tests were followed.
Results: the results of this study are shown in figure 5.4b. The force the actuator can provide at the input distance is added for reference.
Discussion: comparing figures 5.4a and 5.4b a small increase in stiffness from the pressurized graft is noticed. For the most remaining energy concept the force required for closure is 10%. For the lowest stiffness concept this is 19% and the remaining energy within volume this is 30%. However, all concepts remain well under maximum force the actuator can input. From this is can be concluded that all concepts are compatible with the DAS-Actuator. This is with both the mechanisms and the actuator starting at 0mm displacement. As the total displacement of the mechanisms is less, the inner Bowden cable can be shortened to shift the line to the right increasing the force and energy overhead. With this pretension it was found that for the Most Remaining Energy Concept, the Low Volume Concept and the Low Stiffness Concept, all cast in silicone actuated on a pressurized graft, respectively 29%, 30% and 33% of the available energy budget was used.

5.3.1. Silicone stiffness reduction

Research question: Does the deadened silicone centre reduce the overall stiffness as intended?
Method: an identical compliant mechanism was encased in homogenous Platsil 00-25 silicone with OO-30 shore hardness [51]. The result was tested without and with a pressurized graft using the methods described in section 5.3 and section 5.3.
Results: the measurements performed are shown in figure 5.5a.
Discussion: from the results it can be concluded that reducing the hardness of the internal silicone with deadener does reduced stiffness in both tests with and without a pressurized graft. The force required at closure with a pressurized graft is reduced by 7%.

5.3.2. FBR Simulation

Research question: would ingrowth or encapsulation of fibrous tissue limit actuation of the mechanism?
Method: Two models were constructed to simulate two impact cases of FBR. For both models an identical mechanism optimized for maximal remaining energy was encased in silicone including the deadened internals. For the ingrowth simulation model, the areas where a high risk and effect of tissue formation is assumed; around the graft and along the flexures, a harder layer of platsil OO-30 is applied with a shore hardness of A30 is applied. To help identify this material, a few drops of red dye

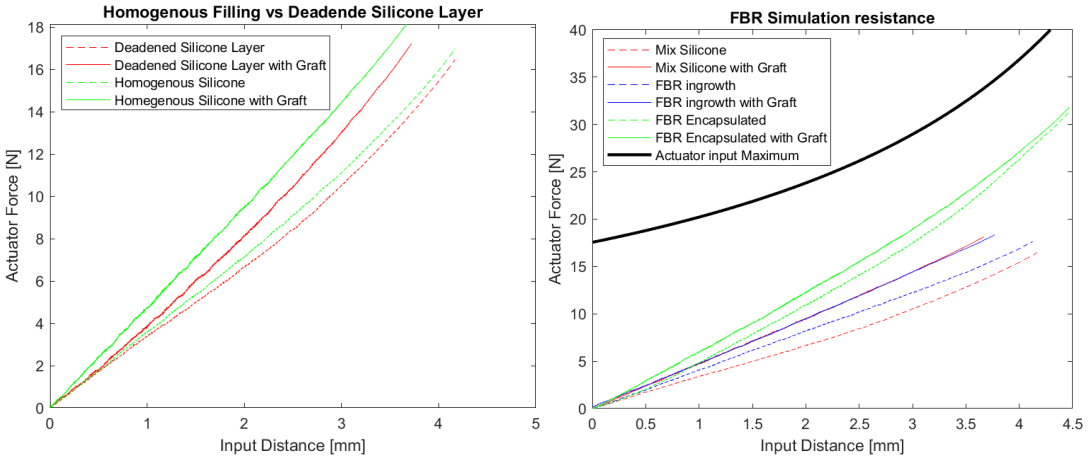

(a) Validation results for the Most Remaining Energy Concept in homogeneous silicone with hardness OO-30 and the same mechanism with deadened silicone internals with hardness OOO-50.

(b) Validation results of effects on stiffnes wiht the simulated tissue ingrowth on a most remaining energy concept.

Figure 5.5

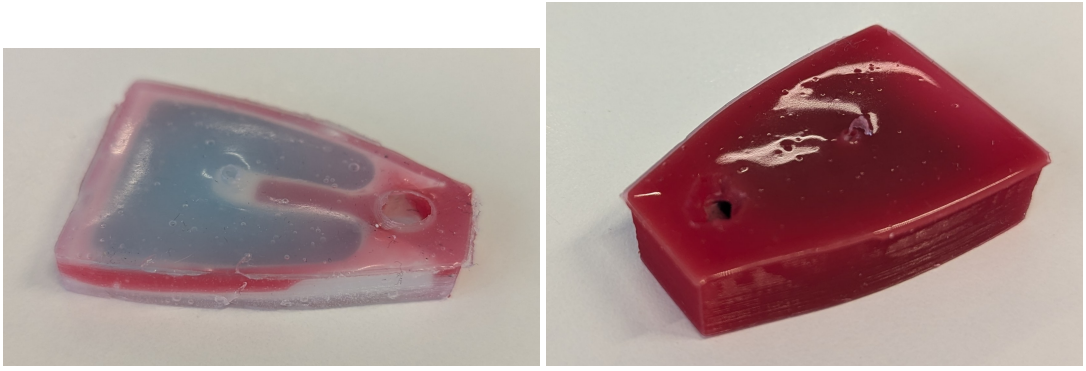

(a) Simulated model of ingrowth on a most remaining energy concept. The transparent silicone is Platsil Gel-00, the blue layer is deadened Platsil and in red is the simulated fibrous tissue in growth of Platsil 00-30 .

(b) Simulated model of encapsulation around a most remaining energy concept. The model as seen in figure 4.19a is completely encased in red simulated fibrous tissue in growth of Platsil 00-30 with a thickness of 4mm.

Figure 5.6: Silicone Models used for FBR simulation

was added to the mixture. Within the Phantomlab this material is used to simulate hard tissue (such as fibrous tissue). For the simulated encapsulation model, the same most remaining energy model with deadened silicone was placed in a second mold and completely encapsulated by platisl OO-30. Based on consultation with experts, it was found that on earlier in-vivo test on a goat model, a tissue layer of thickness around 2-4mm was formed. For this simulation model, a layer of 4mm hard silicone was added around the model to simulate the effects of encapsulation. The resulting mechanisms were tested without and with a pressurized graft using the methods described in section 5.3 and section 5.3.
Result: the results of these test are shown in figure 5.5b.
Discussion: from the tests performed without a pressurized graft, a clear increase in overall stiffness is found for the simulated tissue ingrowth. Adding and pressurizing the graft to 180mmHg yields near similar results to a non affected mechanism. The model with tissue ingrowth required a slightly increased actuation displacement at most. Even with the simulated tissue ingrowth, a clear margin is kept to the actuator limits to ensure the mechanism is still capable of actuation. The effects of simulated encapsulation is more pronounced in figure 5.5b where at closure, 75% of the available force is required to close the pressurized graft. More notably is the increase input distance required to close the graft which with 4.4mm for the pressurized graft just falls within the actuation range of 4.5mm of the actuator. Although these tests with simulated tissue do provide some insight into the affects of tissue ingrowth and encapsulation, further studies have to be performed to ensure in-vivo actuation of the DAS. The

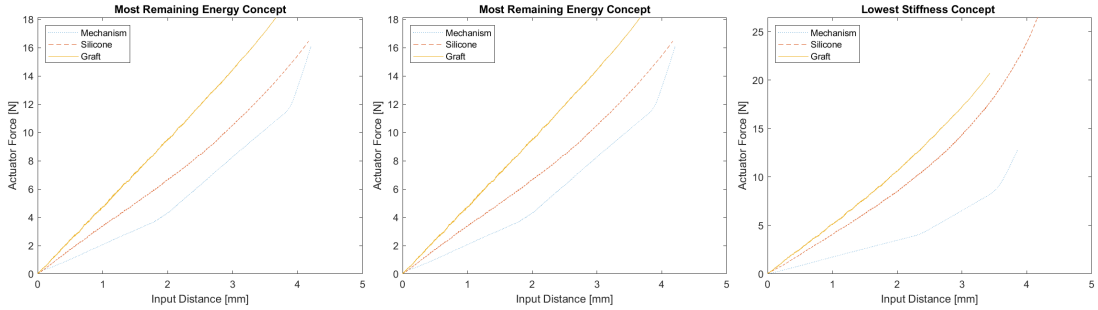

(a) Combined result of stiffness contributions for the most Remaining Energy Concept.

(b) Combined result of stiffness contributions for the most Remaining Energy within Volume Concept.

(c) Combined result of stiffness contributions for the most Remaining Energy within Volume Concept.

Figure 5.7

tests performed here do inspire confidence in the mechanisms ability to withstand these effects.

5.4. Fatigue

Requirement: the dAVF must last for at least 836 cycles, with a cycle defined as the closing and opening of the anastomosis.
Method: the linear stage setup, as seen in figure 5.1, was reused. For this test an unused prototype of the Most Remaining Energy concept was tested in a deadened silicone protection was mounted and actuated upon a pressurized graft (similar to the test discussed in section 5.3). The software used for this linear stage did not allow to program a repeated actuation, thus the actuation was controlled manually. Each one hundred cycles, the closure of the graft was inspected, the silicone surrounding the mechanism was inspected visually for tearing or other forms of damage and the pressure on the graft was checked and if required reset to 0.25bar (equal to 180mmHg systolic pressure).
Results: performing this test resulted in two hours of actuation curves similar to the figure 5.4b. From this data the maximum force measured was extracted for each cycle using the 'findpeaks' function in Matlab. Plotting these peaks for each cycle resulted in the figure 5.8a.

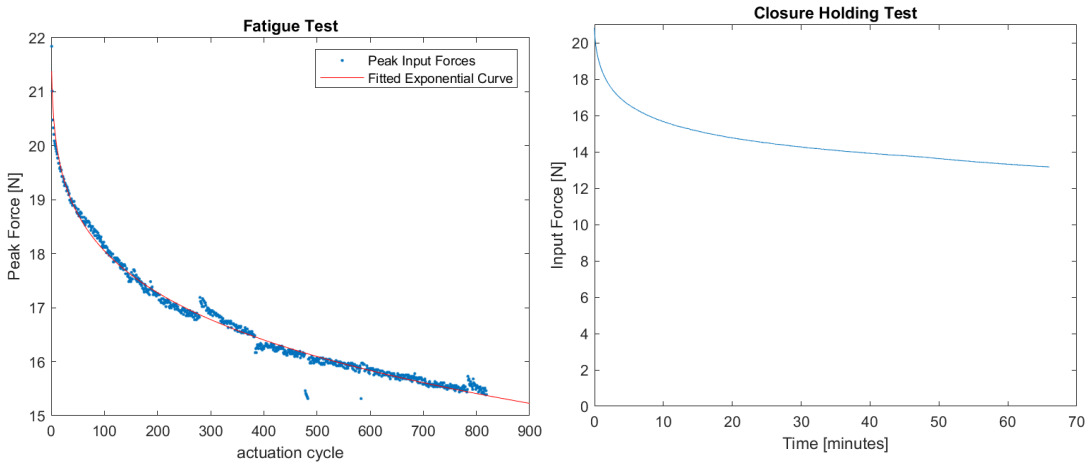

(a) Fatigue test of the Most Remaining Energy concept surrounded in deadened silicone compressing a pressurized graft. The peak force required to close the graft is plotted for each cycle and a exponential curve is fitted through this data.

(b) For this test a unused most remaining energy mechanism encased in a deadened silicone layer was closed using the linear stage and held in position for over an hour. The resulting line of reaction force on the input clearly indicates the non-linear behaviour due to visco-elasticity.

Figure 5.8: Fatigue Testing

Discussion: the main outcome of this test is that the proposed design is performs without failure for the amount of cycles set in the requirement. The compliant mechanism was designed so the stresses in the flexures remain well below the fatigue stress. For the silicone surrounding the mechanism no such expectations could be set, thus proving its capability to exceed the minimal cycles is crucial for the

validation of the compliant dAVF. The goal of achieving 2080 cycles, equal to 10 years of use, could not be validated without automating the test. With manual control over the actuation the allocated testing time would not allow for this. The lack of automation can also be found in the results in figure 5.8a around the 500 cycle mark were a three force measurements are out of line, likely due to opening of the graft before complete closure. Between cycles 300 to 400, a increase in peak force can be identified. It is likely that the pressure on the graft between these cycles was set beyond 180mmHg. Checking the pressure on the graft more often or utilizing a different pressure application that can hold continuous over all cycles could prevent this in the future. Most notably is the negative exponential growth in input force. As the actuation displacement was constant, it must be concluded that the overall stiffness decreased at similar rate. As the prototype was not actuated before, this non linear behaviour can be attributed to large deformation that occur on non-isotropic FDM-printed PLA and a multi-material silicone encasing. To compared this a separate test was performed on a new, but otherwise identical, model. In this test the mechanism was closed and held in position for more than 60 minutes. Similar behaviour was found to the fatigue test, where the longer the mechanism of both flexure and silicone are loaded, the more the input force, and thus stiffness, decreases. This confirms the effects of visco-elasticity of the non-isotropic PLA material. Solutions to this in terms of alternative materials will be discussed in chapter 6. Correct closure of the pressurized graft was confirmed visually. However, for future research it could be beneficial to measure the output force rather than the input force as this would confirm without a doubt that the mechanism can close the anastomosis each cycle.

5.5. Traction on Graft

Requirement: 1f Traction on the Anastomosis must not lead to rupture in the sutures. Based on linearly scaled based on wall-thickness of porcine studies, this force was determined to be no more than 0.38N.
Method: the linear stage used throughout this project was used to actuate the dAVF. However, the FUTEK 45N Loadcell that is previously placed on the input, was connected to a custom made coupling pieced to which a 10mm length of 6mm DL graft was fitted. These connection pieces were designed to be light, as to not introduce a bending moment on the loadcell, as well as stiff to not influence measurement data. An overview of the utilized test setup is given in figure 5.9a.
Results: the data gathered from this test was processed in Matlab. The FUTEK 45N Loadcell has a resolution of 0.0243N, the data was smoothed using a Savitzky-Golay filter for each individual actuation cycle. The result of which is plotted in figure 5.9b.

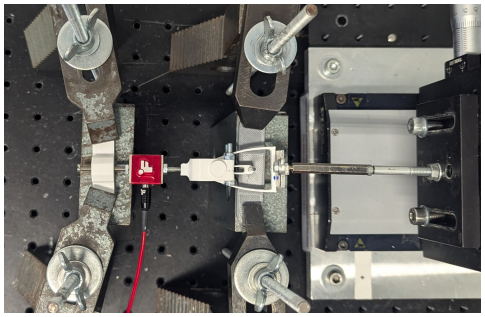

(a) Test setup used to determine the tractive forces on the graft. From right to left linearstage that is used to actuated the compliant mechanism. A 10mm piece of 6mm DL graft is fixated in a holder coupled to the red FUTEK 45N Loadcell which is fixate on the other end.

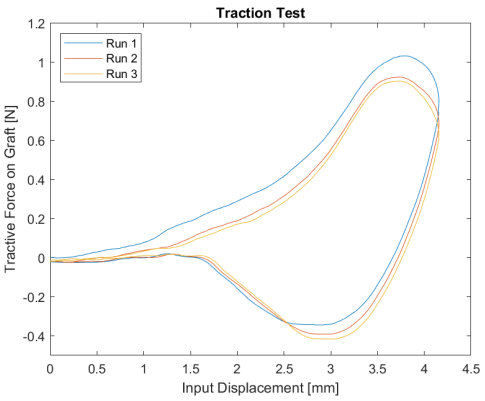

(b) Traction forces measured on the graft over actuation displacement for three runs. A positive force is noted when the graft is pushed away from the dAVF, negative force occurs when the graft is pulled inwards.

Figure 5.9: Traction Test

Discussion: to understand the results shown in figure 5.9b the direction of tractive force is of importance (when a positive force is measured when the graft is pushed away from the dAVF). Upon actuation the rotation of the contact surface will push the graft outwards (the rising line in the graph). The last part of closure, it can be seen that the force is more rapidly increasing. This can be explained at the point indicated in figure 5.3a where the contact surfaces form a new contact point inwards of the mechanism around which they start rotating. This new rotation point is assumed to increase traction forces on

the graft. Around at 3.7mm the tractive force starts reducing which is likely when the graft is closed and further actuation pulls the graft inwards as the outer flexures start buckling. Upon opening of the mechanism the pushing tractive force starts reducing, enters the negative regime (pulling) before returning to zero. The mean maximum force was found at 0.95N. To perform this test, a setup was build with some limitations, not being able to pressurize the graft was already mentioned. Ideally an identical test setup used on the state of the art was used to allow for the best comparison. Unfortunately, neither the original setup nor the design was available. The setup designed for this test had to be compatible with existing equipment. Another limitation is the fixation of the mechanism relative to the graft. The mechanism was fixated with a rigid pin on the input stage of the mechanism. Upon implantation within the body however, there is no rigid connection upon which the dAVF is fixated. From this test as it currently is, it must be concluded that the traction on the graft is exceeded. Further discussion regarding this can be found in chapter 6.

6

Discussion

In this chapter a retrospection on the entirety of this project is given. Following this the results of the validation tests in the previous chapter will be discussed and linked to the requirements set in chapter 2. This chapter will be concluded with recommendations for future research involving this design.

6.1. Design Process Evaluation

6.1.1. Restrictions and Boundaries

As with any engineering project, the design of the compliant dAVF started with an investigation into the problem at hand. Since the fields of medical sciences and engineering are worlds apart, gaining more insight at the start of this project was of vital importance. Asking the five W's [14] (Who's involved, what is the problem, where is it located, when does it occur and why does the problem need solving?) resulted in a clear definition of the stakeholders, desired functionality, restrictions of designing an implant and the biological functionalities affecting (and affected by) the dAVF. Although a large amount of time was invested in understanding the medical and meeting with a nephrologist and a surgeon, this study was always going to be approached from an engineering point of view. Recognizing this, the goal of setting the requirements and criteria was to translate the medical findings, studies and articles into technical requirements. These requirements were to adhere to the VALID-guidelines (similar to SMART) with the goal of applying the engineering design methodologies and allowing for verification and validation of the final design. With this the decision was made to avoid conducting in-depth medical studies as this fall outside of the desired scope. This meant a heavy reliance on available and existing knowledge; for compliant mechanisms, implants and AVFs a plethora of articles and papers were found. In hindsight a clear knowledge gap was identified on the subject of dynamic mechanical implantable devices. A large quantity of implants researched for basing the requirements and criteria on, where either static or did not rely on mechanical solutions (such as pacemakers, cosmetic implants or orthopaedic implants). Within the cardiovascular field stents and artificial heart-valves share some similarities in functionality, however neither are required to be actuated multiple times at will.

Although all requirements and criteria were reevaluated, the decision to not conduct medical studies, meant relying on the data gathered in earlier work on the dAVF. Upon completion of this project and in retrospect this resulted in requirements with specific values based on the very limited knowledge available. For example, the volume requirement is based on a single cadaver study [8]. For this project the dimensions of this volume were followed as a tight limit were in reality this might not be the case when a larger quantity of samples could be tested. Another example is the effects of FBR leading to tissue ingrowth. Although simulating the ingrowth with a silicone model, the exact influence on the compliant dAVF is yet unknown. And this can only be validated using animal studies which are expensive, time consuming and have to be ethically evaluated.

Some other restrictions in this research were self-imposed to limit the scope of this research and focus on the development of the compliant dAVF. An example of this was the choice to use the existing actuator design. Although the performance of this actuator can be adapted without much work, doing so would have increased the design variables and distracted from the scope of the project objective. Nonetheless, further optimizations could be achieved by optimizing the system of both the valve and the

actuator rather than the individual sub-systems. During design optimization it was found that smaller mechanisms would benefit a reduced displacement with an increased force output of the actuator.
Concepts Gathered: For concept generation in chapter 3, a broad and diverse spectrum of mechanisms was considered. A conscious choice was made to focus on existing mechanisms over development of a new mechanism from the ground up due to the large availability of compliant mechanisms with similar functionality. This resulted in the largest possible quantity of compliant mechanisms considered and evaluated for the compliant dAVF within the time allocated for this study. It would be interesting to have utilized advanced techniques like a topology optimization model. However based on experience with optimization, the results will only be as good as the model. Thus the approach used here, upon reflection, was the right one.
Resulting from this broad scope of identified sub-solutions, three concepts were constructed with the help of design focusses. These design focusses helped narrow down the large amount of possible combinations to three promising and varied concepts. Some concepts had to be reiterated upon multiple times before all created concepts matched a similar level of development where the concept would offer a viable solution to the requirements. A critique on the focus approach could be that there is a certain overlap of the focusses and some criteria. For the most important criteria however it would seem reasonable to attempt to construct concepts that would score well on these in the Harris Profile. In a way this overlap can be seen as a sensitivity analysis of the influence that favouring one criteria has on the others.
Concept Selection: for the selection of the best concept based on the criteria; a graphical Harris Profile was favoured over a numerical scored alternative [49]. The main reason for this was to acknowledge the level of uncertainty present at the time of selecting a concept to develop further. The criteria were set such that they could be scored based on some uncertainty and the concepts evaluated were designed to a state were this would be feasible. However, unless each concept was optimized to its best form, there will always be some unknowns due to potential differences in performance. For this reason it was thought best to not score concepts with a score between one to ten and then multiplying this with a weighing factor. At this level of development this could inspire an undesired level of confidence and a small change in scoring and weight factor could unbeknownst to the designer result in a different outcome. In the end both numerical and graphical methods share a lot of similarities; each concept is still scored based on criteria but with a lower range and the criteria ranked on importance to the design objective rather than weighted. This method was favoured for its recognition of the uncertainty present in the concepts and mitigating false confidence.
Optimization Approach: As discussed in section 4.2 on optimization, various models have been considered for optimizing the design upon with varying success, but all models helped gain a better insight in the design of the flexure. A simple PRBM-study was used to gain a insight on the impact of basic parameters on the motion of the mechanism. However, to allow for more rapid iterations and more different geometry it was decided to continue optimization with the use of a FEA. To ensure the model was accurate, two different validation studies were performed confirming acceptable correlation to tested samples as shown in section 4.2.1. A downside of FEA is a significant increase in computation time. However, since the geometry could be evaluated in 2D, a reduction from multiple minutes to twenty seconds per iteration could be achieved.
For both models, PRBM or FAE, only the compliant mechanisms was analysed and optimized. Multiple experts on compliant mechanisms and silicone modelling warned for the complications of multi-material simulations. Simulation of the silicone layer is no more complicated than simulation of the compliant mechanism but interface between materials is hard to predict. To accommodate for this unknown a study on a prototype model was performed from which it was found that without any optimization, the addition of silicone roughly doubled the actuation stiffness of the design. To further accommodate for this uncertainty, the design goal for the optimization was set to extract the most work from the actuator whilst storing the least amount of energy in the compliant mechanism. This leaves a maximal amount of energy for deformation of the silicone. As the silicone was not modelled, this did not take into consideration the effects of dimensioning on the stiffness of the silicone.
For any form of optimization it is important to limit the amount of free variables to maintain an overview of the impact each variable has to the design goal. A optimization model with all free variables set free, large list of constraints and complex design goal could theoretically result in a better design. However, the designer would lose a sense of control over the influence of each design decision. The design goals used in this project are also focussed on the uncertainty of the added stiffness caused by the

Table 6.1: Evaluation results of the proposed design to the requirements.

Requirement	Target	Achieved	Status
1.1 Volume	L<30mm, W<15mm,H<10mm	L=32mm, W=16mm, H=6.5mm	Exceeds requirement, requires minor reiteration of design or reevaluation of the volume requirement
1.2 Mass	<50 grams	<5.96 grams	Confirmed by measurement
1.3 Blood flow in Open state	>600ml/min	TBD	Confirmed by prior use
1.4 Pressure resistance in closed state	>170mmHg	180mmHg	Confirmed by testing with pressurized graft in section 5.3.
1.5 Compatibility with DAS-Actuator	<0.11 J	0.03J	Confirmed by stiffness testing
1.6 Resultant Force on anastomosis	<0.76N	0.95N	Current tests exceed the requirement, a reevaluation of the design, requirement and test setup is required
1.7 Life Cycle	>836 Cycles	>836 Cycles	Confirmed by fatigue testing in section 5.4
1.8 Fail Safety	Return to open position	Returns to open position	Concluded from testing
1.9 Multiple Stages	>three positions	Stable across entire range	Concluded from testing
1.10 Control of opening	>10s opening time	Can be controlled at will	Concluded from testing
2.1 Resistance to Fibrous Tissue	<42.5N	31.8N	Confirmed by measurement of simulation in section 2.4
2.2 Biocompatible material	Confirmed prior use	Prior use confirmed	Confirmed by Literature Study [24]
2.3 Limited tissue ingrowth	4 years	TBD	Confirmed by measurement of simulation
2.5 Removeable	Assessed by surgeon	TBD	To be consulted with Surgeon

silicone. The uncertainty comes from the difficulty of multi-material large deformation simulations. Several experts advised to not pursue this within the set time span of this project. If this could be achieved however, a more in-depth analysis on the entire system could be given leading to a better optimized result.

6.2. Requirement Evaluation

In the table 6.1 the requirements set in chapter 2 are compared to the results found in validation and verification in chapter 5. Where required, extra discussion is provided in the following sections of text.

6.2.1. Volume

In the optimization a focus was determined on extracting the most energy from the actuator and maximizing the energy budget available for silicone deformation. Over the design process this resulted in creating a mechanism with outer dimensions close to the volume requirements. To ensure the requirement was followed, one of the prototypes developed specifically followed to constraints set by the volume. Unfortunately, to increase durability of the silicone layer, the thickness of this layer was increased which lead to exceeding the length requirement with 2 millimetres and the width requirement with 1 millimetre. Upon consultation with an expert, it was concluded that for most patients the increased length of the implant is likely acceptable as this length is parallel to the arm. Concerns were expressed on the widths of this concept and the other prototypes from different optimization goals.

Following the results found in the for this stiffness tests of this concept in silicone on a pressurized graft in figure 5.4b where only one third of the energy available is used. The test on simulated FBR in section 5.3.2 were performed on a different prototype, the results do inspire that, taking into account the effects of tissue encapsulation, the mechanism can be adapted to meet the original volume requirements.
This discussion also confirms the importance of clear requirements. The volume requirement used in this study is based on a single cadaver study. Whilst this does provide a clear indication of the range of volume requirements, future studies would benefit greatly from a larger range of samples that will lead to a better insight in the volume availability near potential locations for the dAVF.

6.2.2. Traction

The tractions tests performed in this study, discussed in more detail in section 5.5, suggested the requirement of 0.76N of tractive force on the anastomosis to be exceeded by 0.19N or by 20%.
This requirement originates form the development of the original dAVF . As specific measurement of traction on the arteriovenous system near the dAVF was not possible, the suture tear out force of other tissue was linearly scaled to the wall thickness of a brachial vein [8]. Due to uncertainty introduced by this approach, a safety factor of two was applied on top of the assumption that all of the traction force could focus on one suture. Based on in-vivo testing of the previous iteration it can be concluded that this requirement will eliminate possible tearout due to tractive forces, however there is a possibility of this requirement being more strict than necessary. Further investigation on the allowed tractive forces on the anastomosis would therefore be recommend. But for the knowledge available at the time of this study, it has to be concluded that the proposed concept does not meet the set requirement.
Limiting the tractive forces on the anastomosis has always been an important design objective of the dAVF [8]. In the generation of concepts in chapter 3, one of the applied focussed was placed on traction reduction. Due to the expected larger amount of energy storage within this concept, among other reasons, the robust concept was favoured over this concept. In the further optimization of the concept, the motion of closure was optimized for with the angle of the grippers. However, due to the complexity, no simulations were performed to assess the tractive forces on the graft. Therefore, determination of these tractive forces relied upon measurements in the verification and validation stage.
As the test setup (design) used in the previous study was no longer available, a new setup had to be designed. The comparison between the state of the art design and the compliant dAVF could not be made. The setup used for traction testing allowed for testing of only the mechanisms without the silicone layer due to interference between the setup and the deformed silicone. Whilst this does allow for test data, it is assumed to be the worst case. The starting position of the graft could not be determined by the graft requiring a manual placement of the graft in the mechanism. Over closure of the dAVF it can be assumed that the added stiffness of the silicone will reduce traction forces. However, this could only be certainly claimed after the setup is altered to fit silicone encased models.

6.2.3. Life cycle

Fatigue testing concluded that the set life cycle of the requirement was achieved. For compliant mechanisms this was to be expected since, as long as the stress in the flexures is kept below the endurance limit [38], no wear or tear occurs. The same holds for the silicone layer, which showed no damages after the set amount of actuations. Although it can be assumed that the complaint dAVF is capable of a large quantity of actuation cycle, the tests performed only reached the amount of cycles set by the requirement. The linear stage used for this study, selected for its fine resolution in both displacement as force actuation, was not able to repeat a programmed set of actuations. This resulted in manual control of the actuation, a time consuming process. In fatigue testing it was found that non-linear effects occur linked to viscoelastic behaviour, this is further discussed in section 5.4 and illustrated in section 5.4. These effects can be reduced by a selecting a material with reduced viscoelastic properties, such as PEEK or titanium, and selecting a manufacturing process that result in an isotropic product, such as milling. The decision for the use of FDM-printed PLA was based on a relatively similar Young's Modulus to PEEK and FDM-printing allowed for rapid prototyping of concepts which proved vital in the development of the compliant dAVF.

6.2.4. Control of dAVF

The requirements 1.8, 1.9 and 1.10 were not subjected to their own tests, however based on the performance of the compliant dAVF in the tests on stiffness in section 5.3, the achievement of these requirements could be confirmed. Fail safety can be confirmed by observing that actuation of the dAVF is only required for closure of the anastomosis. Due to the inherit stiffness of the compliant mechanism, to open the anastomosis only a release of tension in the Bowden cable is required. Thus, if the actuator, bowden cable or even a flexure would fail; the compliant dAVF will return to its minimal energy position which is the open state. Both multiple stages of opening as well as control over the speed of opening, are achieved by remaining below the actuation force limit at all time and the actuator non-backdrivable properties elaborated in section 1.2.

6.2.5. Resistance to Fibrous Tissue

The behaviour and effects of fibrous tissue formation remain hard to predict. For this study a silicone model was chosen over the use of animal studies due to time limitations and ethical considerations. The two tests performed in section 2.4 simulated both complete encapsulation of the compliant dAVF as well as the effects ingrowth of fibrous tissue would have in case of failure of the silicone layer. Exact replication of material properties of fibrous tissue by the silicone (Platsil OO-30) is uncertain, a similarity between this specific silicone and harder tissue in the body was confirmed by an expert of the Phantom Lab. Since casting of silicone was already part of the production process, this approach resulted in fast reiteration times compared to animal models.
Other approaches were considered of researching the compliant dAVFs ability to withstand formation of fibrous tissue. With tissue forming after the introduction of collagen inside the silicone, a test was conceptualized to prove waterproofness of the device. The reasoning being that if the compliant dAVF would be waterproof, no collagen can enter and thus the device would be protected from internal formation of fibrous tissue by prevention. This however would have only been a subset of resistance to fibrous tissue. With the current approach, it is shown that the valve does not have to prevent formation as it is capable of resisting the impact of fibrous tissue.
If development of the compliant dAVF is to be continued, in-vivo testing would be recommended after all of the issues discussed in this chapter are solved.

6.3. Recommendations

The proposed design shows potential. Finishing this development cycle, the following recommendations are given to continue development of the compliant dAVF or other research areas within this field.

- For setting realistic requirements, continuation of medical research into volume constraints and traction on sutures are recommended. The values currently known provide a solid foundation to design a dAVF to, however if further optimization is desired; a larger and more realistic sample set is required to ensure a design can be created that fits the actual needs and functionality.
- In these early stages of development from the mechanical side, the importance of rapid prototyping is not to be underestimated. Due to the complexity of simulation of systems like discussed in this paper, the faster more goal oriented approach can be of great value. In the final stages of this research, based on availability of equipment, the workflow of creating prototypes was fine-tuned such that within 24 hours a new design could be adapted, printed, cast in silicone and tested on the linear stage.
- For the next stage of development for the compliant dAVF, after the issues with traction are resolved, would involve creating a prototype CNC-milled from PEEK. The optimization models used in this process can be reused effectively with new material properties. The silicone used for this study is rated as skin safe [51] and not for implantation. A different supplier would likely be required to ensure the material is biocompatible.

7

Conclusion

Previous iterations of the Dynamic Arteriovenous System relying on pin-hinge mechanisms encountered issues over time during in-vivo testing due to fibrous tissue formation limiting performance. Applying systems engineering principles the problem definition and project objective were set;

Problem Definition: The TUDelft and LUMC research group have found that fibrous tissue forms on critical parts of a valve for the dynamic arteriovenous system placed between the proximal artery and vein after long term implantation of the device. The fibrous tissue formed around the pin-hinges highly influenced both performance and reliability of the valve. Prevention of tissue formation that forms an obstruction in the valve-mechanism is needed to guarantee long term functioning of the valve and a prolongation in life expectancy of those suffering from ESKD.

Project Objective: To reduce the adverse effects of fibrous tissue formation on performance and durability of the DAS valve, a compliant valve is to be designed and tested that performs similarly to previous designs in reducing the negative effects of an AVF treatment but is more resistant against tissue formation.

Requirements were set to measure the performance of the design and to ensure a functional solution to the problem definition. Following concept generation & selection, design optimization and prototyping the multiple prototypes (based on three optimization goals) were tested and evaluated. Due to uncertainty of the added stiffness of the silicone encasing, three models based on three optimization goals were optimized and prototyped. In testing it was found that all three models meet the majority of requirements. Traction on the graft upon closure of the dAVF has to be further investigated. The volume requirement was exceeded by a small margin, based on the performance of the dAVFs and the remaining energy budget, this can likely be resolved in a minor reiteration. Simulated fibrous tissue encapsulation and ingrowth showed the compliant dAVF largely unaffected. This inspires confidence that, with continued development, the compliant dAVF is capable of providing a robust solution against fibrous tissue formation.

References

[1] J. C. Lv and L. X. Zhang, "Prevalence and Disease Burden of Chronic Kidney Disease," *Advances in Experimental Medicine and Biology*, vol. 1165, pp. 3–15, 2019, ISSN: 22148019. DOI: 10.1007/978-981-13-8871-2_1/COVER/. [Online]. Available: https://link.springer.com/chapter/10.1007/978-981-13-8871-2%7B%5C_%7D1.

[2] Nerfrovisie, "Renine Registry Annual Report 2021," Nefrovisie, Utrecht, Tech. Rep., 2021. [Online]. Available: www.nefrovisie.nl.

[3] J. Perl and J. Bargman, "Peritoneal dialysis: From bench to bedside and bedside to bench," *American Journal of Physiology - Renal Physiology*, vol. 311, no. 5, F999–F1004, 2016, ISSN: 15221466. DOI: 10.1152/ajprenal.00012.2016.

[4] J. Malik, C. Lomonte, J. Rotmans, *et al.*, "Hemodialysis vascular access affects heart function and outcomes: Tips for choosing the right access for the individual patient," *Journal of Vascular Access*, vol. 22, no. 1_suppl, pp. 32–41, Nov. 2021, ISSN: 17246032. DOI: 10.1177/1129729820969314.

[5] M. L. Robbin, T. Greene, A. K. Cheung, *et al.*, "Arteriovenous Fistula Development in the First 6 Weeks after creation," *Radiology*, vol. 279, no. 2, pp. 620–629, 2016, ISSN: 15271315. DOI: 10.1148/radiol.2015150385.

[6] P. Roy-Chaudhury, V. P. Sukhatme, and A. K. Cheung, *Hemodialysis vascular access dysfunction: A cellular and molecular viewpoint*, 2006. DOI: 10.1681/ASN.2005050615. [Online]. Available: www.jasn.org..

[7] R. Stolic, "Most important chronic complications of arteriovenous fistulas for hemodialysis," *Medical Principles and Practice*, vol. 22, no. 3, pp. 220–228, 2013, ISSN: 14230151. DOI: 10.1159/000343669.

[8] N. White, "The Design and Validation of a Dynamic Arteriovenous System Valve Mechanism," Ph.D. dissertation, 2021. [Online]. Available: https://repository.tudelft.nl/islandora/object/uuid:582a1501-01c0-4492-99ba-df0a524535de?collection=education.

[9] S. van der Kroft, "Design and validation of a subdermal actuator for use in a dynamic Design and validation of an implantable actuator for use in a novel arteriovenous shunt system," no. January, 2020.

[10] R. Hart, "DAS," pp. 1–11, 2022.

[11] Y. Wu, "The Design and Validation of a Monitoring System for the Dynamic Arteriovenous System," 2023.

[12] N. A. White, S. L. van der Kroft, K. E. van der Bogt, *et al.*, "An implantable magnetic drive mechanism for non-invasive arteriovenous conduit blood flow control," *IEEE Transactions on Biomedical Engineering*, pp. 1–12, 2024, ISSN: 0018-9294. DOI: 10.1109/tbme.2024.3370263.

[13] NASA, "NASA System Engineering Handbook Revision 2," *National Aeronautics and Space Administration*, p. 297, 2007. [Online]. Available: https://www.nasa.gov/sites/default/files/atoms/files/nasa%7B%5C_%7Dsystems%7B%5C_%7Dengineering%7B%5C_%7Dhandbook%7B%5C_%7D0.pdf.

[14] T. Horeman and B. V. Straten, *Design of a Sustainable Medtech solution*, 2023.

[15] *Feiten en cijfers - Nierstichting*. [Online]. Available: https://nierstichting.nl/leven-met-een-nierziekte/feiten-en-cijfers/ (visited on 06/10/2022).

[16] J. Tordoir, B. Canaud, P. Haage, *et al.*, "EBPG on Vascular Access," pp. 88–117, 2007. DOI: 10.1093/ndt/gfm021.

[17] K. Y. Chang, S. H. Kim, Y. O. Kim, *et al.*, “The impact of blood flow rate during hemodialysis on all-cause mortality,” *Korean Journal of Internal Medicine*, vol. 31, no. 6, pp. 1131–1139, 2016, ISSN: 20056648. DOI: 10.3904/kjim.2015.111.

[18] C. E. Lok, T. S. Huber, T. Lee, *et al.*, “KDOQI Clinical Practice Guideline for Vascular Access: 2019 Update,” *American Journal of Kidney Diseases*, vol. 75, no. 4, S1–S164, 2020, ISSN: 15236838. DOI: 10.1053/j.ajkd.2019.12.001. [Online]. Available: https://doi.org/10.1053/j.ajkd.2019.12.001.

[19] N. Depner, Thomas; Krivitski, “Clinical Measurement of Blood Flow in Hemodialysis Access Fistulae and Grafts by Ultrasound Dilution,”

[20] L. Manning, T. G. Robinson, and C. S. Anderson, “Control of blood pressure in hypertensive neurological emergencies,” *Current Hypertension Reports*, vol. 16, no. 6, 2014, ISSN: 15343111. DOI: 10.1007/s11906-014-0436-x.

[21] E. A. Tansey, L. E. Montgomery, J. G. Quinn, S. M. Roe, and C. D. Johnson, “Understanding basic vein physiology and venous blood pressure through simple physical assessments,” *Advances in Physiology Education*, vol. 43, no. 3, pp. 423–429, 2019, ISSN: 15221229. DOI: 10.1152/ADVAN.00182.2018.

[22] K. B. Quencer and R. Oklu, “Hemodialysis access thrombosis,” *Cardiovascular Diagnosis and Therapy*, vol. 7, no. Suppl 3, S299–S308, 2017, ISSN: 22233660. DOI: 10.21037/cdt.2017.09.08.

[23] J. Zilberman-Rudenko, J. L. Sylman, H. H. Lakshmanan, O. J. McCarty, and J. Maddala, “Dynamics of Blood Flow and Thrombus Formation in a Multi-Bypass Microfluidic Ladder Network,” *Cellular and Molecular Bioengineering*, vol. 10, no. 1, pp. 16–29, 2017, ISSN: 18655033. DOI: 10.1007/s12195-016-0470-7.

[24] D. Ulijn, “Biocompatible Materials & Production Methods for Mechanical Implants Literature Review,”

[25] J. Su, H. P. Gonzales, and L. Tang, “Modeling and Simulation of Foreign Body Reactions to Neural Implants,” *Advances in Cognitive Neurodynamics*, pp. 879–883, 2007.

[26] International Institute of Business Analysis, *A Guide to the Business Analysis Body of Knowledge*. Toronto, Canada, 2011, p. 100, ISBN: 9780981129211.

[27] J. Iwanaga, M. C. Fox, H. Rekers, L. Schwartz, and R. S. Tubbs, “Neurovascular anatomy of the adult female medial arm in relationship to potential sites for insertion of the etonogestrel contraceptive implant □ , □□ , □,” *Contraception*, vol. 100, no. 1, pp. 26–30, 2019, ISSN: 0010-7824. DOI: 10.1016/j.contraception.2019.02.007. [Online]. Available: https://doi.org/10.1016/j.contraception.2019.02.007.

[28] M. L. Rocca, A. R. Palumbo, F. Visconti, and C. Di Carlo, “Safety and benefits of contraceptives implants: A systematic review,” *Pharmaceuticals*, vol. 14, no. 6, pp. 1–26, 2021, ISSN: 14248247. DOI: 10.3390/ph14060548.

[29] C.R.Bard GmbH, “Feel and See the NEW Standard of Care ™ Das P ower P ort Portimplantat Eine neue Generation von Ports für die Infusionstherapie P ower P ort Titan Portimplantates : G roshong Ventil Silikon-Katheter : C hrono F lex Polyurethan Katheter haben eine bessere,” no. 8708000, 2010.

[30] S. Plagenhoef, F. Gaynor Evans, and T. Abdelnour, “Anatomical Data for Analyzing Human Motion,” *Research Quarterly for Exercise and Sport*, vol. 54, no. 2, pp. 169–178, 1983, ISSN: 21683824. DOI: 10.1080/02701367.1983.10605290.

[31] S. P. Rodrigues, T. Horeman, J. Dankelman, J. J. Van Den Dobbelsteen, and F. W. Jansen, “Suturing intraabdominal organs: When do we cause tissue damage?” *Surgical Endoscopy*, vol. 26, no. 4, pp. 1005–1009, 2012, ISSN: 14322218. DOI: 10.1007/s00464-011-1986-5.

[32] E. Gill, “Space Systems Engineering (AE4-S12) Slides,” 201000087, 2019, pp. 1–22, ISBN: 9781305968356.

[33] I. W.L. Gore and Associates, *AV ACCESS PORTFOLIO*, 2023.

[34] L. L. Howell, S. P. Magleby, and B. M. Olsen, *Handbook of Compliant Mechanisms*. 2013, ISBN: 9781119953456. DOI: 10.1002/9781118516485.

[35] A. E. Albanesi, V. D. Fachinotti, and M. A. Pucheta, “a Review on Design Methods for Compliant Mechanisms,” *Mecánica Computacional*, vol. XXIX, pp. 59–72, 2010.

[36] JPE, *Precision Point*, 4th. Maastricht, 2019.

[37] S. Visser, *Compliers*, 2022. [Online]. Available: https://www.stevevisser.design/5 (visited on 02/12/2024).

[38] L. L. Howell and A. Midha, “A method for the design of compliant mechanisms with small-length flexural pivots,” *Journal of Mechanical Design, Transactions of the ASME*, vol. 116, no. 1, pp. 280–290, 1994, ISSN: 10500472. DOI: 10.1115/1.2919359.

[39] J. L. Dearden, “Design and Analysis of Two Compliant Mechanism Designs for Use in Minimally Invasive Surgical Instruments BYU ScholarsArchive Citation,” 2016.

[40] C. L. Grames, “Design and Manufacture of Mesoscale Robot- Actuated Surgical Instruments,” 2015.

[41] J. L. Herder, M. J. Horward, and W. Sjoerdsma, “A laparoscopic grasper with force perception,” *Minimally Invasive Therapy and Allied Technologies*, vol. 6, no. 4, pp. 279–286, 1997, ISSN: 13645706. DOI: 10.3109/13645709709153076.

[42] J. L. Sheffield, B. Sargent, and L. L. Howell, “Embedded Linear-Motion Developable Mechanisms on Cylindrical Surfaces,” *Journal of Mechanisms and Robotics*, vol. 16, no. 1, pp. 1–11, 2024, ISSN: 1942-4302. DOI: 10.1115/1.4062133.

[43] J. R. Greenwood, S. P. Magleby, and L. L. Howell, “Developable mechanisms on regular cylindrical surfaces,” *Mechanism and Machine Theory*, vol. 142, 2019, ISSN: 0094114X. DOI: 10.1016/j.mechmachtheory.2019.103584.

[44] V. Arora, P. Kumar, R. Kumar, and J. P. Khatait, “Design of Compliant Iris,” *Lecture Notes in Mechanical Engineering*, pp. 911–917, 2022, ISSN: 21954364. DOI: 10.1007/978-981-16-0550-5_84.

[45] B. M. Kumar, D. K. Badige, S. Hegde, and G. K. Ananthasuresh, “An improved compact compliant mechanism for an external pipe-crawler,” *14th National Conference on Machines and Mechanisms, NaCoMM 2009*, pp. 54–61, 2020.

[46] K. Schreurs, “The design of a compliant shape-preserving ring,” Ph.D. dissertation, 2019.

[47] H. Soemers, *Design Principles for precision mechanisms*. 2017, p. 276, ISBN: 978-90-365-3103-0.

[48] M. Zare, E. R. Ghomi, P. D. Venkatraman, and S. Ramakrishna, “Silicone-based biomaterials for biomedical applications: Antimicrobial strategies and 3D printing technologies,” *Journal of Applied Polymer Science*, vol. 138, no. 38, pp. 1–18, 2021, ISSN: 10974628. DOI: 10.1002/app.50969.

[49] Delft Design, “Harris profile,” vol. 39, no. 16, p. 1995, 1995.

[50] M. Ashby, H. Shercliff, and D. Cebon, *Materials: Engineering, Science, Processing and Design*. 2007, ISBN: 9780750683913.

[51] Polytek Development Corp., *Deadener & Hardener for Platsil Gels: Technical Bulletin*.

[52] J. A. Travieso-Rodriguez, R. Jerez-Mesa, J. Llumà, O. Traver-Ramos, G. Gomez-Gras, and J. J. R. Rovira, “Mechanical properties of 3D-printing polylactic acid parts subjected to bending stress and fatigue testing,” *Materials*, vol. 12, no. 23, 2019, ISSN: 19961944. DOI: 10.3390/ma12233859.

[53] K. W. Xu, Q. Gao, M. Wan, and K. Zhang, “Mock circulatory loop applications for testing cardiovascular assist devices and in vitro studies,” *Frontiers in Physiology*, vol. 14, no. April, pp. 1–17, 2023, ISSN: 1664042X. DOI: 10.3389/fphys.2023.1175919.

A

Experiment I: Graft Collapse under Static Pressure

A.1. Introduction

This test is done during the conceptual design phase for this master thesis project. In researching the selection of a suitable graft, a need arose to compare the collapse force and energy for the identified types and sizes of graft used in DAS. Due to complexity and the unknowns, it was opted to find these values experimentally rather than analytically or numerically through simulations.
Both of these types of graft consist of two layers PTFE material. For the triple layer as layer of silicone is added in the middle. Smaller double layer grafts come with removable rings to hold the graft open, these should be removed before implantation and thus before testing.

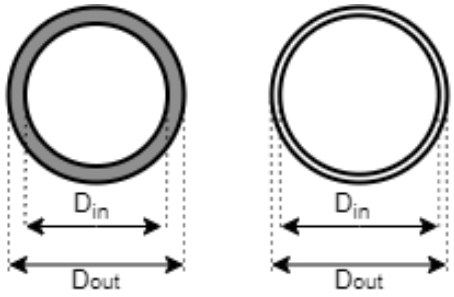

Figure A.1: Schematic representation of the triple layered graft on the left (with the silicone layer in grey) and the double sided graft on the right.

Table A.1: Identified grafts suitable for the DAS. The dimensions are the internal diameters.

Double Layer	Triple Layer
6mm	6mm
7mm	7mm
8mm	8mm

The desired result of this experiment is collection of two types of values;

1. The collapse force required throughout closure of the graft which should result in plots of force over closure distance for each graft.
2. The energy required to close the graft for each type of graft.

A.2. Hypothesis

Al tough the most realistic values are to be found by means of experiments some expectations can be done for this experiment. First the force required to collapse the graft, this is comprised of two forces; the force that results from the mechanical flexure of the graft and the force that is the result of compressing the pressurized fluid within. The material stiffness of the tube is relatively low, with the double layer being significantly less stiff than the triple layered graft. A simplified representation of the graft is given in figure A.2.

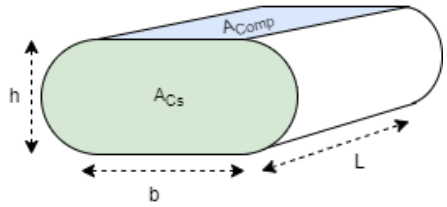

Figure A.2: A simplified figure of the graft halfway through compression with the used dimensions and the two areas used where A_{Cs} is the cross-sectional area and A_{Comp} the area on which the compressor of the DAS will act.

For the material properties the layer thickness was measured for both styles of graft, for all diameters the layer thickness is a constant. The material properties were found taking the average of the range for both Young's Modulus and Poisson Ration from Granta EduPack 2022 R1 (by ANSYS inc., Canonsburg, Pennsylvania).
To find the stiffness of a ring the following equation is used;

$$k = 4.48\frac{ELt^3}{D_{out}(1-v^2)} \tag{A.1a}$$

$$F_{Stiffness} = ks = 4.48\frac{ELt^3}{D_{out}(1-v^2)}s \tag{A.1b}$$

With this equation the force required to overcome the stiffness of both types and all sizes of graft was found. It should already be noted that this equation is only usable for smaller deformations which would lead to linear forces. In the case of a complete collapse of the graft the linear domain will be surpassed into the non linear domain which is not included in these models. Hence the reason for testing the provided samples.
Now to find the total required force the force created by the pressure inside the graft is to be determined. To determine the cross-sectional area it has to be noted that the circumference of the graft will remain a constant such that;

$$\pi D_{in} = 2b + \pi h \tag{A.2}$$

From this the area as well as the collapse force can be found (where it is assumed that two similar surfaces will occur hence the multiplication by 2);

$$A_{Comp} = L\frac{\pi(D_{in}-h)}{2} \tag{A.3a}$$

$$F_{Collapse} = 2pL\frac{\pi(D_{in}-h)}{2} \tag{A.3b}$$

Using the parameters of p is equal to 170 mmHg (or 24 kPa) and a compressor length L of 5 mm, the first results of equation (A.3b) are plotted in appendix A.2. As can already be deduced from equation (A.3b), the relation between Force and opening height, which could be called the spring coefficient for the graft, is linear. This is likely not the case for the final results as the (large) deformation of the material as well as the effects of the internal pressure on areas other than those that are compressed are not accounted for in this approximation of the graft closure.
Now the two forces are added to result in the total force using equation (A.4) which results in the two graphs depicted in appendix A.2.

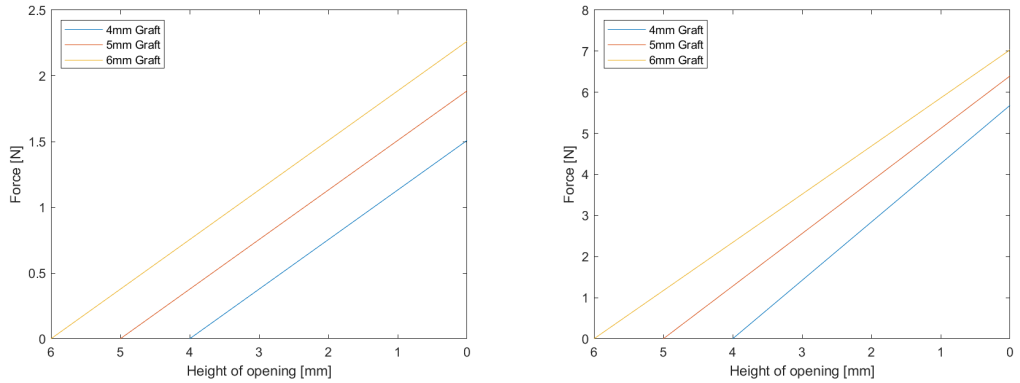

(a) Collapse Force for a double layered graft over closing height for the selected diameters.

(b) Collapse Force for a triple layered graft over closing height for the selected diameters.

Figure A.3: Plots of the hypothetical collapse force for the two types of graft

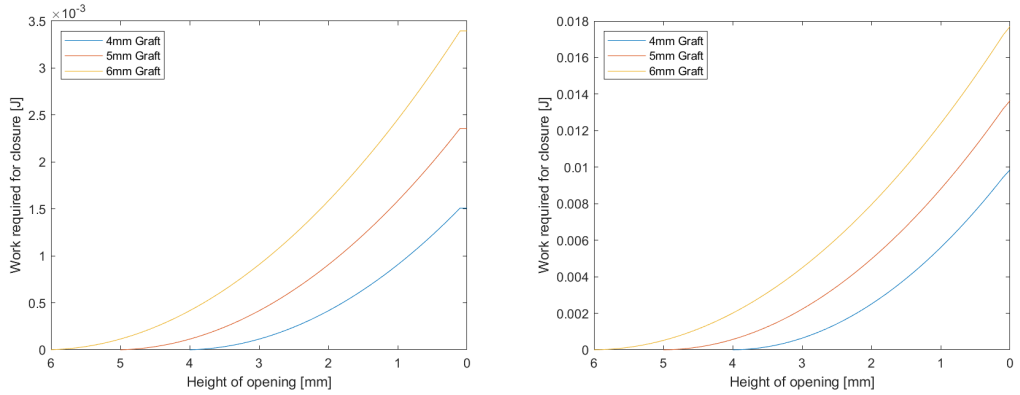

(a) The energy required to close the pressurised double layered graft.

(b) The energy required to close the pressurised triple layered graft.

Figure A.4: Plots of the hypothetical energy required for closing of the graft under static pressure.

$$F_{Collapse} = F_{Stiffness} + F_{Pressure} \tag{A.4}$$

To find the energy required to close the graft the formula in equation (A.5) is used which can be derived from the first law of thermodynamics with the assumption of constant pressure;

$$W = p(V_2 - V_1) \tag{A.5}$$

So in order to find the required work the volume that is compressed has to be found. For this the cross-sectional area in figure A.2 is multiplied by the compressor length (L) to find the volume that is defined as;

$$V_{Compressed} = A_{cross-sec.}L = bh + \frac{\pi h^2}{4} \tag{A.6}$$

With the volumes found in equation (A.6) substituted in equation (A.5) the plot in figure A.4b is generated. Again, as this approximation is solely based on the effects of closing of the pressurized graft, non-linear effects of the large material deformations are not accounted for. However, this graph does give an insight in the expected comparison between graft diameters.

A.3. Method

To test the compression of different grafts at different pressures a test setup as depicted in figure A.5 is proposed. Where a sufficient length of graft is connected to a syringe that can be set and secured a

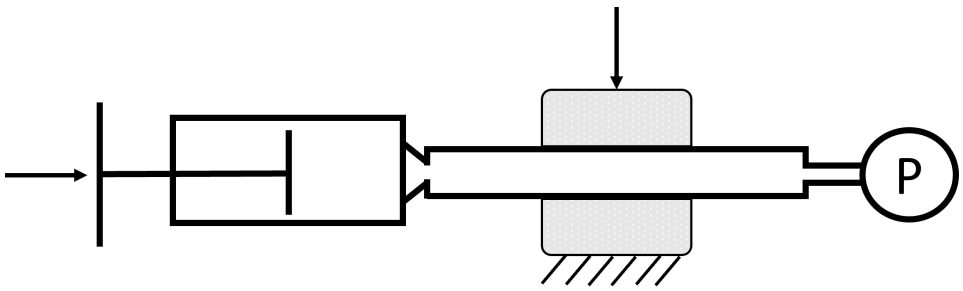

Figure A.5: A diagram of the test setup proposed for the static pressure tests.

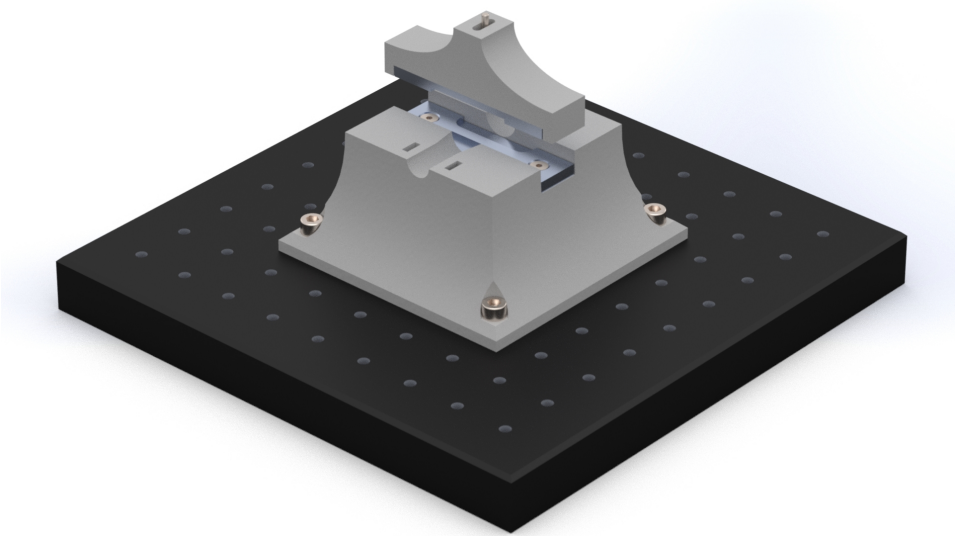

Figure A.6: A render of the custom made parts for static pressure test.

desired pressure on one end. On the other end a manometer is installed to monitor the pressure in the graft. For the fluid water is to be used, in other research a mixture of water and glycerol is used as this gives a similar density and dynamic viscosity as blood [53]. However, as neither of those properties is of interest for this test as no dynamics are involved. The syringe is to be compressed until the desired pressure is read on the manometer. The tests are to be done at 0 mmHg, 120 mmHg and 180mmHg. By measuring the collapse of an unpressurised graft, the effects of pressure can be determined in addition to the material spring stiffness. 120mmHg is considered a healthy systolic (upper pressure limited resulting from a heartbeat) blood pressure where a systolic blood pressure of 180mmHg can result in permanent damage.
For compressing the graft a one axis motion stage coupled to a strain gauge. The motion stage will be set at the grafts outer diameter and is to move downwards until the graft is fully closed all whilst the strain gauge will log the force required to close the graft. For the closing time a duration of 5 second is estimated as this corresponds to the closing time of earlier prototypes. To hold the graft and compression plates two PLA parts are 3D printed, their sole function is to hold the graft and compressor on the right place. Both are over designed to eliminate any lack of stiffness in these parts. The compressors are to be milled to ensure a realistic interface between the graft and the compressor. An overview of this is given in figure A.6.

B

Matlab Code

B.1. Pseudo Rigid Body Model

```
1
2  %% Gripper Pseudo Rigid Body Model
3  % Dirk Ulijn - 4321758
4  %% Setup
5  clear, close
6  clc
7  figure
8  %% Parameters
9  Y0 = 7.5; %[mm] Starting height (half of the design height)
10 RGraft = 3.4;%[mm] Outergraft diameter
11 LC=Y0-RGraft;
12 dMaxActuator = 4.5;%[mm] Maximal Displacement of the actuator
13 %LB = 10;
14 d = dMaxActuator;
15 %% For loop
16 LAV = 15:1:30;
17 LBV = 5:1:15;
18 Yend = zeros(size(LAV,2),size(LBV,2));
19 for n = 1:size(LAV,2)
20 for m = 1:size(LBV,2)
21 %% Variables
22 syms theta0 theta1 theta2
23 %% Equations
24 LA = LAV(n);
25 LB = LBV(m);
26 SumX = LA*cos(theta0)-LC*sin(theta1)-LB*cos(theta2)-LA+LB+d; %Sum of X Remove cos sin x3 for
       SumMDirk
27 SumY = -LA*sin(theta0)-LC*cos(theta1)+LB*sin(theta2)+LC; %Sum of Y
28 % SumM = LB/LA*theta1-theta2; %Sum of moments DIRK
29 %SumM = theta0+theta1-2*theta2; % Sum of moments THOMAS
30 SumM = (theta0+theta1)/LA-(2*theta2)/LB; %Sum of moments Combined
31 %eqn4 = -LA*sin(theta0)+LC*cos(theta1)-y2; %Displacement of Y2
32 %% Solver
33 [theta0solved, theta1solved, theta2solved]=vpasolve(SumX,SumY,SumM,[theta0 theta1 theta2
       ],[0.1 0.1 0.1]);
34 %% Displacements
35 X0 = 0;
36 %Y0=Y0;
37
38 X1 = X0+LA*cos(theta0solved);
39 Y1 = Y0-LA*sin(theta0solved);
40
41 X2 = X1-LC*sin(theta1solved);
42 Y2 = Y1-LC*cos(theta1solved);
43
44 X3 = X2-LB*cos(theta2solved);
45 Y3 = Y2+LB*sin(theta2solved);
46
```

```
X=[X0, X1, X2, X3];
Y=[Y0, Y1, Y2, Y3];

Yend(n,m)=Y2; % The end point is assumed to be Y2
AngleEndEffector(n,m)=rad2deg(double(theta2solved)); % Angle theta2, less rotational movement
     will result in a reduced traction on the graft. CHECK IF CORRECT

plot(X,Y);
hold on
end
end
x0 = 0;
y0 = Y0;

x1 = x0+LA;
y1 = y0;

x2 = x1;
y2 = y1-LC;

x3 = x2-LB;
y3 = y2;

x=[x0, x1, x2, x3];
y=[y0, y1, y2, y3];
plot(x,y);
axis equal
xlabel('x[mm]')
ylabel('y[mm]')

figure
surf(LAV,LBV,Yend');
hold on
contour3(LAV,LBV,Yend',[0 0], '-r','LineWidth',5)
title('Closure Displacement')
xlabel('Length of Flexure A [mm]')
ylabel('Length of Flexure B [mm]')
zlabel('Distance between end effectors on closure')

figure
surf(LAV,LBV,AngleEndEffector')
title('Closure Rotation')
xlabel('Length of Flexure A [mm]')
ylabel('Length of Flexure B [mm]')
zlabel('Rotation of end effectors on closure')
```

B.2. Variation Study

```
%% Design Variations Stiffness experiment
% Dirk Ulijn 18-06-2024
clc, clear,% close all
%% Import data
A20B9 = readmatrix("20_9_5x_3mm_run1.xlsx");
A20B11 = readmatrix("20_11_5x_3mm_run1.xlsx");
A25B10 = readmatrix("25_10_5x_2p5mm_run1.xlsx");
A25B12 = readmatrix("25_12_5x_2mm_run1.xlsx");
A25B15 = readmatrix("25_15_5x_1p5mm_run2.xlsx");
A30B11 = readmatrix("30_11_5x_2p5mm_run1.xlsx");
A30B14 = readmatrix("30_14_5x_3mm_run1.xlsx");

%% Data conditioning
% Offset Displacement and Absolute Force
[A20B9Open,A20B9Close,A20B9Both]=Clean(A20B9);
[A20B11Open,A20B11Close,A20B11Both]=Clean(A20B11);
[A25B10Open,A25B10Close,A25B10Both]=Clean(A25B10);
[A25B12Open,A25B12Close,A25B12Both]=Clean(A25B12);
[A25B15Open,A25B15Close,A25B15Both]=Clean(A25B15);
[A30B11Open,A30B11Close,A30B11Both]=Clean(A30B11);
[A30B14Open,A30B14Close,A30B14Both]=Clean(A30B14);
```

```
22
23 %% Calculate Means
24 window =100;
25
26 MeanA20B9Open = movmean(A20B9Open,window);
27 MeanA20B9Close = movmean(A20B9Close,window);
28 MeanA20B9Both = movmean(A20B9Both,window);
29
30 MeanA20B11Open = movmean(A20B11Open,window);
31 MeanA20B11Close = movmean(A20B11Close,window);
32 MeanA20B11Both = movmean(A20B11Both,window);
33
34 MeanA25B10Open = movmean(A25B10Open,window);
35 MeanA25B10Close = movmean(A25B10Close,window);
36 MeanA25B10Both = movmean(A25B10Both,window);
37
38 MeanA25B12Open = movmean(A25B12Open,window);
39 MeanA25B12Close = movmean(A25B12Close,window);
40 MeanA25B12Both = movmean(A25B12Both,window);
41
42 MeanA25B15Open = movmean(A25B15Open,window);
43 MeanA25B15Close = movmean(A25B15Close,window);
44 MeanA25B15Both = movmean(A25B15Both,window);
45
46 MeanA30B11Open = movmean(A30B11Open,window);
47 MeanA30B11Close = movmean(A30B11Close,window);
48 MeanA30B11Both = movmean(A30B11Both,window);
49
50 MeanA30B14Open = movmean(A30B14Open,window);
51 MeanA30B14Close = movmean(A30B14Close,window);
52 MeanA30B14Both = movmean(A30B14Both,window);
53
54
55 %% Plot
56 figure
57 plot(MeanA20B9Both(1:2495,1),MeanA20B9Both(1:2495,2),'r','LineWidth',2)
58 hold on
59 % plot(MeanA20B9Open(:,1),MeanA20B9Open(:,2),'r','LineWidth',2)
60 % plot(MeanA20B9Close(:,1),MeanA20B9Close(:,2),'r','LineWidth',2)
61
62 plot(MeanA20B11Both(1:2288,1),MeanA20B11Both(1:2288,2),'g','LineWidth',2)
63 % plot(MeanA20B11Open(:,1),MeanA20B11Open(:,2),'g','LineWidth',2)
64 % plot(MeanA20B11Close(:,1),MeanA20B11Close(:,2),'g','LineWidth',2)
65
66 plot(MeanA25B10Both(1:2360,1),MeanA25B10Both(1:2360,2),'b','LineWidth',2)
67 % plot(MeanA25B10Open(:,1),MeanA25B10Open(:,2),'b','LineWidth',2)
68 % plot(MeanA25B10Close(:,1),MeanA25B10Close(:,2),'b','LineWidth',2)
69
70 plot(MeanA25B12Both(1:2037,1),MeanA25B12Both(1:2037,2),'c','LineWidth',2)
71 % plot(MeanA25B12Open(:,1),MeanA25B12Open(:,2),'c','LineWidth',2)
72 % plot(MeanA25B12Close(:,1),MeanA25B12Close(:,2),'c','LineWidth',2)
73
74 plot(MeanA25B15Both(1:1320,1),MeanA25B15Both(1:1320,2),'m','LineWidth',2)
75 % plot(MeanA25B15Open(:,1),MeanA25B15Open(:,2),'m','LineWidth',2)
76 % plot(MeanA25B15Close(:,1),MeanA25B15Close(:,2),'m','LineWidth',2)
77
78 plot(MeanA30B11Both(1:2677,1),MeanA30B11Both(1:2677,2),'y','LineWidth',2)
79 % plot(MeanA30B11Open(:,1),MeanA30B11Open(:,2),'y','LineWidth',2)
80 % plot(MeanA30B11Close(:,1),MeanA30B11Close(:,2),'y','LineWidth',2)
81
82 plot(MeanA30B14Both(1:3208,1),MeanA30B14Both(1:3208,2),'k','LineWidth',2)
83 % plot(MeanA30B14Open(:,1),MeanA30B14Open(:,2),'k','LineWidth',2)
84 % plot(MeanA30B14Close(:,1),MeanA30B14Close(:,2),'k','LineWidth',2)
85
86 title('Stiffness profiles of varying flexure lengths')
87 xlabel('Input Displacement [mm]')
88 ylabel('Input Force [N]')
89 legend('A20B9', 'A20B11','A25B10','A25B12','A25B15','A30B11','A30B14' ,'Location','northwest
       ')
90 axis([0 2.5 0 20])
91 grid on
```

```
%% Save data
save('VariationStudyResults','MeanA30B14Close","MeanA30B14Open")
%% Clean Function
% This function will delete data where the stage is stationairy and
% differentiate opening movements from closing movements for the inputted
% data.
function [open,close,both] = Clean(Data)
% Offset Displacement and Absolute Force
Data(:,1) = Data(:,1)-Data(1,1); %Set first position to zero
Data(:,2) = abs(Data(:,2)); %Make force vector positives
index1=find(Data(:,1)<0.01); %Finds all points where stages rests at minimal displacement
Data(index1,:)=[]; % Removes all entries at zero position
index2=find(Data(:,1)>(max(Data)-0.01)); %Finds all points where stage rests at maximum
    position
Data(index2,:)=[]; % Removes all entries at max position
index3=find(diff(Data(:,1))==0); %Finds other stationairy points
Data(index3,:)=[]; %Removes all stationairy points
index4=find(diff(Data(:,1))>0); %Finds all closing motions
DataClose = Data(index4,:); %Defines closing movements
DataOpen = Data;
DataOpen(index4,:)=[]; % Defines opening movements

open=DataOpen;
open(open==0)=NaN;
open=sortrows(open);

close = DataClose;
close(close==0)=NaN;
close = sortrows(close);

both=[open;close];
both = sortrows(both);


end

%% Mean Function
% find the mean for each row of displacements and each row of force.
% Outputs [MeanDisplacements MeanForces]
function A = NonZeroMean(B)
% B(B==0)=NaN;
d=mean(B(:,1:2:size(B,2)-1),2,'omitNaN');
f=mean(B(:,2:2:size(B,2)),2,'omitNaN');
A= [d f];
end
```

B.3. Evaluation of verification results

```
        %% Concept Evaluation
        % Dirk Ulijn
        clc; clear ; close

        % Todo: Fix allignment in input so all lines start at the same point
        %% Load Data
        load("Actuator.mat")

        LowResMechanism = readmatrix("LowResConcept_Mechanism_4mm_5x.tmp.xlsx");
        LowResSiliconeHard = readmatrix("LowRes_HardSiliconeOnly_6mm_5x.tmp.xlsx");
        LowResSiliconeHardGraft = readmatrix("LowRes_HardSiliconeGraft_6mm_5x.tmp.xlsx");

        LowResSiliconeMix = readmatrix("LowRes_HardSoftSilicone_6mm_5x.xlsx");
        LowResSiliconeMixGraft = readmatrix("LowRes_HardSoftSiliconeGraft_6mm_5x.tmp.xlsx");

        LowResSiliconeIngrowth = readmatrix("LowRes_IngrowthSim_6mm_5x.tmp.xlsx");
        LowResSiliconeIngrowthGraft = readmatrix("LowRes_IngrowthSimGraft_6mm_5x.tmp.xlsx");
        LowResSiliconeEncap = readmatrix("LowResSiliconeMixFBRCap7mm5x.tmp.xlsx");
        LowResSiliconeEncapGraft = readmatrix( "LowResSiliconeMixFBRCapPresGraft7mm5x.tmp.
            xlsx");

```

```
        LowResSiliconePretension = readmatrix("LowRes_Pretension_5mm_5x.tmp.xlsx");

        LowVolMechanism = readmatrix("LowVolumeConcept_Mechanism_2p5mm_5x.tmp.xlsx");
        LowVolSiliconeMix = readmatrix("LowVol_HardSoftSilicone_4p5mm_5x.tmp.xlsx");
        LowVolSiliconeMixGraft = readmatrix("LowVol_HardSoftSiliconeGraft_5mm_5x.tmp.xlsx");

        LowStifMechansim = readmatrix("LowStiffnessConcept_Mechanism_3p5mm_5x.tmp.xlsx");
        LowStifMechanism2 = readmatrix("LowStiffnessConcept2_Mechanism_3p5mm_5x.tmp.xlsx");
        LowStifMechanism3 = readmatrix("LowStiffnessConcept3_Mechanism_3p5mm_5x.tmp.xlsx");
        LowStifSiliconeMix = readmatrix("LowStiff_HardSoftSilicone_6mm_5x.tmp.xlsx");
        LowStifSiliconeMixGraft = readmatrix("LowStiff_HardSoftSiliconeGraft_6mm_5x.tmp.xlsx
            ");

        load("Actuator.mat")
        %% Clean Data
        [LowResMechanismOpen,LowResMechanismClose,LowResMechanismBoth]=Clean(LowResMechanism)
            ;
        [LowResSiliconeHardOpen,LowResSiliconeHardClose,LowResSiliconeHardBoth]=Clean(
            LowResSiliconeHard);
        [LowResSiliconeHardGraftOpen,LowResSiliconeHardGraftClose,LowResSiliconeHardGraftBoth
            ]=Clean(LowResSiliconeHardGraft);

        [LowResSiliconeMixOpen,LowResSiliconeMixClose,LowResSiliconeMixBoth]=Clean(
            LowResSiliconeMix);
        [LowResSiliconeMixGraftOpen,LowResSiliconeMixGraftClose,LowResSiliconeMixGraftBoth]=
            Clean(LowResSiliconeMixGraft);

        [LowResSiliconeIngrowthOpen,LowResSiliconeIngrowthClose,LowResSiliconeIngrowthBoth]=
            Clean(LowResSiliconeIngrowth);
        [LowResSiliconeIngrowthGraftOpen,LowResSiliconeIngrowthGraftClose,
            LowResSiliconeIngrowthGraftBoth]=Clean(LowResSiliconeIngrowthGraft);
        [LowResSiliconeEncapOpen,LowResSiliconeEncapClose,LowResSiliconeEncapBoth]=Clean(
            LowResSiliconeEncap);
        [LowResSiliconeEncapGraftOpen,LowResSiliconeEncapGraftClose,
            LowResSiliconeEncapGraftBoth]=Clean(LowResSiliconeEncapGraft);

        [LowResSiliconePretensionOpen,LowResSiliconePretensionClose,
            LowResSiliconePretensionBoth]=Clean(LowResSiliconePretension);

        [LowVolMechanismOpen,LowVolMechanismClose,LowVolMechanismBoth]=Clean(LowVolMechanism)
            ;
        [LowVolSiliconeMixOpen,LowVolSiliconeMixClose,LowVolSiliconeMixBoth]=Clean(
            LowVolSiliconeMix);
        [LowVolSiliconeMixGraftOpen,LowVolSiliconeMixGraftClose,LowVolSiliconeMixGraftBoth]=
            Clean(LowVolSiliconeMixGraft);

        [LowStifMechanismOpen,LowStifMechanismClose,LowStifMechanismBoth]=Clean(
            LowStifMechansim);
        [LowStifMechansim2Open,LowStifMechansim2Close,LowStifMechansim2Both]=Clean(
            LowStifMechanism2);
        [LowStifMechansim3Open,LowStifMechansim3Close,LowStifMechansim3Both]=Clean(
            LowStifMechanism3);
        [LowStifSiliconeMixOpen,LowStifSiliconeMixClose,LowStifSiliconeMixBoth]=Clean(
            LowStifSiliconeMix);
        [LowStifSiliconeMixGraftOpen,LowStifSiliconeMixGraftClose,LowStifSiliconeMixGraftBoth
            ]=Clean(LowStifSiliconeMixGraft);
        %% Find Means
        window =100;

        LowResMechanismOpenMean = movmean(LowResMechanismOpen,window);
        LowResMechansimCloseMean = movmean(LowResMechanismClose,window);
        LowResMechansimBothMean = movmean(LowResMechanismBoth,window);

        LowResSiliconeHardOpenMean = movmean(LowResSiliconeHardOpen,window);
        LowResSiliconeHardCloseMean = movmean(LowResSiliconeHardClose,window);
        LowResSiliconeHardBothMean = movmean(LowResSiliconeHardBoth,window);

        LowResSiliconeHardGraftOpenMean = movmean(LowResSiliconeHardGraftOpen,window);
        LowResSiliconeHardGraftCloseMean = movmean(LowResSiliconeHardGraftClose,window);
        LowResSiliconeHardGraftBothMean = movmean(LowResSiliconeHardGraftBoth,window);

```

```
        LowResSiliconeMixOpenMean = movmean(LowResSiliconeMixOpen,window);
        LowResSiliconeMixCloseMean = movmean(LowResSiliconeMixClose,window);
        LowResSiliconeMixBothMean = movmean(LowResSiliconeMixBoth,window);

        LowResSiliconeMixGraftOpenMean = movmean(LowResSiliconeMixGraftOpen,window);
        LowResSiliconeMixGraftCloseMean = movmean(LowResSiliconeMixGraftClose,window);
        LowResSiliconeMixGraftBothMean = movmean(LowResSiliconeMixGraftBoth,window);

        LowResSiliconeIngrowthOpenMean = movmean(LowResSiliconeIngrowthOpen,window);
        LowResSiliconeIngrowthCloseMean = movmean(LowResSiliconeIngrowthClose,window);
        LowResSiliconeIngrowthBothMean = movmean(LowResSiliconeIngrowthBoth,window);

        LowResSiliconeIngrowthGraftOpenMean = movmean(LowResSiliconeIngrowthGraftOpen,window)
            ;
        LowResSiliconeIngrowthGraftCloseMean = movmean(LowResSiliconeIngrowthGraftClose,
            window);
        LowResSiliconeIngrowthGraftBothMean = movmean(LowResSiliconeIngrowthGraftBoth,window)
            ;

        LowResSiliconeEncapOpenMean = movmean(LowResSiliconeEncapOpen,window);
        LowResSiliconeEncapCloseMean = movmean(LowResSiliconeEncapClose,window);
        LowResSiliconeEncapBothMean = movmean(LowResSiliconeEncapBoth,window);

        LowResSiliconeEncapGraftOpenMean = movmean(LowResSiliconeEncapGraftOpen,window);
        LowResSiliconeEncapGraftCloseMean = movmean(LowResSiliconeEncapGraftClose,window);
        LowResSiliconeEncapGraftBothMean = movmean(LowResSiliconeEncapGraftBoth,window);

        LowResSiliconePretensionOpenMean = movmean(LowResSiliconePretensionOpen,window);
        LowResSiliconePretensionCloseMean = movmean(LowResSiliconePretensionClose,window);
        LowResSiliconePretensionBothMean = movmean(LowResSiliconePretensionBoth,window);
        % Volume Concept

        LowVolMechansimOpenMean = movmean(LowVolMechanismOpen,window);
        LowVolMechansimCloseMean = movmean(LowVolMechanismClose,window);
        LowVolMechansimBothMean = movmean(LowVolMechanismBoth,window);

        LowVolSiliconeMixOpenMean = movmean(LowVolSiliconeMixOpen,window);
        LowVolSiliconeMixCloseMean = movmean(LowVolSiliconeMixClose,window);
        LowVolSiliconeMixBothMean = movmean(LowVolSiliconeMixBoth,window);

        LowVolSiliconeMixGraftOpenMean = movmean(LowVolSiliconeMixGraftOpen,window);
        LowVolSiliconeMixGraftCloseMean = movmean(LowVolSiliconeMixGraftClose,window);
        LowVolSiliconeMixGraftBothMean = movmean(LowVolSiliconeMixGraftBoth,window);
        % Stiffness Concept

        LowStifMechansimOpenMean = movmean(LowStifMechanismOpen,window);
        LowStifMechansimCloseMean = movmean(LowStifMechanismClose,window);
        LowStifMechansimBothMean = movmean(LowStifMechanismBoth,window);

        LowStif2MechanismOpenMean = movmean(LowStifMechansim2Open,window);
        LowStif2MechanismCloseMean = movmean(LowStifMechansim2Close,window);
        LowStif2MechanismBothMean = movmean(LowStifMechansim2Both,window);

        LowStif3MechanismOpenMean = movmean(LowStifMechansim3Open,window);
        LowStif3MechanismCloseMean = movmean(LowStifMechansim3Close,window);
        LowStif3MechanismBothMean = movmean(LowStifMechansim3Both,window);

        LowStifSiliconeMixOpenMean = movmean(LowStifSiliconeMixOpen,window);
        LowStifSiliconeMixCloseMean = movmean(LowStifSiliconeMixClose,window);
        LowStifSiliconeMixBothMean = movmean(LowStifSiliconeMixBoth,window);

        LowStifSiliconeMixGraftOpenMean = movmean(LowStifSiliconeMixGraftOpen,window);
        LowStifSiliconeMixGraftCloseMean = movmean(LowStifSiliconeMixGraftClose,window);
        LowStifSiliconeMixGraftBothMean = movmean(LowStifSiliconeMixGraftBoth,window);

        %% Plot
        figure(1)

        plot(LowResMechansimBothMean(:,1),LowResMechansimBothMean(:,2), 'r')
        hold on
        % plot(LowResOpenMean(:,1),LowResOpenMean(:,2), 'r')
```

```
141         % plot(LowResCloseMean(:,1),LowResCloseMean(:,2),'r')
142
143         plot(LowVolMechansimBothMean(:,1),LowVolMechansimBothMean(:,2), 'g')
144         % plot(LowVolOpenMean(:,1),LowVolOpenMean(:,2),'g')
145         % plot(LowVolCloseMean(:,1),LowVolCloseMean(:,2),'g')
146
147         plot(LowStifMechansimBothMean(:,1),LowStifMechansimBothMean(:,2), 'b')
148         % plot(LowStifOpenMean(:,1),LowStifOpenMean(:,2),'b')
149         % plot(LowStifCloseMean(:,1),LowStifCloseMean(:,2),'b')
150
151         title('Concept Mechanism Only Comparisson')
152         xlabel('Input Distance [mm]')
153         ylabel('Actuator Force [N]')
154         legend('Most Residual Energy', 'Most Residual Energy within Volume Constraint', 'Low
                Stiffness','Location','north')
155
156         %% Plot Silicone of all concepts
157         figure(2)
158         plot(LowResSiliconeMixBothMean(:,1),LowResSiliconeMixBothMean(:,2),'r')
159         hold on
160         plot(LowVolSiliconeMixBothMean(:,1),LowVolSiliconeMixBothMean(:,2),'g')
161         plot(LowStifSiliconeMixBothMean(:,1),LowStifSiliconeMixBothMean(:,2),'b')
162         %plot(LowResSiliconeHardBothMean(:,1),LowResSiliconeHardBothMean(:,2),'k')'% REMOVE
                FROM PLOT
163         title('Concept Comparisson Mechanism in Silicone')
164         xlabel('Input Distance [mm]')
165         ylabel('Actuator Force [N]')
166         legend('Most Remaining Energy ', 'Most Remaining Energy within Volume', 'Lowest
                Stiffness','Location','southeast')
167         axis([0 5 0 17])
168
169         %% Plot Silicone + Graft of all concepts
170
171         figure(3)
172         plot(LowResSiliconeMixGraftBothMean(:,1),LowResSiliconeMixGraftBothMean(:,2),'r')
173         hold on
174         plot(LowVolSiliconeMixGraftBothMean(:,1),LowVolSiliconeMixGraftBothMean(:,2),'g')
175         plot(LowStifSiliconeMixGraftBothMean(:,1),LowStifSiliconeMixGraftBothMean(:,2),'b')
176         %plot(LowResSiliconeHardGraftBothMean(:,1),LowResSiliconeHardGraftBothMean(:,2),'k')
                '% REMOVE FROM PLOT
177         plot(displ*1000,Fp,'k','LineWidth',2)%Actuator
178         title('Concept Comparisson Mechanism in Silicone with Graft')
179         xlabel('Input Distance [mm]')
180         ylabel('Actuator Force [N]')
181         legend('Most Remaining Energy ', 'Most Remaining Energy within Volume', 'Lowest
                Stiffness','Actuator Input Maximum','Location','northwest')
182         axis([0 4 0 35])
183
184         %% Res Energy Concept
185
186         figure(4)
187         plot(1.25.*LowResMechansimBothMean(:,1),LowResMechansimBothMean(:,2),':')%Plot
                Mechanism only
188         hold on
189         plot(LowResSiliconeMixBothMean(:,1),LowResSiliconeMixBothMean(:,2),'--') %Plot
                Mechanism with Silicone
190         plot(LowResSiliconeMixGraftBothMean(:,1),LowResSiliconeMixGraftBothMean(:,2)) % Plot
                Mechanism with Silicone and pres Graft
191         title('Most Remaining Energy Concept')
192         xlabel('Input Distance [mm]')
193         ylabel('Actuator Force [N]')
194         legend('Mechanism ', 'Silicone', 'Graft','Location','northwest')
195         axis([0 5 0 inf])
196
197         %% Res Energy within Volume Concept
198
199         figure(5)
200         plot(1.5.*LowVolMechansimBothMean(:,1),LowVolMechansimBothMean(:,2),':')%Plot
                Mechanism only
201         hold on
202         plot(LowVolSiliconeMixBothMean(:,1),LowVolSiliconeMixBothMean(:,2),'--') %Plot
```

```
            Mechanism with Silicone
203         plot(LowVolSiliconeMixGraftBothMean(:,1),LowVolSiliconeMixGraftBothMean(:,2)) % Plot
                Mechanism with Silicone and pres Graft
204         title('Most Remaining Energy within Volume Concept ')
205         xlabel('Input Distance [mm]')
206         ylabel('Actuator Force [N]')
207         legend('Mechanism ', 'Silicone', 'Graft','Location','northwest')
208         axis([0 3 0 inf])
209
210         %% Low Stif Concept
211
212         figure(6)
213         plot(1.3.*LowStifMechansimBothMean(:,1),LowStifMechansimBothMean(:,2),':')%Plot
                Mechanism only
214         hold on
215         plot(LowStifSiliconeMixBothMean(:,1),LowStifSiliconeMixBothMean(:,2),'--') %Plot
                Mechanism with Silicone
216         plot(LowStifSiliconeMixGraftBothMean(:,1),LowStifSiliconeMixGraftBothMean(:,2)) %
                Plot Mechanism with Silicone and pres Graft
217         title('Lowest Stiffness Concept ')
218         xlabel('Input Distance [mm]')
219         ylabel('Actuator Force [N]')
220         legend('Mechanism ', 'Silicone', 'Graft','Location','northwest')
221         axis([0 5 0 inf])
222
223         %% Plot Production
224         figure(7)
225         plot(LowStifMechansimBothMean(:,1),LowStifMechansimBothMean(:,2), 'r')
226         hold on
227         plot(LowStif2MechanismBothMean(:,1),LowStif2MechanismBothMean(:,2), 'g')
228         plot(LowStif3MechanismBothMean(:,1),LowStif3MechanismBothMean(:,2), 'b')
229
230         title('Identical Mechanism Comparisson')
231         xlabel('Input Distance [mm]')
232         ylabel('Actuator Force [N]')
233         legend('Mechansim 1', 'Mechanism 2', 'Mechanism 3','Location','northwest')
234         axis([0 3 0 inf])
235
236
237         %% Plot Low Res Energy homogenous vs gel filling
238         figure(8)
239         plot(LowResSiliconeMixBothMean(:,1),LowResSiliconeMixBothMean(:,2),'--r')
240         hold on
241         plot(LowResSiliconeHardGraftBothMean(:,1),LowResSiliconeHardGraftBothMean(:,2),'r')
242         plot(LowResSiliconeHardBothMean(:,1),LowResSiliconeHardBothMean(:,2),'--g')
243         plot(LowResSiliconeMixGraftBothMean(:,1),LowResSiliconeMixGraftBothMean(:,2),'g')
244         title('Homogenous Filling vs Multi hardness Silicone')
245         xlabel('Input Distance [mm]')
246         ylabel('Actuator Force [N]')
247         legend('Mix Silicone', 'Mix Silicone with Graft', 'Homogenous Silicone','Homegenous
                Silicone with Graft','Location','northwest')
248         axis([0 5 0 inf])
249
250
251         %% Plot Low Res Energy FBR Sim
252         figure(9)
253         plot(LowResSiliconeMixBothMean(:,1),LowResSiliconeMixBothMean(:,2),'--r')
254         hold on
255         plot(LowResSiliconeMixGraftBothMean(:,1),LowResSiliconeMixGraftBothMean(:,2),'r')
256         plot(LowResSiliconeIngrowthBothMean(:,1),LowResSiliconeIngrowthBothMean(:,2),'--b')
257         plot(LowResSiliconeIngrowthGraftBothMean(:,1),LowResSiliconeIngrowthGraftBothMean
                (:,2),'b')
258         plot(LowResSiliconeEncapBothMean(:,1),LowResSiliconeEncapBothMean(:,2),'--g')
259         plot(LowResSiliconeEncapGraftBothMean(:,1),LowResSiliconeEncapGraftBothMean(:,2),'g')
260
261         plot(displ*1000,Fp,'k','LineWidth',2)%Actuator
262         title('FBR Simulation resistance')
263         xlabel('Input Distance [mm]')
264         ylabel('Actuator Force [N]')
265         legend('Mix Silicone', 'Mix Silicone with Graft', 'FBR ingrowth','FBR ingrowth with
                Graft','FBR Encapsulated','FBR Encapsulated with Graft','Actuator input Maximum
```

```
        ','Location','southeast')
266     axis([0 4.5 0 40])
267
268     %% Trapz
269     % EAct = 0.0722;
270
271     LowResSiliconeMixGraftBothMean(isnan(LowResSiliconeMixGraftBothMean))=0;
272     LowResSiliconeMixGraftBothMean(:,1)=LowResSiliconeMixGraftBothMean(:,1)*0.001;
273     ELowRes=trapz(LowResSiliconeMixGraftBothMean(:,1),LowResSiliconeMixGraftBothMean(:,2)
            );
274     EActLowRes=trapz(displ(80:end),Fp(80:end));
275
276     pLowRes = ELowRes/EActLowRes;
277
278     LowVolSiliconeMixGraftBothMean(isnan(LowVolSiliconeMixGraftBothMean))=0;
279     LowVolSiliconeMixGraftBothMean(:,1)=LowVolSiliconeMixGraftBothMean(:,1)*0.001;
280     ELowVol=trapz(LowVolSiliconeMixGraftBothMean(:,1),LowVolSiliconeMixGraftBothMean(:,2)
            );
281     EActLowVol=trapz(displ(130:end),Fp(130:end));
282
283     pLowVol=ELowVol/EActLowVol;
284
285     LowStifSiliconeMixGraftBothMean(isnan(LowStifSiliconeMixGraftBothMean))=0;
286     LowStifSiliconeMixGraftBothMean(:,1)=LowStifSiliconeMixGraftBothMean(:,1)*0.001;
287     ELowStif=trapz(LowStifSiliconeMixGraftBothMean(:,1),LowStifSiliconeMixGraftBothMean
            (:,2));
288     EActLowStif=trapz(displ(101:end),Fp(101:end));
289
290     pLowStif=ELowStif/EActLowStif;
291
292
293
294     %% Clean Function
295     % This function will delete data where the stage is stationairy and
296     % differentiate opening movements from closing movements for the inputted
297     % data.
298     function [open,close,both] = Clean(Data)
299     % Offset Displacement and Absolute Force
300     Data(:,1) = Data(:,1)-Data(1,1); %Set first position to zero
301     Data(:,2) = abs(Data(:,2)); %Make force vector positives
302     index1=find(Data(:,1)<0.01); %Finds all points where stages rests at minimal
            displacement
303     Data(index1,:)=[]; % Removes all entries at zero position
304     index2=find(Data(:,1)>(max(Data)-0.01)); %Finds all points where stage rests at
            maximum position
305     Data(index2,:)=[]; % Removes all entries at max position
306     index3=find(diff(Data(:,1))==0); %Finds other stationairy points
307     Data(index3,:)=[]; %Removes all stationairy points
308     index4=find(diff(Data(:,1))>0); %Finds all closing motions
309     DataClose = Data(index4,:); %Defines closing movements
310     DataOpen = Data;
311     DataOpen(index4,:)=[]; % Defines opening movements
312
313     open=DataOpen;
314     open(open==0)=NaN;
315     open=sortrows(open);
316
317     close = DataClose;
318     close(close==0)=NaN;
319     close = sortrows(close);
320
321     both=[open;close];
322     both = sortrows(both);
323
324     end
325
326     %% Mean Function
327     % find the mean for each row of displacements and each row of force.
328     % Outputs [MeanDisplacements MeanForces]
329     function A = NonZeroMean(B)
330     % B(B==0)=NaN;
```

```
        d=mean(B(:,1:2:size(B,2)-1),2,'omitNaN');
        f=mean(B(:,2:2:size(B,2)),2,'omitNaN');
        A= [d f];
        end
```

B.4. Fatigue Study

```
        %% Fatigue Study
        % Dirk Ulijn - 4321758
        clc
        %clear, close all
        %% Load Data
        data = readmatrix("Fatigue836x.tmp.xlsx");
        %% Data interpretation
        Force = data(:,2); % Select force from data
        %Distance = data(:,1);
        peaks = findpeaks(Force,'MinPeakDistance',13,'MinPeakHeight',15.3);
        %peaks(peaks<5)=[ ];

        %%Curve fit
        xfit=(1:1:size(peaks))';
        % fit=fit(xfit,peaks,'log10');
        %% Plot
        figure(1)
        plot(peaks,'.')
        hold on
        plot(fittedmodel)
        xlabel('actuation cycle')
        ylabel('Peak Force [N]')
        title('Fatigue Test')
        legend('Peak Input Forces','Fitted Exponential Curve')
```

B.5. Traction Test

```
        %% Traction Test
        % Dirk Ulijn 4321758
        clc
        close all, clear
        %% Load data
        data_Mechanism = readmatrix("TractionLowResMech4p5mm3x.tmp.xlsx");
        data_Mechanism(:,1)=data_Mechanism(:,1)-50.35;
        % data_Mechanism = smoothdata(data_Mechanism);
        run1=data_Mechanism(1:1167,:);
        run2=data_Mechanism(1168:2271,:);
        run3=data_Mechanism(2271:end,:);

        run1smooth=smoothdata(run1,"sgolay",50);
        run2smooth=smoothdata(run2,"sgolay",50);
        run3smooth=smoothdata(run3,"sgolay",50);
        %% Plotting
        % plot(data_Mechanism(:,1),data_Mechanism(:,2))
        % % hold on
        % data_Mechanism = smoothdata(data_Mechanism,"sgolay",50);
        % plot(data_Mechanism(:,1),data_Mechanism(:,2))

        plot(run1smooth(:,1),run1smooth(:,2))
        hold on
        plot(run2smooth(:,1),run2smooth(:,2))
        plot(run3smooth(:,1),run3smooth(:,2))

        title('Traction Test')
        xlabel('Input Displacement [mm]')
        ylabel('Tractive Force on Graft [N]')
        legend('Run 1', 'Run 2','Run 3', "Location","northwest")
        axis([0 4.5 -0.5 1.2])
```

B.6. Input-Output study for video analysis - Unused

```
vidObj = VideoReader("LowStifMech.mp4");
s = struct("cdata",zeros(vidObj.Height,vidObj.Width,3,"uint8"),colormap=[]);

vidObj.CurrentTime = 0.0; % seconds
endtime = 48;% seconds
k = 1;
while vidObj.CurrentTime <= endtime
s(k).cdata = readFrame(vidObj);
k = k+1;
end
whos s
%%
set(gcf, 'Units', 'Normalized', 'OuterPosition', [0 0 1 1]);
framerate = ceil(vidObj.FrameRate);

[n ,numofframes] = size(s);

imshow(s(1).cdata)
title('set 2 points to measure width of the base and one point in the middle and the botom tip (x4)');
[xb,yb] = getpts();

basewith = 0.025;% m, 15mm

D = {};
Dapp = {};

basewithhpx = sqrt((yb(2)-yb(1))^2 + (xb(2)-xb(1))^2);
pixelsize= basewith/basewithhpx;
Dapp = {0 0 0 0 xb yb 0 0};
D = [D;Dapp];

D = {};
Dapp = {};

framerate = 0.2*framerate;

for i = 1:framerate:numofframes  %% verander framerate waarde om meerof minder datapunten te hebben

figure(1)
% set(gcf, 'Units', 'Normalized', 'OuterPosition', [0 0 1 1]);
imshow(s(i).cdata)
title('select 1 points of gripper and 1 on actuator input middle');
[x,y] = getpts();


%tipdistance = sqrt((y(2)-y(1))^2 + (x(2)-x(1))^2)*pixelsize;
tipdistancex = (x(1)-xb(4))*pixelsize;
tipdistancey = (y(1)-yb(4))*pixelsize;
%tipdistance = sqrt((y(2)-yb(4))^2 + (x(2)-xb(4))^2)*pixelsize;
%inputdistance = sqrt((y(3)-yb(3))^2 + (x(3)-xb(3))^2)*pixelsize;
inputdistancex = (x(2)-xb(3))*pixelsize;
inputdistancey = (y(2)-yb(3))*pixelsize;
Dapp = {(i/framerate) tipdistancex tipdistancey inputdistancex inputdistancey basewithhpx pixelsize xb yb x y};
D = [D;Dapp];

end

%%
% datat = cell2table(D);
% datat.Properties.VariableNames = ["time","tipdistancex","tipdistancey","inputdistancex","inputdistancey","basewithhpx","pixelsize","xb","yb","x","y"];
%  writetable(datat,'LowStiffMech.csv');
```